

NPS-MR-99-001

# NAVAL POSTGRADUATE SCHOOL MONTEREY, CALIFORNIA



## THESIS

### OBSERVATION AND ANALYSIS OF COASTALLY TRAPPED WIND REVERSALS

by

Steven P. Sopko

December 1998

Thesis Advisor:

Wendell A. Nuss

Approved for public release; distribution is unlimited.

19990209 096

Prepared for:  
Office of Naval Research  
800 N. Quincy Street  
Arlington, VA 22217

DTIC QUALITY INSPECTED 2

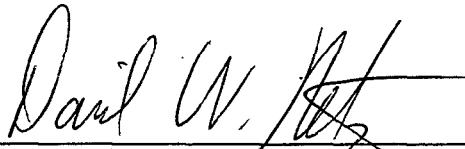
**NAVAL POSTGRADUATE SCHOOL  
MONTEREY, CALIFORNIA**

Rear Admiral Robert C. Chaplin  
Superintendent

This thesis was prepared in conjunction with research sponsored in part by the Office of Naval Research, 800 N. Quincy Street, Arlington, VA 22217.

Reproduction of all or part of this report is authorized.

Released by:

A handwritten signature in dark ink, appearing to read "David W. Netzer", is written over a horizontal line.

David W. Netzer, Associate Provost and Dean of Research

REPORT DOCUMENTATION PAGE			Form Approved OMB No. 0704-0188	
Public reporting burden for this collection of information is estimated to average 1 hour per response, including the time for reviewing instruction, searching existing data sources, gathering and maintaining the data needed, and completing and reviewing the collection of information. Send comments regarding this burden estimate or any other aspect of this collection of information, including suggestions for reducing this burden, to Washington Headquarters Services, Directorate for Information Operations and Reports, 1215 Jefferson Davis Highway, Suite 1204, Arlington, VA 22202-4302, and to the Office of Management and Budget, Paperwork Reduction Project (0704-0188) Washington DC 20503.				
1. AGENCY USE ONLY (Leave blank)	2. REPORT DATE December 1998	3. REPORT TYPE AND DATES COVERED Master's Thesis		
4. TITLE AND SUBTITLE OBSERVATION AND ANALYSIS OF COASTALLY TRAPPED WIND REVERSALS		5. FUNDING NUMBERS N0001498WR30111		
6. AUTHOR(S) Steven P. Sopko in conjunction with Dr. Wendell A. Nuss				
7. PERFORMING ORGANIZATION NAME(S) AND ADDRESS(ES) Naval Postgraduate School Monterey, CA 93943-5000		8. PERFORMING ORGANIZATION REPORT NUMBER NPS-MR-99-001		
9. SPONSORING/MONITORING AGENCY NAME(S) AND ADDRESS(ES) Office of Naval Research 800 N. Quincy Street, Arlington, VA 22217		10. SPONSORING/MONITORING AGENCY REPORT NUMBER		
11. SUPPLEMENTARY NOTES The views expressed in this thesis are those of the author and do not reflect the official policy or position of the Department of Defense or the U.S. Government.				
12a. DISTRIBUTION/AVAILABILITY STATEMENT Approved for public release; distribution is unlimited.		12b. DISTRIBUTION CODE		
13. ABSTRACT (maximum 200 words) <p>During the warm season (April-September), the California coast is under the influence of persistent northwesterly flow. Periodically, this flow is replaced by a narrow band of southerly winds along the coast. The transition to southerly flow is often accompanied by a rise in sea-level pressure, lower temperatures, coastal stratus, and fog. The mesoscale disturbance responsible for this southerly transition has become known as a coastally trapped wind reversal (CTWR). While it is clear that these mesoscale disturbances are forced by the interaction of the coastal topography with the synoptic-scale flow, the exact mechanisms for their development and their governing dynamics remain the subject of much debate.</p> <p>The present study examines three cases from 1996 that appear to have the characteristics of a CTWR. Each case is analyzed to determine the associated synoptic-scale forcing and the respective mesoscale structure. The observed synoptic-scale forcing is compared to the results of a climatological study conducted by Mass and Bond (1996). Results from a modeling study by Skamarock et al. (1998) are used to create a conceptual model for comparison with the observed development and mesoscale structure of each event. Results of this study show that only two of the cases can be classified as a CTWR. The study also shows that variability exists in the synoptic-scale forcing associated with the initiation of a CTWR. Two mechanisms for the development of the offshore mesoscale low, and ultimately the CTWR, have been identified. The variability of the mesoscale structure in each CTWR is also documented.</p>				
14. SUBJECT TERMS Coastal meteorology, Environmental effects		15. NUMBER OF PAGES 146		
		16. PRICE CODE		
17. SECURITY CLASSIFICATION OF REPORT Unclassified	18. SECURITY CLASSIFICATION OF THIS PAGE Unclassified	19. SECURITY CLASSIFICATION OF ABSTRACT Unclassified	20. LIMITATION OF ABSTRACT UL	

Approved for public release; distribution is unlimited.

**OBSERVATION AND ANALYSIS OF  
COASTALLY TRAPPED WIND REVERSALS**

Steven P. Sopko  
Lieutenant Commander, United States Navy  
B.S., Texas A&M University, 1988

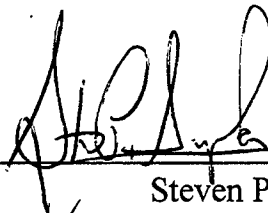
Submitted in partial fulfillment  
of the requirements for the degree of

**MASTER OF SCIENCE IN  
METEOROLOGY AND PHYSICAL OCEANOGRAPHY**

from the

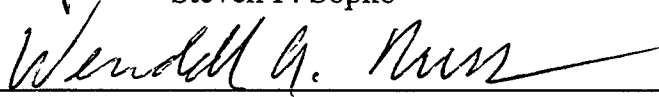
**NAVAL POSTGRADUATE SCHOOL  
December 1998**

Author:

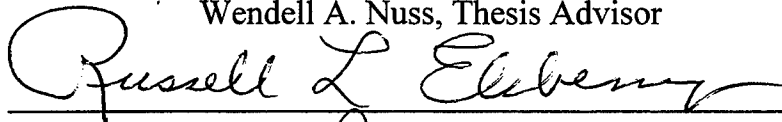


Steven P. Sopko

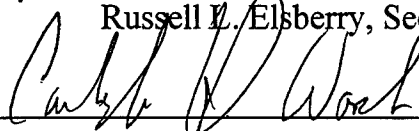
Approved by:



Wendell A. Nuss, Thesis Advisor



Russell L. Elsberry, Second Reader



Carlyle H. Wash, Chairman  
Department of Meteorology

## ABSTRACT

During the warm season (April-September), the California coast is under the influence of persistent northwesterly flow. Periodically, this flow is replaced by a narrow band of southerly winds along the coast. The transition to southerly flow is often accompanied by a rise in sea-level pressure, lower temperatures, coastal stratus, and fog. The mesoscale disturbance responsible for this southerly transition has become known as a coastally trapped wind reversal (CTWR). While it is clear that these mesoscale disturbances are forced by the interaction of the coastal topography with the synoptic-scale flow, the exact mechanisms for their development and their governing dynamics remain the subject of much debate.

The present study examines three cases from 1996 that appear to have the characteristics of a CTWR. Each case is analyzed to determine the associated synoptic-scale forcing and the respective mesoscale structure. The observed synoptic-scale forcing is compared to the results of a climatological study conducted by Mass and Bond (1996). Results of a modeling study by Skamarock et al. (1998) are used to create a conceptual model for comparison with the observed evolution of the mesoscale structure of each case. Results of this study show that only two of the cases can be classified as a CTWR. The study also shows that variability exists in the synoptic-scale forcing associated with the initiation of a CTWR. Two mechanisms for the development of the offshore mesoscale low, and ultimately the CTWR, have been identified. The variability of the mesoscale structure of each CTWR is also documented.

## TABLE OF CONTENTS

I.	INTRODUCTION .....	1
II.	SYNOPTIC-SCALE EVOLUTION .....	7
	A. BACKGROUND .....	7
	B. MODEL DESCRIPTION .....	9
	C. METHOD OF ANALYSIS .....	11
	D. ANALYSIS OF THE 1996 CASES .....	12
	1. 21-24 July 1996 Case .....	12
	2. 1-4 September 1996 Case .....	20
	3. 4-7 June 1996 Case .....	27
III.	MESOSCALE STRUCTURE .....	41
	A. BACKGROUND .....	41
	B. METHOD OF ANALYSIS .....	42
	C. SURFACE EVOLUTION .....	45
	1. 21-24 July 1996 Case .....	45
	2. 1-4 September 1996 Case .....	50
	3. 4-7 June 1996 Case .....	55
	D. DEVELOPMENT OF THE OFFSHORE MESOSCALE LOW .....	59
	1. Conceptual Model .....	59
	2. 21-24 July 1996 Case .....	60
	3. 1-4 September 1996 Case .....	65
	E. REVERSAL OF THE ALONG-COAST PRESSURE GRADIENT .....	69
	1. 21-24 July 1996 Case .....	69
	2. 1-4 September 1996 Case .....	73
	F. PROPAGATION AND VERTICAL EXTENT OF THE CTWR .....	75
	1. 21-24 July 1996 Case .....	75
	2. 1-4 September 1996 Case .....	76

IV. SUMMARY AND CONCLUSIONS .....	121
LIST OF REFERENCES .....	127
INITIAL DISTRIBUTION LIST .....	131

## LIST OF FIGURES

2.1. The evolution of the composite fields of 500 mb geopotential height, 850 mb geopotential height, and sea-level pressure for 2 days prior to 2 days after strong coastally trapped wind reversals at buoy 46013 (from Mass and Bond 1996) .....	32
2.2. Domain for the eta model analyses used in analyzing the evolution of the synoptic-scale pattern .....	34
2.3. Eta model analyses for the 21-24 July 1996 case for 500 mb, 850 mb, and the surface .....	35
2.4. Eta model analyses for the 1-4 September 1996 case for 500 mb, 850 mb, and the surface .....	37
2.5. Eta model analyses for the 4-7 June 1996 case for 500 mb, 850 mb, and the surface. ....	39
3.1. Summary of a coastally trapped wind reversal (from Skamarock et al. 1998) .....	79
3.2. Horizontal cross-sections at $z = 300$ m from the reference simulation (from Skamarock et al. 1998) .....	80
3.3. Domain for the hand-drawn mesoscale analyses of sea-level pressure .....	81
3.4. Surface evolution of the 21-24 July 1996 case as depicted by hand-drawn analyses of sea-level pressure .....	82
3.5. Satellite imagery from NOAA polar orbiting satellites for the 21-24 July 1996 coastally trapped wind reversal .....	88
3.6. Surface evolution of the 1-4 September 1996 case as depicted by hand-drawn analyses of sea-level pressure .....	90



3.7. Satellite imagery from NOAA polar orbiting satellites for the 01-04 September 1996 coastally trapped wind reversal .....	96
3.8. Surface evolution of the 4-7 June 1996 case as depicted by hand-drawn analyses of sea-level pressure .....	98
3.9. Satellite imagery from NOAA polar orbiting satellites for the 04-06 June 1996 ...	106
3.10. Along-coast vertical cross sections of the cross-coast wind component and temperature for the 21-24 July 1996 coastally trapped wind reversal .....	108
3.11. A time series of sea-level pressure for the moored coastal buoys for the period from 1200 UTC 19 July to 0600 UTC 24 July .....	109
3.12. A time series of marine layer depth for the coastal wind profiler sites for the period from 0000 UTC 21 July to 2300 UTC 23 July .....	110
3.13. Along-coast vertical cross sections of the cross-coast wind component and temperature for the 1-4 September 1996 coastally trapped wind reversal .....	111
3.14. A time series of sea-level pressure for the moored coastal buoys for the period from 0000 UTC 31 August to 0600 UTC 04 September .....	112
3.15. A time series of marine layer depth for the coastal wind profiler sites for the period from 0000 UTC 01 September to 2300 UTC 03 September .....	113
3.16. A series of along-coast depictions of sea-level pressure for the moored coastal buoys and marine layer depth for the coastal wind profiler sites for the 21-24 July 1996 coastally trapped wind reversal .....	114
3.17. A series of along-coast depictions of sea-level pressure for the moored coastal buoys and marine layer depth for the coastal wind profiler sites for the 1-4 September 1996 coastally trapped wind reversal .....	117

## ACKNOWLEDGEMENT

I would like to thank my advisor, Dr. Wendell Nuss, for his exceptional professional guidance and advice, which has made this study possible. His willingness to engage in thought-provoking discussion and convey his vast knowledge greatly enhanced my intellectual capacity for original thought and provided the motivation for this work. The constructive advice provided by Dr. Russell Elsberry, as second reader, significantly improved the focus and quality of this work, and was greatly appreciated. I would like to recognize Mr. Dick Lind for his invaluable assistance in obtaining and plotting wind profiler data, which greatly assisted my efforts in this endeavor. I would also like to thank Mr. Bob Creasey and Mr. Kurt Nielsen for their assistance in obtaining and processing the satellite imagery used in this study.

## I. INTRODUCTION

Local weather conditions along the west coast of the United States can be strongly influenced by orography. Coastal mountain ranges extend along the entire length of the U.S. west coast and act as barrier to lower-tropospheric flow. Their interaction with the synoptic-scale flow results in a variety of mesoscale, trapped atmospheric phenomena within approximately 100 km of the coastline (Nuss 1996). These mesoscale features greatly influence local weather conditions near the coast. The warm season (April-September) features a well-defined, shallow marine layer capped by a strong low-level inversion. The marine layer depth increases in the offshore direction, which causes a large cross-coast pressure gradient and a strong northwesterly coastal jet in the lower troposphere. Periodically, these prevailing conditions are interrupted by a mesoscale disturbance called a coastally trapped wind reversal (CTWR), which produces a narrow band of southerly winds along the coast. Although the transition to southerly flow is often gradual (e.g., 8 m/s change in the along-shore wind over 4-10 hours; Bond et al. 1996), it can be abrupt in some cases (e.g., 15 m/s within a few minutes; Mass and Albright 1987). These disturbances are often, but not always, accompanied by rising pressure, cooling at the surface of up to 10° C, and a transition from clear to overcast sky conditions with stratus and fog. The low ceilings and reduced visibility associated with these weather conditions can have a large impact on aviation and maritime operations.

Changes in the depth of the marine layer and the strength of the capping inversion can affect the distribution of air pollution along the coast.

Forecasting the transition from northerly to southerly winds has proven to be a difficult problem for operational weather forecasters. In one case during 1982, strong northerly winds and moderate seas were forecast for a current meter recovery cruise off the coast of California (Dorman 1985). Instead, the winds were light and southerly, while the seas were relatively calm. An examination of the surface weather charts revealed that the winds were blowing against the synoptic-scale pressure gradient (Dorman 1985). Some mesoscale feature, not depicted by synoptic-scale weather charts, influenced the weather conditions near the coast. Even today, similar mesoscale atmospheric phenomena are not resolvable by the current observational network due to inadequate spatial resolution. Efforts to simulate realistically the evolution of CTWRs with operational numerical weather prediction models are ongoing. Recent modeling efforts using the Navy's Coupled Ocean and Atmosphere Mesoscale Prediction System (COAMPS) have been successful in capturing many features of a CTWR (Thompson et al. 1997, Thompson and Bane 1998). Such studies demonstrate the vast potential of mesoscale models in forecasting mesoscale phenomena that were previously unresolvable by global-scale models.

A climatological study by Mass and Bond (1996) documents the evolution of the synoptic-scale conditions associated with CTWRs by creating composites of surface and upper-air analyses (500 mb and 850 mb). Mass and Bond (1996) do an excellent job of

establishing the general synoptic-scale patterns associated with CTWRs; however, the composites fail to show differences in the synoptic-scale forcing that may occur in many cases. The lack of variability indicated in Mass and Bond (1996) can be attributed to the coarse resolution of the gridded fields used in the compositing process. The compositing process can also be expected to smooth out any small features (e.g., short-wave troughs), and thus omit any case to case variability.

The present study examines three cases from a 1996 field experiment (4-7 June, 21-24 July, and 1-4 September) that appear to exhibit some features (e.g., coastal southerlies and coastal stratus) that are characteristic of past CTWRs. A qualitative analysis of National Center for Environmental Prediction (NCEP) eta model analyses at 500 mb, 700 mb, 850 mb, and the surface is conducted for the three 1996 cases. Results of this analysis indicate that the evolution of their general synoptic-scale patterns are similar in some aspects to those depicted in Mass and Bond (1996); however, significant differences are found in each event. These differences illustrate the observed variability in the evolution of a CTWR and its respective mesoscale structure. The present study focuses on the synoptic-scale conditions associated with the initiation of a CTWR.

Variability in the mesoscale structure of CTWRs has been documented in past studies and has led to many theories regarding the governing dynamics. Those studies focus around the initiation, propagation, and structure of CTWRs. The earliest such study (Dorman 1985) interprets these disturbances as freely propagating Kelvin waves. Other interpretations characterize CTWRs as topographically trapped density currents

(Dorman 1987; Mass and Albright 1987), or as mesoscale responses to the along-shore pressure gradients produced by orography and the synoptic-scale flow (Mass et al. 1986; Mass and Albright 1988; Overland and Bond 1994). The relative importance of Kelvin wave and density current dynamics versus the synoptic-scale flow was studied by Reason and Steyn (1992), who suggest that both marine boundary layer processes and synoptic-scale processes contribute to the initiation and evolution of a CTWR, which seemed to have been confirmed in a field study conducted in 1994 (Nuss 1996).

A recent numerical modeling study by Skamarock et al. (1998) attempts to simulate many of the observed features of a CTWR. This study superposes a large-scale offshore flow at 850 mb across coastal topography on a climatological mean atmospheric state for 3 days. Their simulations use two-dimensional dynamics and a three-dimensional non-hydrostatic model. These simulations have many of the features associated with observed CTWRs in past studies. These features include the offshore displacement of the northerly coastal jet and marine layer, the formation of a coastal trough and offshore mesoscale low, and a layer of deep southerlies along the coast. It is important to note that these idealized simulations exclude some effects that may influence or alter the evolution of CTWRs. For example, the superposed barotropic offshore flow does not include a north-south temperature gradient (Skamarock et al. 1998). Furthermore, the simulations do not include mechanisms that maintain (sea surface fluxes) or erode (radiation, diurnal processes) the marine layer, or complex vertical structure in the inversion above the marine layer. The simulated coastal topography is a

smooth coastal plateau with no along-coast variation (Skamarock et al. 1998). Although the Skamarock et al. (1998) study provides an excellent conceptual model of the evolution of a CTWR for comparison with observed events, it fails to address the case to case variability found in past studies (Dorman 1985, Mass and Albright 1987, and Ralph et al. 1998).

The present study examines the evolution and some aspects of the mesoscale structure of the three 1996 cases, and compares the observed features with those in Skamarock et al. (1998) through a qualitative analysis of sea-level pressure, lower tropospheric winds, thermal advection, and marine layer depth. The variability in the evolution of these events and their mesoscale features are also documented. The mechanisms for the formation of the coastal troughing and the offshore mesoscale low, and their correlation to the eventual initiation of a CTWR are addressed. Ultimately, the present study shows that differences in the synoptic-scale environment for each event result in variability in the initiation of each CTWR and their respective mesoscale structures. The 21-24 July and 1-4 September cases are excellent cases to study for two reasons. First, these two cases occur near buoy 46013, so they can be readily compared with the Mass and Bond climatological study. Second, both cases are determined to be CTWRs, even though they have different synoptic-scale forcing patterns and mesoscale structures. Although the 4-7 June case has some characteristic features of a CTWR, the analysis of the synoptic-scale evolution and mesoscale structure indicates that this case is not a well-defined CTWR.

## II. SYNOPTIC-SCALE EVOLUTION

### A. BACKGROUND

Mass and Bond (1996) examine the synoptic evolution associated with CTWRs occurring at various places along the U.S. west coast. Composites of surface and upper-air analyses were constructed for four coastal buoy locations: 46010, off the mouth of the Columbia River; 46027, near the California-Oregon border; 46013, just north of San Francisco Bay; and 46028, north of San Luis Obispo on the central California coast (Mass and Bond 1996). The composites were created for CTWRs occurring between April and September during 1981-1991 by averaging NCEP operational analyses (0000 UTC and 1200 UTC) with a horizontal resolution of 380 km (Mass and Bond 1996). The composite analyses are from 48 hours prior to the initiation of the CTWR to 48 hours after the transition. The 21-24 July and 1-4 September cases are initiated near buoy 46013 and the 4-7 June case is initiated south of buoy 46028. Therefore, the synoptic-scale evolutions for buoys 46013 and 46028 presented in Mass and Bond (1996) are the focus of this discussion. For this study, the annotation (- hh or + hh) refers to the approximate number of hours prior to or after the initiation of the coastally trapped wind reversal (e.g., (-24) indicates 24 hours prior to the initiation of the CTWR).

Evolution of the synoptic-scale pattern for CTWRs occurring near buoy 46013 is illustrated in Figure 2.1. The figures referenced in the text are at the end of each chapter. Mass and Bond (1996) find that synoptic height and pressure fields resemble normal



climatological conditions three days prior to the initiation of CTWRs near buoy 46013. A 500 mb ridge over the eastern North Pacific amplifies and drifts eastward during the 48 hours prior to the transition. At the time of transition, highly anomalous ridging is found over the eastern Pacific with weak troughing that extends from the Rocky Mountains to northwestern Mexico. The ridge is maintained during the first 24 hours (+12, +24) of the CTWR, and then rapidly attenuates during the subsequent 24 hours (+36, +48). At 850 mb, the eastern Pacific high intensifies and builds northeastward over the Pacific Northwest, while an inland trough extends southwestward from Nevada to extreme southern California. This synoptic-scale pattern results in enhanced offshore (northeasterly) flow over northern California. Above-normal temperatures are evident over much of the California coast and offshore waters, with the largest anomalies coincident with the region of strongest offshore flow. A trough over southern California also becomes better defined during the 48 hours prior to the transition. This pattern weakens slowly during the first day (+12, +24) of the transition, and then more rapidly during the second day (+36, +48). At the surface, the eastern Pacific high builds over the Pacific Northwest, while a thermal trough expands westward from the Central Valley of California to the coast during the two days prior to the wind reversal. At the time of the transition, a surface trough extends from the interior of California to San Francisco Bay with a strong (and highly anomalous) pressure gradient along the northern California coast. The trough weakens considerably after the first day (+24) of the event.

Mass and Bond (1996) also indicate that the evolution of the synoptic-scale pattern for CTWRs initiated near buoy 46028 are very similar to those initiated near buoy 46013. The significant synoptic-scale features are weaker and are shifted southward for CTWRs initiated near buoy 46028. Mass and Bond also find that the evolution of the synoptic-scale pattern for strong and weak CTWRs at buoy 46013 are very similar -- the main differences are some attenuation in the amplitudes of the synoptic-scale features for the weak CTWRs.

## **B. MODEL DESCRIPTION**

In this study, National Center for Environmental Prediction (NCEP) eta model analyses are used to examine the evolution of the synoptic-scale pattern associated with the three cases. The eta coordinate as defined by Mesinger (1984) is a generalization of the terrain-following sigma coordinate (Rogers et al. 1995) normalized from 0 to 1 with respect to sea-level pressure. The model orography is configured in discrete steps that exactly coincide with model interfaces. The step-mountains are computed using a "silhouette-mean" orography method (Mesinger and Collins 1987), so that their heights are maximized based upon the input 10-min surface elevation data of Joseph (1980). At land points where the observed topography is concave (e.g., a valley), the silhouette elevation is replaced by the average elevation (Rogers et al. 1995). The horizontal domain of the operational model that was in use during the period of this study covered much of the Northern Hemisphere and extended from the western Pacific Ocean to the

eastern Atlantic Ocean with a horizontal resolution of 80 km and 38 vertical layers. The pressure at the top of the model was 50 mb.

The eta model is a hydrostatic model that employs the semi-staggered Arakawa e-grid (Arakawa and Lamb 1977) in which wind points are adjacent to mass points (Rogers et al. 1995). The model uses a split-explicit time differencing scheme. Physical parameterizations include the modified Betts-Miller (1986) convective adjustment scheme for deep and shallow convection, and the Mellor-Yamada (1974, 1982) level 2.5 model for free atmosphere vertical turbulent exchange and Mellor-Yamada level 2.0 model near the surface. Parameterization of the viscous sublayer over the water is based on Liu et al. (1979) and Mangarella et al. (1973). Specific details on eta model dynamics and physical parameterizations can be found in Black (1988, 1994), Janjic (1990, 1994), Mesinger et al. (1988), and Gerrity et al. (1994).

The eta model employs an optimum interpolation scheme to generate the initial conditions (Rogers et al. 1995). A 6-hour forecast from the NCEP global spectral model is used as the first guess. Boundary conditions are obtained from the previous run of the NCEP global spectral model. The procedure for processing observations for the analysis is identical to the one described by DiMego (1988) except for the time window of data acceptance (2145-0115 for 0000 UTC and 0945-1315 for 1200 UTC) (Rogers et al. 1995). The ingested data undergo a hydrostatic quality control check, and are then transformed to spectral grid space. After the optimum interpolation scheme is performed

and all analysis corrections are computed, the analysis fields are interpolated back to the full analysis grid. The data are then added to the first-guess field for analysis.

### **C. METHOD OF ANALYSIS**

The eta model gridded fields used in this study are in GEMPAK format. The GEMPAK files are displayed using the Visual Meteorological Diagnostic and Display Program. Eta model analyses for 0000 UTC and 1200 UTC are displayed on a domain that covers the western U.S., southwestern British Columbia, and the eastern Pacific Ocean (Figure 2.2). The levels examined include 500 mb, 700 mb, 850 mb, and the surface. Geopotential height and temperature are displayed on the 500 mb, 700 mb and 850 mb analyses. Sea-level pressure is depicted on the surface analyses. Although both 0000 UTC and 1200 UTC analyses are examined, the 1200 UTC (0400 L) analyses are chosen to describe the synoptic forcing in each case to minimize the diurnal variation associated with daytime heating over land, especially in the lower troposphere. The use of only the 1200 UTC charts creates more continuity, and thus provides a clearer picture of the evolution of the synoptic-scale forcing in each case.

The synoptic-scale evolution for buoy 46013 depicted by Mass and Bond (1996) is compared with the 21-24 July and 1-4 September cases, while the synoptic-scale evolution for buoy 46028 is used for the June case. This study focuses on the initiation of a CTWR; therefore, the evolution of the synoptic-scale pattern is analyzed at least 48 hours prior to through 24 hours after the initiation of the CTWR. The analysis for 48

hours prior to initiation is compared with the climatological mean synoptic-scale conditions. If this analysis differs significantly from the mean pattern, then analyses prior to that time are also examined. The 500 mb, 850 mb, and surface analyses are compared directly with the Mass and Bond (1996) study to determine any variability among the three cases. Additionally, the 500 mb and 700 mb analyses are examined for a possible coupling between mid-tropospheric features and marine boundary layer processes in the initiation of a CTWR. The 850 mb and surface analyses are examined to determine the role of the lower tropospheric synoptic-scale processes in the relaxation of the strong along-coast pressure gradient and the development of the mesoscale coastal trough and offshore low. The development of an offshore mesoscale low at the surface appears to initiate the CTWR, as shown by Skamarock et al. (1998) and as observed by Ralph et al. (1998).

#### **D. ANALYSIS OF THE 1996 CASES**

##### **1. 21-24 July 1996 Case**

The examination of this case begins at 1200 UTC 18 July (-72) due to the anomalous synoptic conditions preceding the period of interest. The evolution of the synoptic-scale pattern for this case differs substantially from that of Mass and Bond (1996) as illustrated in Figure 2.3. In this case, the key feature at 500 mb is the development of a thermal ridge over the western U.S., instead of the eastern North Pacific as in the Mass and Bond (1996) composites. At 500 mb, a migratory closed low is the

vicinity of Vancouver Island with a deep trough extending south along the entire U.S. west coast (Figure 2.3). Over the next 24 hours, this system drifts slowly to the east-northeast as a ridge builds over the eastern North Pacific (west of the domain). By 19/1200 UTC (-48), a 500 mb trough exists over the U.S. west coast. This trough has greater amplitude than in the climatological study by Mass and Bond (1996), which had a much more zonal 500 mb flow over the analysis domain. At -48 hours, the Mass and Bond composite (Figure 2.1) has only a weak trough extending southwestward from Nevada across extreme southern California and a weak ridge over the eastern North Pacific Ocean. Over the next 24 hours, the 500 mb trough over the U.S. west coast weakens as a ridge builds from the south and east over the western U.S. An analysis of the 500 mb thermal pattern indicates that this ridge is associated with warming, as indicated by the northward expansion of the 8°C isotherm (heavy dashed line) after 20/1200 UTC. At 20/1200 UTC (-24), the 500 mb pattern is somewhat similar to the Mass and Bond composite with ridging over the eastern Pacific and predominantly zonal flow over the Pacific Northwest. However, Mass and Bond (1996) indicate the presence of a trough over the southwestern U.S. ahead of the ridge over the eastern North Pacific, which acts to amplify the ridge and the subsidence ahead of it over the U.S. west coast. No troughing ahead of the ridge is indicated in this case. The presence of a short-wave trough along the west coast also differs from the climatological study. At 21/0000 UTC (-12) (not shown), the 500 mb ridge reaches the U.S. west coast with a short-wave trough extending from southern Oregon to northern California embedded in the flow. At

21/1200 UTC (00), the amplitude of the 500 mb ridge and the trough ahead of it are much less than indicated in the Mass and Bond composite. The thermal ridge building from the southeast covers a broad area over the eastern Pacific and western U.S., and becomes the dominant synoptic-scale feature in the domain. Associated with the building of the ridge from the southeast, the 500 mb flow over the area of the coastally trapped wind reversal is actually west-southwesterly vice northwesterly as depicted in Mass and Bond (1996). The short-wave trough at 500 mb dampens by the transition time (21/1200 UTC). Similarly, it does not appear that the mid-tropospheric short-wave plays a role in the development of the offshore mesoscale low. Over the next 12 hours, the 500 mb thermal ridge over the western U.S. builds significantly from the southeast with the ridge axis extending southeast to northwest across the U.S. West Coast. The ridge axis is shifted slightly inland over southern Oregon and northern California. By 22/0000 UTC (+12) (not shown), the amplitude of the thermal ridge is much greater in this case, and the ridge axis is farther to the east than the composite pattern of Mass and Bond (1996). At 22/1200 UTC (+24), the pattern remains essentially unchanged, with the 500 mb thermal ridge over the western U.S. remaining the dominant feature, which differs significantly from the climatological study of Mass and Bond (1996).

As Mass and Bond (1996) do not address the 700 mb level in their study, no comparison is possible. Although the evolution of the 700 mb geopotential height pattern essentially reflects the pattern at 500 mb, these analyses (not shown) are examined to determine the thermal structure and how it may relate to the evolution of the synoptic-

scale pattern above and below 700 mb. The significant feature at 700 mb is the development of the thermal ridge over the eastern Pacific and western U.S. The 19/1200 UTC (-48) analysis indicates a 700 mb thermal ridge building from the south and east over the western U.S. and the eastern Pacific. Over the next 48 hours, the trough over the western U.S. becomes flat as the thermal ridge builds northward. The thermal ridge is associated with mid-tropospheric warming. By 21/1200 UTC (00), as the migratory synoptic features are displaced to the north, the thermal ridge has become the dominant synoptic feature over the western U.S. and eastern Pacific. Over the next 24 hours, the thermal ridge remains the dominant synoptic forcing feature as it continues to build in response to further warming of the mid-troposphere over the domain. The evolution of the thermal pattern in the mid-troposphere clearly indicates that the ridge at 500 mb and 700 mb is associated with warming in the mid-troposphere.

Although the 850 mb evolution (Figure 2.3) is somewhat similar to the Mass and Bond composites (Figure 2.1), it differs in several aspects that can be related to the evolution aloft of the thermal structure aloft. In this case, the key features at 850 mb include the ridge over the Pacific Northwest, the development of offshore flow over northern California, increasing temperatures along the California coast, and the westward displacement of the trough across the California coast. At 18/1200 UTC (-72), a 850 mb migratory closed low associated with the deep trough at 500 mb is located just west of Vancouver Island with an associated trough extending south along the U.S. west coast to southern Oregon. A lobe of the eastern Pacific high extends eastward over central



California in a more pronounced way than the Mass and Bond (1996) composite. Over the next 24 hours, the migratory closed low translates to the northeast and its associated trough weakens as the eastern Pacific high begins to build offshore as well as over the western U.S. By 19/0000 UTC (-60) (not shown), weak offshore flow is implied by the height gradient to the south of the 850 mb ridge along the California coast from Point Conception to Crescent City. By 19/1200 UTC (-48), a thermal trough begins to move westward toward the California coast, and the offshore flow persists along the California coast, with the strongest flow located over the San Francisco Bay area. The westward movement of the thermal trough is accompanied by increasing temperatures along the coast and offshore, as shown by the westward displacement of the 16°C isotherm (heavy dashed line) after 19/1200 UTC (-48). This thermal pattern is in agreement with Mass and Bond (1996), which indicates a warm anomaly at 850 mb over this same region (not shown). By 20/1200 UTC (-24), the ridge over the Pacific Northwest builds eastward and southward, and the thermal trough has shifted west and now lies along the California coast. The pattern differs from Mass and Bond (1996) at -24 hours in that the ridge over the Pacific Northwest is stronger and extends farther inland. Although the geopotential height pattern implies substantially weaker offshore geostrophic flow than indicated in the Mass and Bond composite, weak offshore flow along the coast is revealed in the observed winds (not shown). At 21/0000 UTC (-12) (not shown), the pattern is in closer agreement with Mass and Bond (1996). As the thermal trough recedes inland somewhat, the ridge over the Pacific Northwest continues to move north.

The evolution of the 850 mb synoptic pattern (Figure 2.3) over the next 24 hours is similar to the Mass and Bond composite with a pronounced coastal trough and the 850-mb high positioned near 42°N offshore. The axis of the ridge over the Pacific Northwest shifts north as the eastern Pacific high moves to near 47°N, 133°W. As a result, the area of offshore flow expands northward to northern Washington. The thermal trough begins to expand northward along the coast and westward (offshore) as a result of the thermal forcing aloft. By 22/1200 UTC (+24), southerly flow develops east of the inverted trough (or closed low) from Monterey Bay, California to Bodega Bay, California. This coastal inverted trough (or closed low) is missing in the (+24) composite in Mass and Bond (1996).

The surface evolution (Figure 2.3) also differs somewhat from the Mass and Bond composites, particularly over the coastal California region. In this case, the key features at the surface include a ridge over the Pacific Northwest and the westward displacement of the thermal trough across the California coast. At 18/1200 UTC (-72), a migratory closed low that is associated with the deep trough aloft located southwest of Vancouver Island. A surface ridge extends southwest to northeast across the northern California coast into Oregon with a weak thermal trough over southern Nevada. Over the next 24 hours, the migratory low located off Vancouver Island weakens significantly as the eastern Pacific high builds into the Pacific Northwest. At 19/1200 UTC (-48), the pronounced thermal trough over the California coast is much more developed than depicted by Mass and Bond (1996). Similarly, the ridge over the Pacific Northwest is

much stronger for this event as indicated by the inland extension of the 1024 mb isobar (heavy solid line). During the next 24 hours, the thermal trough intensifies over inland California while the ridge strengthens over the Pacific Northwest and extends south to Nevada. At 20/1200 UTC (-24), the pattern closely resembles that of Mass and Bond (1996) except that the ridge over the Pacific Northwest is stronger in this event.

By 21/1200 UTC (00), the thermal trough over the California coast has further intensified. The northwesterly flow along the California coast weakens considerably as the tight pressure gradient between the eastern Pacific high and the thermal trough is pushed offshore at this time, which compares favorably with the Mass and Bond (1996) composite at the time of transition. The only notable difference is that the composite has weaker ridging over the Pacific Northwest. The eastern Pacific high is centered at approximately 47°N, 133°W with the inland ridge axis shifted to the northeast over southwestern British Columbia. As discussed above, this northward shift is found at 850 mb as well, and is forced by the strong thermal ridging aloft. By 22/1200 UTC (+24) a closed low develops off the central California coast as the thermal trough moves offshore. The associated trough extends northward along the entire U.S. west coast. Southerly flow extends north to Point Arena, California and south to buoy 46028. The coastal trough and cyclonic circulation are much more pronounced than that indicated in the Mass and Bond (1996) composite; i.e., the offshore and northern extent of the surface trough is much greater in this case.

In summary, the synoptic evolution for this case differs significantly from that of Mass and Bond (1996). One key difference is that the synoptic-scale conditions 72 hours prior to the initiation of this event are anomalous, with the passage of a deep short-wave trough over the western U.S. Another key difference includes the development of a thermal ridge in the mid-troposphere over the western U.S. The northward and westward warm advection over the western U.S. appears to be responsible for the development of the mid-tropospheric ridge and the troughing in the lower troposphere. With maximum synoptic-scale warming between 850 mb and 700 mb, this should result in rising geopotential heights above and falling geopotential heights below. This is consistent with the geopotential height and temperature patterns observed in this event and explains the close agreement of the 850 mb thermal pattern with the geopotential height patterns above and below this level.

Another key difference in this event as compared to the Mass and Bond composites is the northward expansion over the western U.S. of the thermal trough and the northward movement of the ridge axis over the Pacific Northwest in the lower troposphere. After initiation of the CTWR, the warming continues to expand northward. It should also be noted that the westward advection of warm air across the coast over the region of the CTWR stops once the event is initiated.

The synoptic evolution of this event does resemble that of Mass and Bond (1996) in some aspects, especially in the lower troposphere. Approximately 48 hours prior to the initiation of the CTWR, the eastern Pacific high builds over the Pacific Northwest in the

lower troposphere, which results in an area of offshore flow over northern California. This offshore flow causes a localized westward advection of warm air across the northern and central California coast, and results in the westward expansion of thermal troughing across the coast. Anomalously warm air develops along the California coast as evidenced by the temperature maximum west of Point Reyes (Figure 2.3). This temperature maximum is associated with the development of the lower tropospheric offshore flow, and coincides with the position of the offshore mesoscale low at the surface (as discussed in the following chapter). The connection between the lower tropospheric offshore flow and the development of the temperature maximum is examined further in the next chapter. As discussed above, this temperature maximum coincides with the development of an offshore mesoscale low at 21/1600 UTC. Approximately 20 hours later 22/1200 UTC (+24), a cyclonic circulation is indicated at 850 mb with coastal southerly winds extending to just south of Point Arena.

## **2. 1-4 September 1996 Case**

The September case (Figure 2.4) differs substantially from the Mass and Bond composites, as illustrated by the evolution of the synoptic-scale pattern for this case. The initiation of this CTWR occurs at approximately 01/1800 UTC (as discussed in the following chapter); therefore neither the 0000 UTC nor 1200 UTC analyses provide an exact time match with the Mass and Bond composites. The 1200 UTC analyses are used for this discussion, since these analyses are not affected by daytime heating over land,

which causes a diurnal variation in the geopotential height and thermal structures (as discussed previously). In this case, the key features at 500 mb include the ridge over the eastern North Pacific and the development of a short-wave trough along the northern California coast. At 30/1200 UTC (-54), the 500 mb analysis has a large ridge that dominates the western U.S., while a very strong short-wave trough approaches the Pacific Northwest from the eastern Pacific Ocean. Over the next 24 hours, the short-wave trough weakens as it rides up over the ridge. At 31/1200 UTC (-30), the short-wave trough moves inland over the Pacific Northwest, while the primary trough axis remains off the northern California coast. This pattern is similar to the Mass and Bond (1996) composite for (-24) in that a 500 mb ridge begins to amplify over the eastern Pacific near 135°W-140°W. However, that Mass and Bond (1996) composite does not indicate a short-wave trough along the U.S. west coast as in this case.

Over the next 24 hours, a very interesting evolution occurs over northern California as the primary trough moves east over the Northern Plains states and southern Canada, and the offshore ridge builds to the east. The 01/1200 UTC (-06) analysis has a pronounced short-wave trough along the U.S. west coast from central Oregon to central California. This short-wave trough coincides with an area of relatively warm temperatures as shown by the northward displacement of the 8°C isotherm (heavy dashed line). This thermal pattern suggests that the short-wave trough is warm-core. At this same time, the ridge over the eastern Pacific begins to weaken. The 02/0000 UTC (+06) synoptic-scale pattern (not shown) is similar to that depicted in the Mass and Bond

(1996) composite for (00), except that the features have smaller amplitudes and the short-wave trough over northern California is present just off the coast. By 02/1200 UTC (+18), the short-wave trough weakens substantially. The flow over the northeastern Pacific and Pacific Northwest has become zonal, which suggests an upper-level flow pattern more like the Mass and Bond (1996) composite for (+48). The rapid decay of the upper-level ridge is indicative of a more progressive synoptic-scale flow pattern than is typical for most CTWRs.

The 700 mb analyses (not shown) depict a similar geopotential height pattern to that seen at 500 mb. The most notable aspect at this level is that the thermal structure suggests that the short-wave trough along the northern California coast is a warm-core feature. As for the July case, the 700 mb level is examined to determine the thermal structure and its effects on the synoptic-scale evolution for this case. At 30/1200 UTC (-54), a migratory short-wave trough that is associated with the 500 mb short-wave approaches the Pacific Northwest, and a thermal ridge dominates the western U.S. Over the next 24 hours the migratory short-wave trough weakens as it makes landfall over the Pacific Northwest and the thermal ridge retreats to the southwest. By 31/1200 UTC (-30), another short-wave trough begins to develop along the U.S. west coast in the northwesterly ahead of a 700 mb ridge that is building over the eastern Pacific. Over the next 24 hours, the ridge over the eastern Pacific continues to build to the north. Ahead of this ridge, the short-wave trough along the U.S. west coast deepens with a closed low circulation indicated just offshore of the California/Oregon border. The thermal pattern

has a tongue of relatively warm air extending northward along the coast associated with the deepening short-wave trough. This area of warming can be attributed to subsidence associated with the building ridge over the eastern Pacific. At 01/1200 UTC (-06), the short-wave trough continues to deepen, and coincides with a local temperature maximum off the coast of northern California. Because the geopotential height and thermal patterns coincide, this feature is considered a thermal trough/warm-core low. Over the next 24 hours, a migratory closed low begins moving southeastward toward the Pacific Northwest. By 02/1200 UTC (+18), the thermal trough weakens significantly, as does the 700 mb ridge over the eastern Pacific. However, the thermal pattern remains intact with the local temperature maximum over the California coast.

The 850 mb analyses (Figure 2.4) depict an evolution quite different from the Mass and Bond (1996) composites, and clearly show the development of a cyclonic circulation along the northern California coast. At 30/1200 UTC (-54), the 850 mb analysis has a frontal trough moving into the Pacific Northwest with an enhanced thermal gradient across central Oregon and Washington. At 31/1200 UTC (-30), high pressure develops over the eastern Pacific, and ridging is evident over western Oregon and Washington. The thermal analysis at this time has substantial temperature decreases over Oregon and Washington as the front moves east to the Rocky Mountains in Montana. The 850 mb geopotential height analysis differs from the Mass and Bond (1996) composites in that a pronounced low develops over the northern California coast. This low coincides with thermal ridge (warm air) oriented in the north-south direction over the



same area, and lies between the region of cold advection behind the front and the region of warm advection associated with thermal troughing to the south. This thermal pattern suggests that the low is a warm-core feature. The localized warming along the coast, shown by the northward displacement of the 16°C isotherm (heavy dashed line), appears to be related to the subsidence aloft ahead of the mid-tropospheric ridge rather than warm advection across the coast from offshore flow. Offshore flow does develop over the California/Oregon border at the same time that the thermal trough and cyclonic circulation develop across the northern California coast. This pattern suggests that the offshore flow is initially the result of the development of the thermal trough across the coast rather than ridging over the Pacific Northwest as shown in the Mass and Bond (1996) composites. A weak ridge develops over central California, possibly in response to onshore flow south of the trough. At 01/1200 UTC (-06), the trough along the U.S. west coast expands to the north and west, and a closed low develops offshore between Point Arena and Cape Mendocino, California. Onshore flow is evident from the San Francisco Bay area to Point Conception. The presence of a closed low at 850 mb is not indicated in the Mass and Bond (1996) composites, and the trough over the California coast is deeper and extends farther west than indicated in the climatological study.

Over the next 24 hours, the offshore low moves slightly northward along the coast. The high pressure over the Pacific Northwest weakens as a migratory low-pressure system approaches from the Gulf of Alaska. As a result, the geostrophic offshore flow pattern weakens considerably. At 02/1200 UTC (+18), the trough along the California

coast persists. At this time, the ridging over the Pacific Northwest is weaker than indicated in the Mass and Bond (1996) composite for (+12), but the troughing along the coast is more defined. Over the next 24 hours, the trough over the California coast weakens, and the offshore flow pattern breaks down.

At the surface (Figure 2.4), the evolution of this case is very similar to the Mass and Bond (1996) composites as the ridge builds over the Pacific Northwest and a pronounced coastal trough/low develops along the northern California coast. The 30/1200 UTC (-54) analysis has a frontal trough approaching the coasts of Oregon and Washington as a ridge builds to the northeast across northern California and Oregon. The thermal trough is confined to the central and southern California coastal regions, and northerly flow persists along the California coast. Over the next 24 hours, the frontal trough moves across the Pacific Northwest and weakens as high pressure develops offshore and over the Pacific Northwest. The 31/1200 UTC (-30) analysis shows that the thermal trough has expanded to the north and west to cover the entire California coast. Northerly flow continues to persist along the California coast. At 01/1200 UTC (-06), a closed low develops in the thermal trough just offshore of Point Arena, California. The northerly flow pattern along the California coast weakens considerably with a weak onshore component evident from south of the low to San Francisco Bay. At 02/0000 UTC (+06) (not shown), troughing is evident over the northern California coast. The southerly wind and pressure minimum at buoy 46014 indicates the possible presence of an offshore mesoscale low not depicted by the eta model analysis. Onshore flow

develops south of the coastal low from Buoy 46013 to Monterey Bay and results in the development of a weak ridge from Point Conception to San Francisco Bay. This synoptic pattern for the approximate time of initiation agrees well with the Mass and Bond (1996) composite, except for the presence of the weak ridging along the central California coast. At 02/1200 UTC (+18), a closed low is analyzed west of Point Arena. Southerly flow is established from Buoy 46013 to Point Arena, California. As the next migratory low pressure system begins to approach the Pacific Northwest from the Gulf of Alaska, onshore ridging from the eastern Pacific high. At 03/0000 UTC (+30) (not shown), the coastal trough shifts to the south and expands to the southwest with a weak ridge to the east. The Mass and Bond (1996) composite completely misses this feature. Southerly flow is evident along the coast from buoy 46028 to Cape Mendocino.

In summary, the synoptic-scale evolution of this case is different from that of the July event and the Mass and Bond (1996) composites. Specifically, this case differs from the Mass and Bond (1996) composites in that the event begins after the passage of a deep migratory short-wave trough. In this case, a thermal trough/warm-core low develops through a deep layer of the atmosphere, and the event breaks down with the approach of another deep migratory trough. Also, it should be noted that the 500 mb ridge never reaches the California coast. This case also lacks a strong thermal ridge over the western U.S. as in the July case.

This case differs from the July case in that the thermal forcing (warming) results in the development of a short-wave trough in the mid-troposphere. This warming is

attributed to subsidence in the flow ahead of the building ridge over the eastern Pacific in the mid-troposphere. Although the synoptic-scale trough at 500 mb and 700 mb is flat at 31/0000 UTC (-42) (not shown), weak perturbations are present in the flow. At 31/1200 UTC, a thermal trough develops along the California coast at 850 mb, and by 01/1200 UTC a closed low indicated. Analysis of the thermal structure at 500 mb, 700 mb and 850 mb suggests that these features are thermally forced and warm-core. The warming at 850 mb is confined to the coast and does not extend significantly offshore as in the July case. Offshore flow does not develop at 850 mb until after the thermal trough is across the California coast. These two facts suggest that subsidence warming from the ridge aloft, and not warm advection in the lower troposphere, are responsible for the development of the thermal trough. The surface low does not develop until approximately 30 hours after the 850 mb trough and offshore flow. The exact mechanism for the development of the offshore mesoscale low is addressed in Chapter III.

### **3. 4-7 June 1996 Case**

Figure 2.5 is an illustration of the evolution of the synoptic-scale pattern for this event, which differs substantially from the previous cases as well as the Mass and Bond (1996) composites. As the 04/1200 UTC eta model analysis was not available, the 04/0000 UTC analysis will be used to set the synoptic-scale pattern preceding the onset of southerly flow in the lower troposphere along the southern California Bight region. The 500 mb analysis at 04/0000 UTC has a long-wave ridge that extends northward from the southwestern U.S. to eastern British Columbia. A migratory closed low is northwest

of Vancouver Island. Southwesterly flow prevails over the eastern Pacific and the Pacific Northwest. Over the next 36 hours, the long-wave ridge decreases in amplitude, which results in zonal (westerly) flow across the eastern Pacific and western U.S. The migratory closed low weakens and moves over the ridge in Canada. The 500 mb analysis at 05/1200 UTC has a developing transient ridge over the eastern Pacific just offshore of the U.S. west coast. Unlike the scenario depicted by Bond and Mass (1996), this ridge does not remain stationary off the west coast, but propagates to the east over the U.S. as a deep trough moves towards the coast. In the 06/1200 UTC analysis, the transient ridge has moved inland and now extends north from southern Nevada to western Canada. Over the next 24 hours, the ridge continues to drift eastward, as a trough approaches the Pacific Northwest from the Gulf of Alaska as seen in the 07/1200 UTC analysis.

The 700 mb analyses (Figure 2.5) depict geopotential height and thermal structures that differ significantly from the previous cases. The key feature at this level is the development of a thermal ridge over the western U.S., which is favorable for the development of a CTWR. Unlike the July case, this feature is moved to the east as a deep trough approaches the Pacific Northwest. At 04/0000 UTC, a 700 mb ridge is over the western U.S. and a trough approaches the Pacific Northwest from the Gulf of Alaska. The isotherm pattern suggests that the ridge is thermally forced (Figure 2.6b). Over the next 36 hours, the thermal ridge weakens as cooler air is advected over the western U.S. associated with the approach of a migratory trough. By 05/1200 UTC, the thermal ridge begins to build from the south over the eastern Pacific as the atmosphere warms over this

region. Over the next 24 hours, the thermal ridge moves to the east over the western U.S., and the atmosphere continues to warm. The geopotential height and thermal patterns at 06/1200 UTC resemble those of the July case (see Figure 2.3), and appear to be favorable for development of a CTWR. However, the thermal ridge over the next 24 hours continues to move east over the Northern Plains states as a deep trough approaches the Pacific Northwest.

The 850 mb analyses (Figure 2.5) show an evolution similar to the Mass and Bond (1996) composites, except the features in this case are weaker and less persistent. The 850 mb analysis at 04/0000 UTC has a closed low located northwest of Vancouver Island with an associated trough extending south-southeast along the Washington and Oregon coasts. A weak ridge from the eastern Pacific high extends to the northeast over central Oregon. Another closed low is west of the California Bight with an inverted trough that extends north along the central California coast. Over the next 24 hours, the eastern Pacific high builds over the northeast Pacific and the Pacific Northwest. By 05/0000 UTC (not shown), a weak thermal trough lies over coastal California, which is typical of the synoptic evolution associated with a coastally trapped wind reversal. As shown by the 05/1200 UTC analysis, the thermal trough then recedes inland as the eastern Pacific high pushes toward the California coast, and only a weak offshore flow pattern develops over northern California and southern Oregon.

Over the next 24 hours, the 850 mb ridge over the Pacific Northwest pinches off from the eastern Pacific high and propagates to the east as a closed low moves toward the

Pacific Northwest from the Gulf of Alaska, as seen in the 06/1200 UTC analysis. As a consequence of this eastward movement of the high over the Pacific Northwest, easterly flow over northern California is replaced by northerly flow, and the thermal trough recedes farther inland over northern and central California. This synoptic-scale pattern differs significantly from Mass and Bond (1996), since the ridge over the Pacific Northwest is weak and is never established for an extended period of time. Over the next 24 hours, the high over the Pacific Northwest moves much farther east and the thermal trough is located well inland over the interior western U.S.

The surface analyses (Figure 2.5) depict a synoptic evolution similar to other coastally trapped wind reversal events, except the features in this event are less persistent. At 04/0000 UTC, the eastern Pacific high is along the Oregon and Washington coasts, and a migratory low pressure system is west of Vancouver Island. Over the next 36 hours, the ridge builds over the Pacific Northwest and the thermal trough begins to expand toward the California coast. By 05/1200 UTC, the center of the eastern Pacific high begins to move to the northeast, and the thermal trough has expanded farther west over coastal California. Over the next 24 hours, the center of the high continues to move east. At 06/1200 UTC, the thermal trough persists over the California coast. This evolution differs from the typical synoptic evolution in Mass and Bond (1996), who suggest westward movement of the thermal trough offshore. By this time, a migratory low-pressure system is moving southeast out of the Gulf of Alaska toward the Pacific Northwest. At 07/1200 UTC, the thermal trough has receded inland. Northwestern flow

remains well established through the entire period along the California coast, except over the southern California Bight region.

Synoptic-scale conditions required for the development of a CTWR along the central California coast do develop for a brief period on 5 June. However, the synoptic-scale features develop farther north than is typical for a CTWR and are more transient in nature. At 500 mb and 700 mb, the ridge does not remain stationary off the U.S. west coast as seen in the prior two cases and indicated by Mass and Bond (1996). At 850 mb, the ridge over the Pacific Northwest is not of sufficient strength and does not remain over that area long enough for a strong offshore flow pattern to develop. The short-lived nature of the offshore flow pattern results in little or no warm advection toward the coast and little or no lee troughing along the coast. The lack of a strong offshore flow pattern and coastward warm advection impede the establishment of a coastal thermal trough and development of an offshore mesoscale low, which appear to be the key to the development of coastal southerlies. In this case, weak southerly flow develops along the central California coast only at 950 mb for a period of approximately 24 hours. However, the surface winds do not reverse except near Point Conception and the southern California Bight region. Consequently, this event does not appear to be a well-defined CTWR. These marginal cases are helpful in indicating both the necessary and sufficient conditions for the cases in which a CTWR does develop.



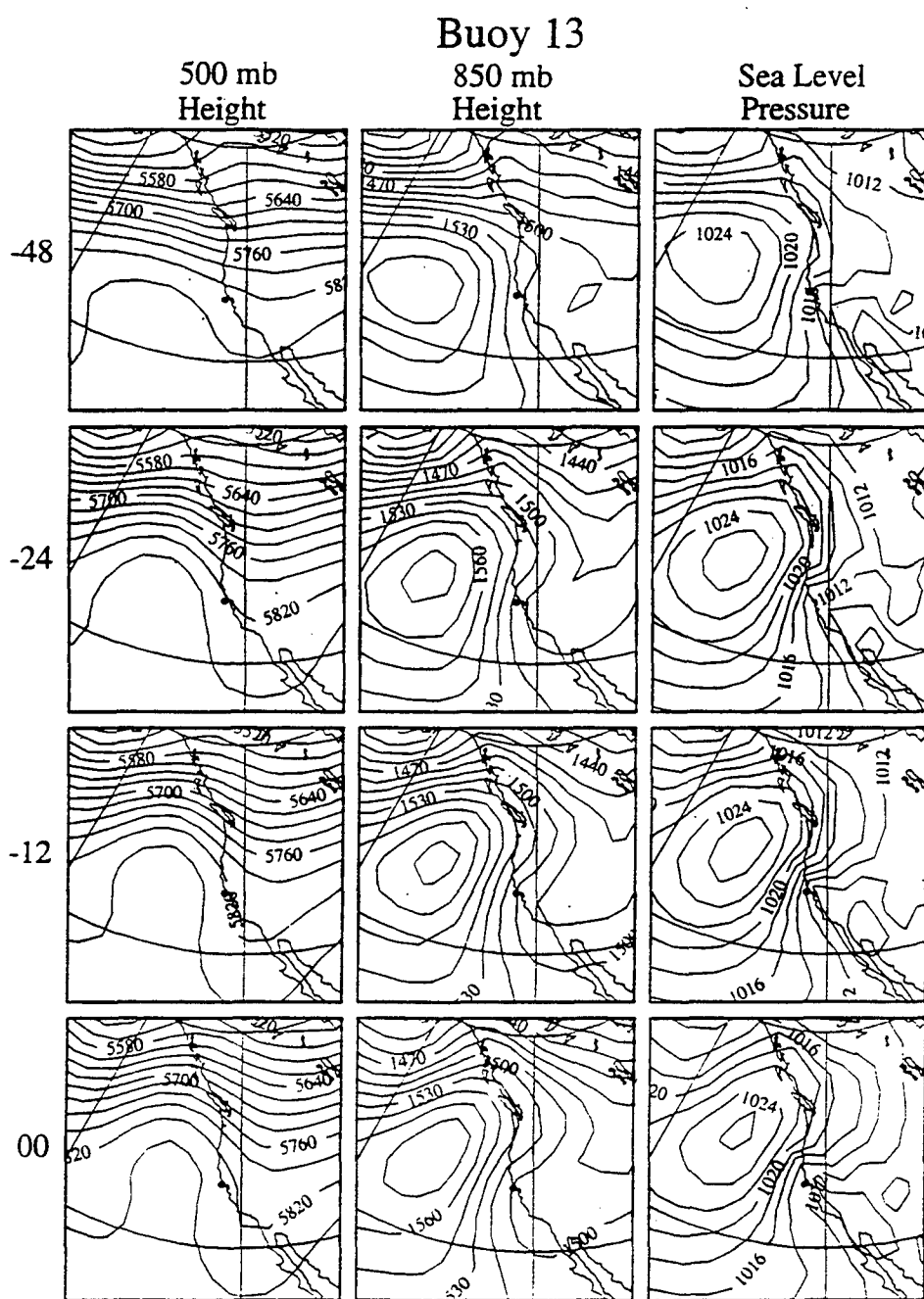


**Figure 2.1.** The evolution of the composite fields of 500 mb geopotential height, 850 mb geopotential height, and sea-level pressure for 2 days prior to 2 days after strong coastally trapped wind reversals at buoy 46013. Contour intervals are 30 gpm for 500-mb, 15 gpm for 850-mb, and 2 mb for sea level pressure. The location of buoy 46013 is indicated by the black dot (from Mass and Bond 1996).

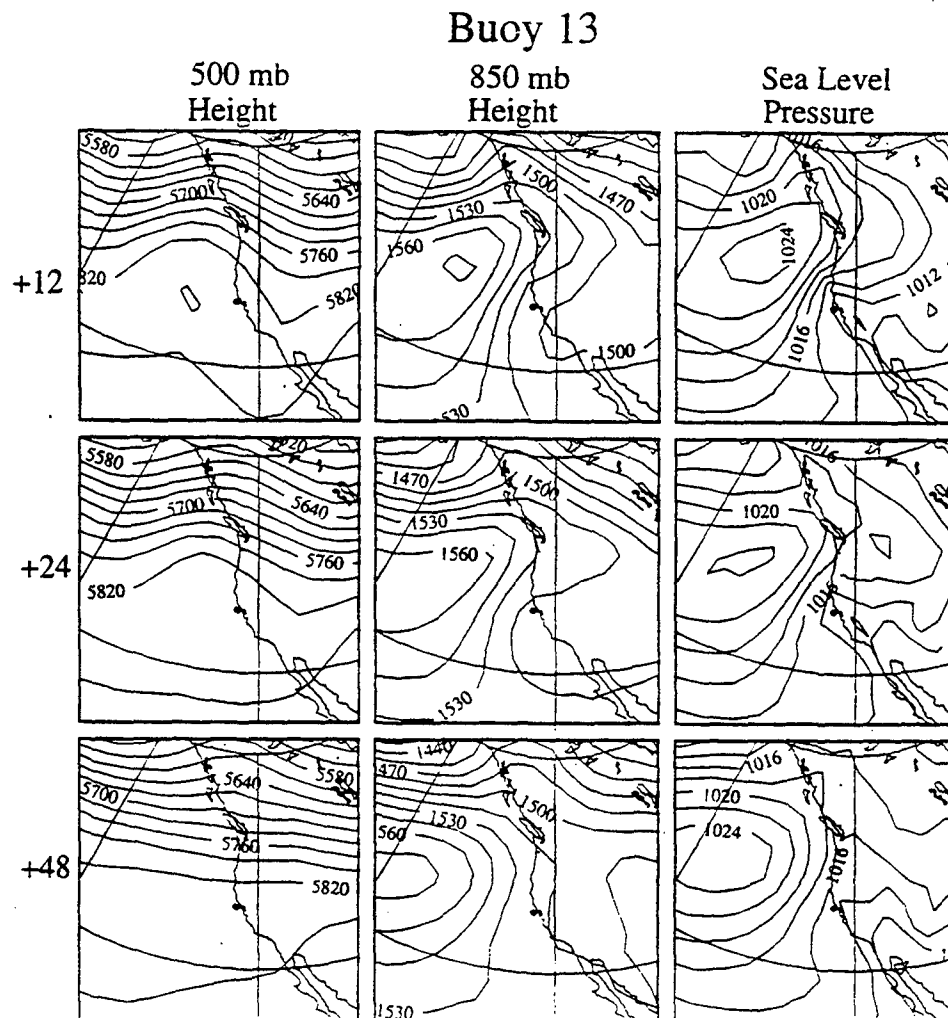
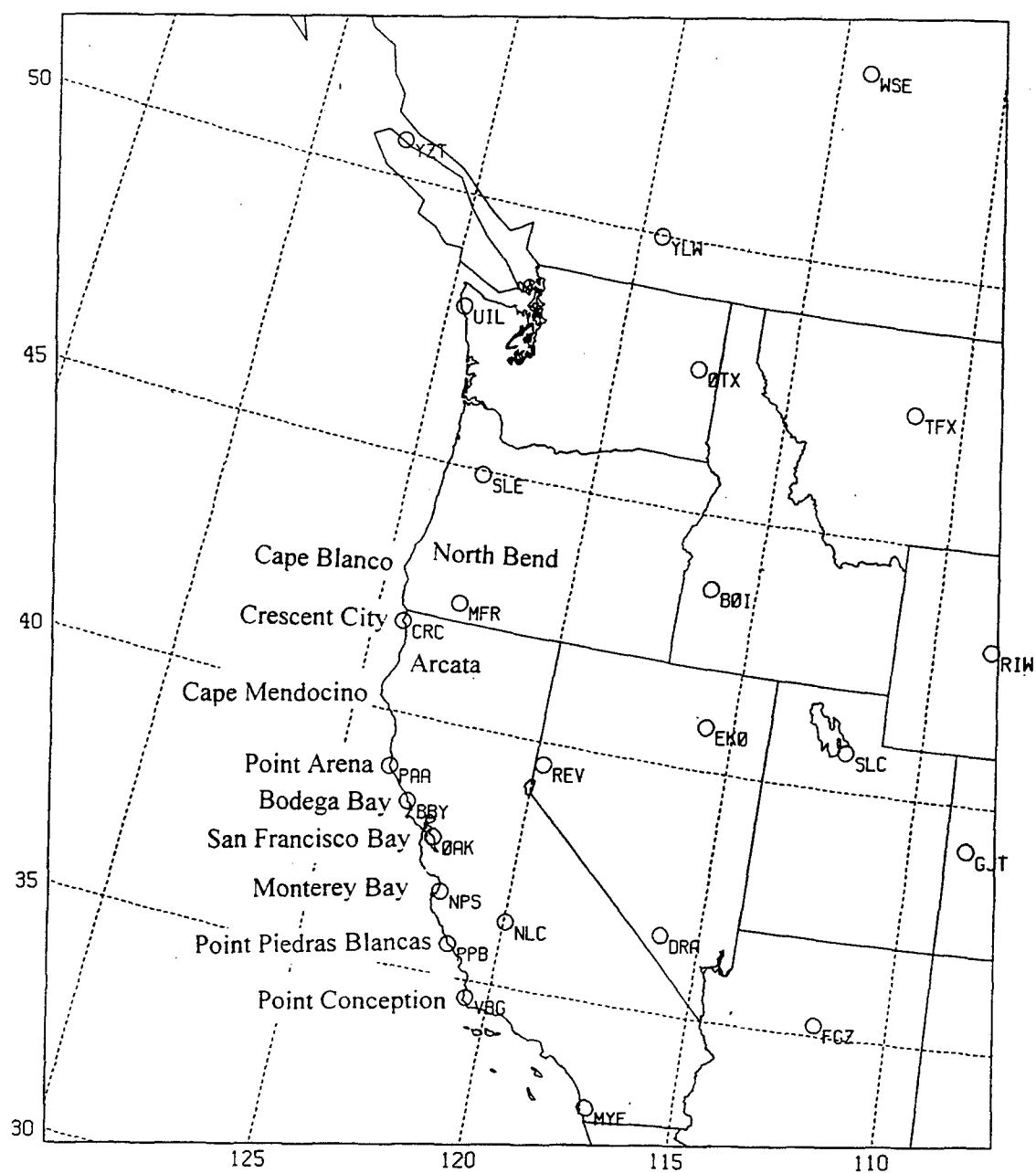
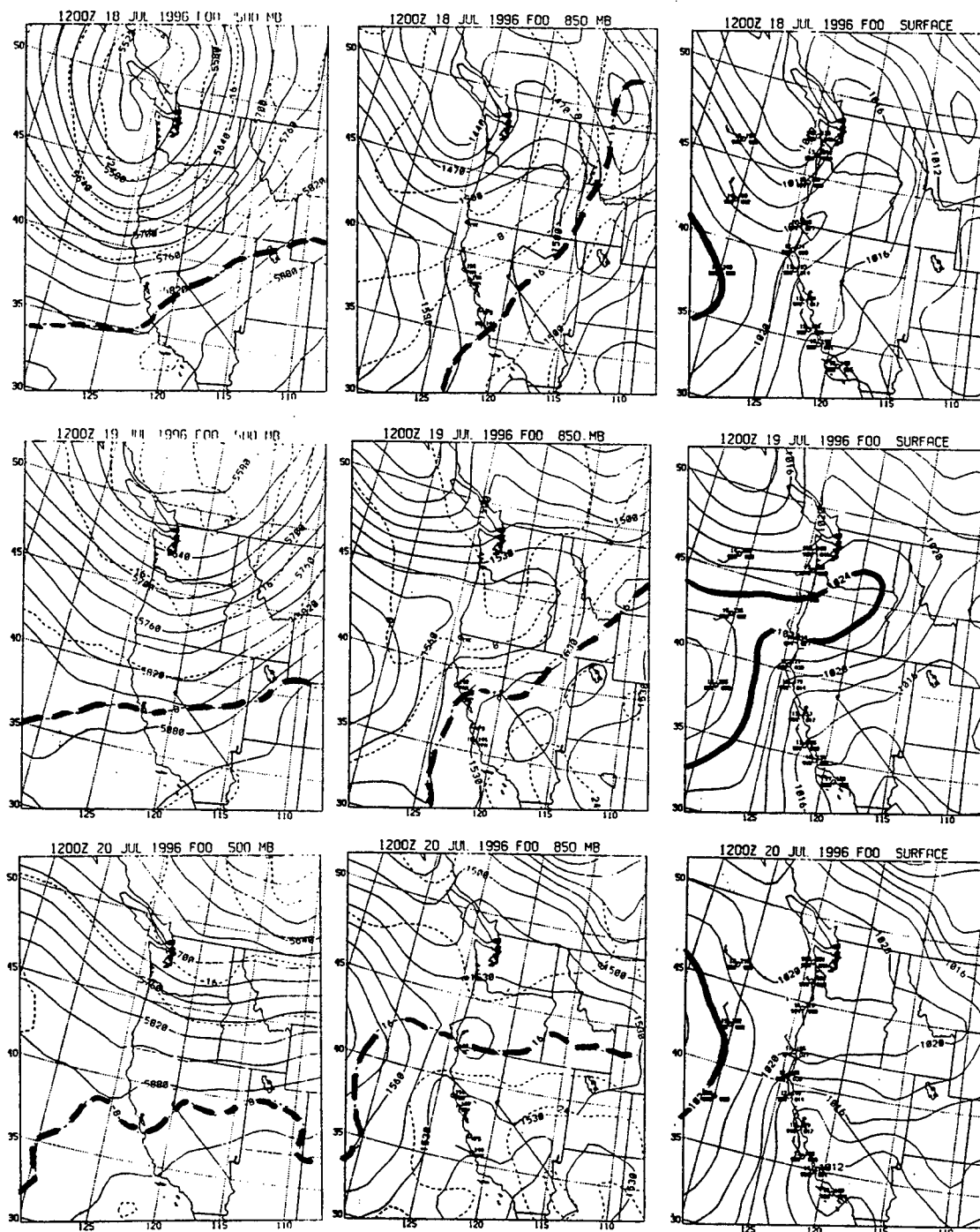


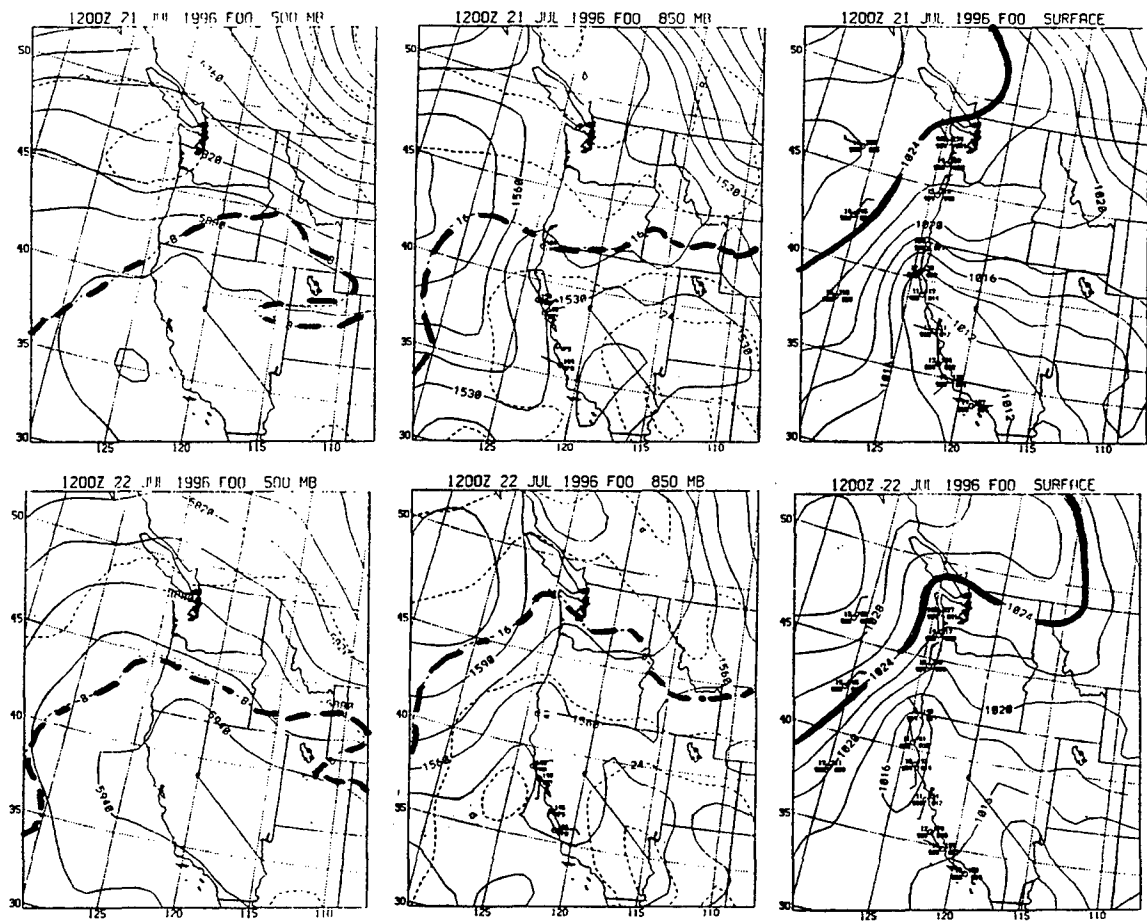
Figure 2.1. (cont.)



**Figure 2.2.** Domain for the Eta model analyses used in analyzing the evolution of the synoptic-scale pattern. The domain covers an area from 51.5°N, 137°W to 55°N, 110°W and 30°N, 130°W to 32.5°N, 108°W. Selected upper air reporting stations, wind profiler sites, moored buoy positions, and geographical landmarks are denoted.



**Figure 2.3.** Eta model analyses for the July 1996 case for 500 mb, 850 mb, and the surface. The 500 mb charts depict geopotential height and temperature with contour intervals of 30 gpm and 4°C, respectively. The 850 mb charts depict geopotential height and temperature with contour intervals of 15 gpm and 4°C, respectively. The surface charts depict sea-level pressure with a contour interval of 2 mb.



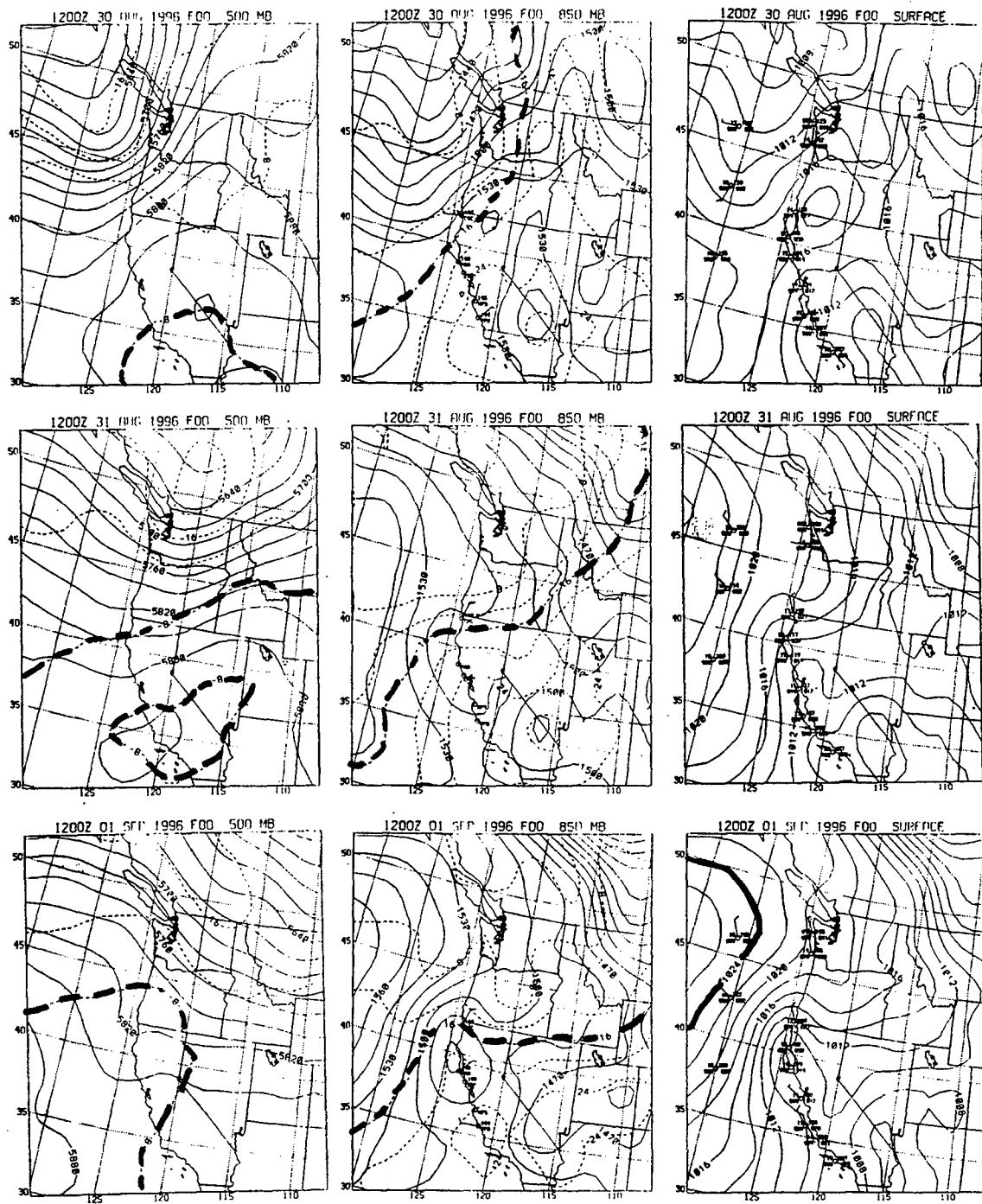


**Figure 2.4.** Eta model analyses for the September 1996 case for 500 mb, 850 mb, and the surface. The 500 mb charts depict geopotential height and temperature with contour intervals of 30 gpm and 4°C, respectively. The 850 mb charts depict geopotential height and temperature with contour intervals of 15 gpm and 4°C, respectively. The surface charts depict sea-level pressure with a contour interval of 2 mb.

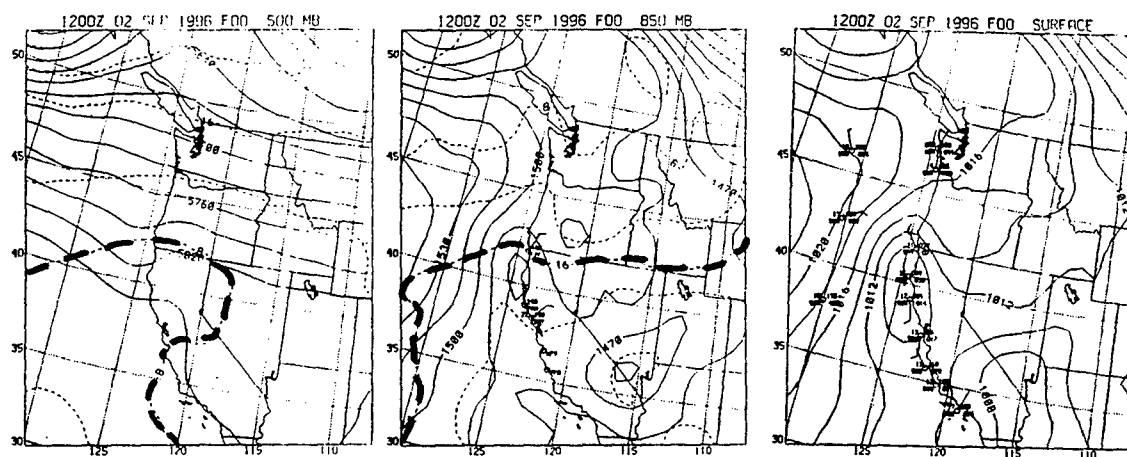
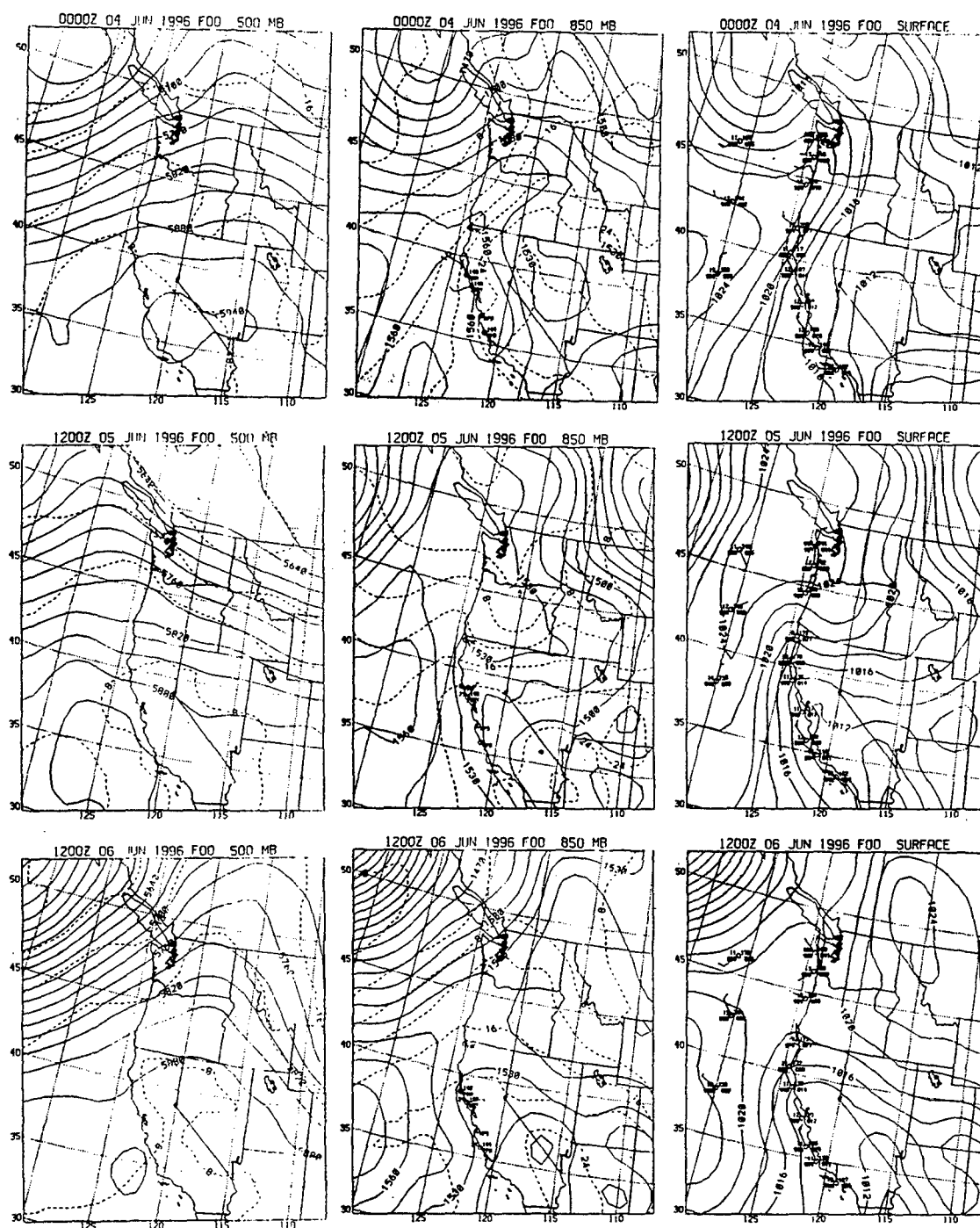


Figure 2.4 (cont.)



**Figure 2.5.** Eta model analyses for the June 1996 case for 500 mb, 850 mb, and the surface. The 500 mb charts depict geopotential height and temperature with contour intervals of 30 gpm and 4°C, respectively. The 850 mb charts depict geopotential height and temperature with contour intervals of 15 gpm and 4°C, respectively. The surface charts depict sea-level pressure with a contour interval of 2 mb.



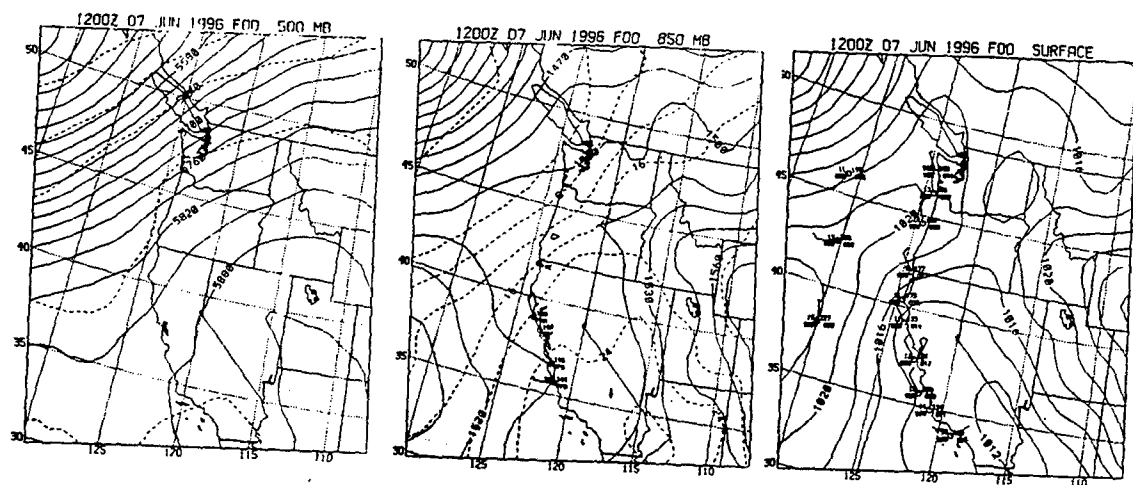


Figure 2.5 (cont.)

### III. MESOSCALE STRUCTURE

#### A. BACKGROUND

Skamarock et al. (1998) examine the role of offshore flow at 850 mb in the development of a CTWR. An offshore flow of  $-6$  m/s is superposed on a coastal domain at 850 mb for 3 days. In these simulations, the coastline is straight and the idealized topography has a general rise from the coast to the Sierra Nevada with no coastal mountain range. A summary of the evolution of a CTWR based on these simulations is illustrated in Figures 3.1 and 3.2. The two-dimensional simulations show the offshore displacement of the marine layer and the coastal northerly jet when offshore flow is imposed (Skamarock et al. 1998). Other features of the two-dimensional simulations include the relaxation of the pressure gradient along the coast, the formation of an area of low pressure along the coast, and the appearance of southerly flow along the coast (Skamarock et al. 1998) (Figure 3.2). These features are amplified by increasing the stratification above the marine layer or increasing the height of the coastal topography in three-dimensional simulations (Skamarock et al. 1998).

The simulations using the three-dimensional non-hydrostatic model show that the imposed offshore flow weakens the prevailing northerly flow along the coast and lowers the pressure near the coast. The flow around the developing area of low pressure approaches geostrophic balance. The onshore flow at the southern end of the low encounters the coastal range and subsequently deepens the marine layer in this region. The elevated marine layer begins propagating poleward parallel to the coast as a Kelvin

wave and may later steepen into an internal bore or gravity current. The three-dimensional simulations also indicate deep southerly flow along the coast. Strong stability above the marine layer can result in topographically trapped Rossby waves and stronger southerly winds associated with the CTWRs (Skamarock et al. 1998). The CTWRs in these simulations are interpreted by Skamarock et al. (1998) as being freely propagating once they are initiated by the localized deepening of the marine layer that results from onshore flow south of the coastal low, which is produced by the lower tropospheric offshore flow. This interpretation is based on the fact that the region of localized deepening of the marine layer does not propagate.

## **B. METHOD OF ANALYSIS**

To analyze the surface evolution in more detail for each case, hourly hand-drawn analyses of sea-level pressure were prepared for a domain roughly covering California, Oregon, Nevada, and the eastern Pacific Ocean extending a few hundred kilometers offshore. Key features include the relaxation of the cross-coast pressure gradient, a coastal trough and offshore mesoscale low, reversal of the along-coast pressure gradient, and a coastal mesoscale ridge that roughly coincides with the southerly winds, stratus, and marine layer along the coast. Data sources for these analyses include land surface observations, moored and drifting buoy observations, and ship observations. Figure 3.3 illustrates the domain for the hand-drawn analyses as well as the locations of the moored

buoy and the wind profiler sites. The hand-drawn analyses were checked against the eta model analyses of sea-level pressure and each other to ensure time continuity.

Along-coast vertical cross sections depicting temperature and the cross-coast wind component were created from the eta model analyses to examine the strength and the extent of offshore flow in the area of development of the CTWR. The cross sections extend parallel to the coast from approximately 40°N, 125°W (west of Cape Mendocino) to just west of Monterey Bay as shown in Figure 3.3. The cross sections are for a layer from the surface to 700 mb to allow for the analysis of the synoptic-scale offshore flow along the coast, which has been suggested by Mass and Bond (1996) and Nuss (1998) as an important factor in the development of CTWRs. As in the previous chapter, the 1200 UTC cross sections are chosen to describe the along-coast evolution to minimize diurnal effects.

Visible and infrared satellite imagery from the National Oceanic and Atmospheric Administration (NOAA) polar-orbiting satellites (NOAA-12 and NOAA-14) and a NOAA geostationary satellite (GOES-9) with resolutions of 1.1 km and 4 km, respectively, were analyzed as part of the present study. A multi-channel algorithm from Dykes (1991) was used on the nighttime passes of the polar-orbiting satellites to enhance infrared imagery for better detection of stratus clouds along the California coast. The satellite imagery is used to compare the extent of the signature "tongue of stratus" associated with many CTWRs with the location of the southerly wind transition and the

coastal mesoscale ridge at the surface and as a data source for preparing the hand-drawn mesoscale surface analyses.

Time series of wind and virtual temperature are available from 915 MHZ wind profilers with the Radio Acoustic Sounding System (RASS) at Point Piedras Blancas (PPB), Monterey Bay (FTO), Bodega Bay (BBY), Point Arena (PAA), and Crescent City (CRC) along the California coast. The wind data are analyzed to determine the horizontal and vertical extent, as well as the duration, of the lower tropospheric offshore flow and coastal southerly flow during the CTWR. The height of the base of the lower tropospheric inversion is estimated for each profiler site using the virtual temperature data. The base of the lower tropospheric inversion capping the marine layer was found to be where the virtual temperature begins increasing with height in a layer in which the vertical temperature gradient strengthens significantly. These data are used to construct a time series of marine layer depth for each profiler site and to create three-hourly along-coast profiles of marine layer depth.

Time series for each coastal moored buoy and three-hourly along-coast profiles of sea-level pressure data are constructed. Time series and along-coast profiles of MBL depth and sea-level pressure were compared. Specifically, the reversal in the along-coast sea-level pressure gradient should correspond to a reversal in the along-coast gradient in MBL depth. Past studies have suggested that the reversal of these along-coast gradients is the key to the development of ageostrophic southerly winds along the coast. These profiles are also examined for their correlation with the expansion of the thermal trough

across the coast, the formation of the offshore mesoscale low and coastal mesoscale ridge, and the propagation of these features along the coast.

## **C. SURFACE EVOLUTION**

### **1. 21-24 July 1996 Case**

The hand-drawn analyses of sea-level pressure (Figure 3.4) were used to examine the initiation and propagation of this case. Figure 3.5 contains polar-orbiting satellite imagery (1.1 km resolution) for various times during this event, and illustrates the development and propagation of the coastal stratus. The initiation of this CTWR occurs at approximately 21/1500 UTC. The offshore displacement of an area of low sea-level pressure characterizes the evolution of this event prior to this time. As noted in the synoptic discussion, the eastern Pacific high builds eastward over the Pacific Northwest, and results in weak offshore flow at 850 mb along the northern and central California coast by 19/1200 UTC. Subsequently, temperatures begin to increase offshore and the thermal trough moves west over the California coast at 850 mb. The 21/0000 UTC surface analysis has a thermal trough over the Central Valley of California, which is typical of the climatological summertime conditions. Although the pressure gradient is somewhat relaxed along the California coast south of Point Arena, the pressure gradient remains tight along the northern California coast north of Point Arena, and northwesterly flow is evident in the buoy observations along the California coast from the Oregon border to Point Piedras Blancas. A noticeable depression in sea-level pressure develops

along the coast from roughly Point Arena to Monterey Bay by 21/0600 UTC as shown in Figure 3.4 as the pressure gradient and winds along the northern and central California coast weaken considerably. The relaxed pressure gradient and winds along the coast suggest that the coastal jet has been displaced offshore.

The wind observations from buoy 46026 near San Francisco Bay are the first indications of the developing trough along the coast as the wind turns onshore with a west wind of less than 5 kt reported at 21/0700 UTC. Whereas the wind at buoy 46026 then develops a southerly component by 21/0800 UTC, the wind direction varies until it becomes southerly at 21/1100 UTC. The onshore and southerly winds at buoy 46026 occur to the south of the developing offshore mesoscale low, which is similar to the simulations by Skamarock et al. (1998). The wind at buoy 46012 does not develop a southerly component until 21/1500 UTC, when the CTWR is fully initiated. The sea-level pressure at buoy 46026 is the lowest along the California coast at this time with the exception of a 0.1 mb lower pressure at buoy 46012, which is typical throughout the event and suggests a low bias. The wind and pressure data indicate that the trough is centered in the area near buoy 46026 at 21/1500 UTC, although by 21/1200 UTC the trough is located farther north near Point Reyes. Winds at the southern edge of the trough develop a stronger onshore component as evidenced by the 21/1200 UTC wind report for buoy 46012. Over the next 3 hours, the trough continues to expand and also extend farther offshore and to the south, and by 21/1500 UTC a narrow ridge begins building onshore over Monterey Bay to the south of the offshore trough. This ridge represents an

area of marine air building up against the coast in response to onshore flow. At this same time, the wind at buoy 46012 develops a more persistent southerly component, which strongly suggests the initiation of this event at 21/1500 UTC. At 21/1600 UTC, satellite imagery (not shown) reveals a tongue of coastal stratus forming in the vicinity of Point Reyes and a cyclonic eddy evident in the stratus just west of Point Reyes.

The next 48 hours (next nine analyses in Figure 3.4) represent the period during which the CTWR propagates poleward along the coast. During this period, the synoptic-scale ridge over the Pacific Northwest and the area of offshore flow in the lower troposphere shift northward (Figure 2.3). As a result, the pressure gradient and winds near the coast weaken farther north along the U.S. west coast. The ensuing surface evolution is very similar to that found by Skamarock et al. (1998), although the propagation is not uniform over the entire period. The 21/1800 UTC analysis in Figure 3.4 has an offshore mesoscale low east of buoy 46012 and a coastal mesoscale ridge that extends from Point Sur to Point Reyes. After a brief period of stalling, the coastal mesoscale ridge propagates north during next 9 hours, and reaches buoy 46014 (Point Arena) by 22/0300 UTC. Satellite imagery for 21/2108 UTC (Figure 3.5) continues to indicate the cyclonic eddy west of Point Reyes and the northward progression of the coastal stratus. The 22/0000 UTC analysis has the head of the coastal mesoscale ridge north of buoy 46013 with weak southerly flow at buoys 46012 and 46013. At this same time, the coastal trough is confined to a small area that extends from the head of the coastal ridge to just north of Point Arena. During this period, the offshore mesoscale low



drifts to the southwest as the trough continues to elongate to the south, and the localized coastal trough across the coast begins to propagate northward, as revealed in the falling sea-level pressure at buoy 46014. This northward propagation occurs as the axis of the synoptic-scale ridge over the Pacific Northwest shifts to the north. The southerly flow under the coastal ridge remains light at 5 knots or less. The offshore mesoscale low drifts slightly to the west and is located west of Monterey Bay at 22/0600 UTC. The localized coastal trough ahead of the coastal mesoscale ridge moves northward between 22/0300 UTC and 22/0600 UTC and is located just south of Cape Mendocino on the 22/0600 UTC analysis. At 22/0300 UTC, the offshore trough and mesoscale low begin to slowly fill, which relaxes the pressure gradient to its west. The sea-level pressure rises significantly under the coastal mesoscale ridge during this period. When the propagation of the coastal ridge stalls between 22/0300 UTC and 22/0600 UTC, the coastal ridge and southerly transition are at Point Arena.

During the next 8 hours, the mesoscale structure changes very little along the coast, as seen by comparing the 22/0600 UTC and 22/1200 UTC analyses in Figure 3.4. No progression of the coastal stratus is evident in Figure 3.5 between 21/2108 UTC and 22/1111 UTC. The wind reversal reaches buoy 46030 (Cape Mendocino) by 22/1400 UTC, and the 22/1500 UTC analysis in Figure 3.4 shows the transition to southerly flow and the coastal mesoscale ridge located just north of Cape Mendocino. The coastal ridge and southerly transition propagate northward along the coast during this period, and reach the California/Oregon border by 22/1600 UTC, Cape Blanco by 23/0000 UTC, and North

Bend, Oregon by 23/12000 UTC, which is its northernmost extent. The coastal stratus nearly coincides with the coastal mesoscale ridge and southerly transition as shown in the 22/1620 UTC image in Figure 3.5. The southerly flow under the coastal ridge remains light (ranging from less than 5 knots to 10 knots), and the highest sea-level pressure is located at the southern edges of the coastal ridge in the area of onshore flow during most of this period. The offshore mesoscale low near Monterey Bay continues to fill during this period, and after 23/0000 UTC the offshore low begins to propagate northward. After 23/1100 UTC, this CTWR rapidly decays over a period of 12-18 hours.

The evolution of this case is very similar to the conceptual model from Skamarock et al. (1998). Many aspects of the evolution shown in Figures 3.1 and 3.2 are observed at the surface in this case, including the relaxation of the pressure gradient near the coast, the development of a surface depression, and the offshore displacement of the coastal jet. Subsequently, onshore flow develops south of the coastal depression, and thus leads to the development of a mesoscale ridge and southerly winds along the coast, and finally the offshore mesoscale low.

In this case, the timing of the initial mesoscale response at the surface to the 850 mb offshore flow is much slower than in the Skamarock et al. (1998) model. The surface depression begins to develop approximately 48 hours after the onset on offshore at 850 mb instead of 24 hours after as in Skamarock et al. (1998). This case also differs from the Skamarock et al. (1998) model in that the dynamic forcing (850 mb offshore flow) and, thus the thermal trough, shift poleward along the coast as the synoptic-scale ridge

over the Pacific Northwest shifts northward instead of remaining stationary (see Figure 2.3). The poleward shift of the synoptic forcing relaxes the pressure gradient along the coast farther north and allows the CTWR to propagate well north of the original area of forcing, which suggests that the evolution of the synoptic forcing is at least partially contributes to the propagation characteristics of this CTWR.

## **2. 1-4 September 1996 Case**

Hand-drawn analyses of sea-level pressure depicting the initiation, propagation, and decay of this CTWR (Figure 3.6) depict an evolution similar to the previous case. The most notable differences are its less uniform propagation and a more southward point of maximum propagation. Figure 3.7 contains selected imagery (1.1 km resolution) from polar-orbiting satellites.

As discussed in the previous chapter, offshore flow at 850 mb develops by 1200 UTC 31 August (Figure 2.4). The surface analysis for 0000 UTC 1 September depicts the typical precursor structure with a thermal trough over the Central Valley of California and a lobe of the eastern Pacific high over the Pacific Northwest. Northwestern flow prevails along the California coast from the Oregon border to Point Conception at this initial time. Over the next 6 hours, as the thermal trough expands westward across the California coast, and the pressure gradient along the California coast weakens from Point Arena to San Francisco Bay. The westward expansion of the thermal trough is evident by the noticeable depression in sea-level pressure along the coast between Point Arena and Point Reyes in the 01/0600 UTC analysis. Onshore flow does develop at the surface over

the San Francisco Bay area south of this trough. Over the next 6 hours, the sea-level pressure gradient west of the developing trough strengthens, which suggests an acceleration of the northerly flow over this region. In response to the accelerating northerly flow, the offshore trough begins to elongate to the south, and by 01/1500 UTC (not shown) the area of onshore flow expands southward to Monterey Bay. The onshore flow in this area results in weak ridging over this area, most likely in response to the build up of marine air against the coastal mountains. During this period, the sky conditions along the coast change from clear at 01/0000 UTC to overcast, with stratus filling in along the coast from Point Arena to the Southern California Bight (Figure 3.7). It is interesting that the coastal stratus is present in the 01/1027 UTC and 01/1445 UTC images prior to the initiation of the CTWR. The 01/1700 UTC is the first analysis that indicates the wind at buoy 46012 has developed a southerly component. In addition, a narrow, coastal mesoscale ridge is established that begins to rapidly propagate northward along the coast, which marks the beginning of this event. The initiation of this event occurs much faster (approximately 18 hours after onshore flow at 850 mb) than in the July case (approximately 48 hours), and matches that shown in Figure 3.2.

The propagation phase of this event occurs over the next 24-30 hours and is characterized by a very non-uniform propagation pattern. At 01/1900 UTC, the coastal mesoscale ridge has separated the southern end of the trough from the coast, and an offshore mesoscale low is analyzed west-southwest of San Francisco Bay. The 01/1900 UTC analysis also has the head of the coastal ridge is just south of Point Arena, which

coincides with the northern extent of southerly winds, as indicated by the light southerly wind at buoy 46014. Although this northward extension occurs within 2 hours of the initiation of the CTWR, it subsequently stalls until after 02/1200 UTC. However, the coastal stratus continues to move northward along the coast ahead of the coastal mesoscale ridge and southerly transition (e.g. the 02/0206 UTC image in Figure 3.7). A localized trough across the coast extends from the head of the coastal mesoscale ridge to Cape Mendocino. In this case, the northward extension of the coastal trough is attributed to the westward retreat of the synoptic-scale ridge over the Pacific Northwest, rather than a northward shift of this ridge axis as in the July event, and as noted in past studies.

Over the next 6 hours, the pattern then remains essentially unchanged. By 02/0600 UTC, the sea-level pressure under the coastal mesoscale ridge begins rising at the same time as the offshore mesoscale low begins to fill, which results in a weaker pressure gradient offshore but a very pronounced coastal mesoscale ridge (Figure 3.6). The coastal mesoscale ridge begins to propagate to the north and the northern edge of the ridge then extends north of Point Arena. Over the next 6-7 hours, the coastal mesoscale ridge and southerly transition reach Cape Mendocino, as evidenced by the increasing sea-level pressure and southerly flow at buoy 46030 at 02/1300 UTC (not shown).

Over the next few hours, the coastal mesoscale ridge propagates to the north along the coast and the leading edge reaches Arcata (ACV) by 02/1500 UTC with light southerly winds (Figure 3.6). Since the coastal stratus is located north of Cape Mendocino, it now slightly lags the arrival of the coastal mesoscale ridge and southerly

transition during this period (see the 02/1603 UTC image in Figure 3.6). Winds are southerly from buoy 46042 to Arcata. Wind speeds are 10 knots in the southern three-fourths of the coastal ridge and 5 knots or less near the leading edge to the north.

Even though the coastal trough has shifted northward and lies between Arcata (ACV) and Crescent City (CEC), the position of the offshore mesoscale low does not change. Moderate northerly flow still exists west of the offshore trough, although the pressure gradient appears to have slackened. It bears noting that the sea-level pressure at the California-Oregon border falls significantly (see the buoy 46027 observation) against the diurnal cycle when the pressure should rise. However, the winds remain northwesterly at 20 knots.

Over the next 6 hours, the coastal mesoscale ridge and the southerly wind transition appear to propagate slowly along the coast and reach Crescent City by 02/2200 UTC. During this same period, the coastal stratus retreats to just south of Cape Mendocino (Figure 3.7). The area of coastal troughing expands to the north to include part of the southern Oregon coast, as the synoptic-scale ridge over the Pacific Northwest weakens. The 03/0000 UTC analysis shows that the southerly flow under the coastal mesoscale ridge has weakened considerably to 5 knots or less, and the northerly flow west of the mesoscale low appears to weaken as well. This event begins to decay shortly after 03/0000 UTC.

As in the July case, the surface evolution of the CTWR in this case is remarkably similar to the Skamarock et al. (1998) model, despite the differences in the synoptic forcing. This case has many aspects of the evolution shown in Figures 3.1 and 3.2 including the relaxation of the pressure gradient near the coast, the development of a surface depression, and the offshore displacement of the coastal jet. Subsequently, onshore flow develops south of the coastal depression, and thus leads to the development of a mesoscale ridge and southerly winds along the coast, and finally the offshore mesoscale low. In this case, the timing of the initial surface mesoscale response to the 850 mb offshore flow is in closer agreement to the Skamarock et al. (1998) model than the July case (18 hours versus 48 hours).

As in the July case, the northern-most extent of the propagation of this CTWR is at least partially related to the synoptic forcing in the lower troposphere. In this case, the region of dynamic forcing (850 mb offshore flow) and the thermal trough do not shift as far north as in the July case (see Figures 2.3 and 2.4). The synoptic forcing also breaks down much faster, which is attributed to the more progressive nature of the synoptic-scale features as discussed in the previous chapter. Subsequently, the CTWR fails to reach the California/Oregon border before it begins to break down and retreat equatorward along the coast.

### 3. 4-7 June 1996 Case

Hand-drawn analyses of sea-level pressure (Figure 3.8) show that this event fails to develop into an extended CTWR as found in the previous cases. It will be shown that the development, diurnal modulation, and decay of a Catalina Eddy extended north of Point Conception on 5 June for only a brief period of time. Figure 3.9 contains selected satellite imagery illustrating the evolution of the coastal stratus.

The 04/0000 UTC analysis has a thermal trough over the Central Valley of California similar to the other cases and the climatological pattern. The eastern Pacific high lies near the U.S. west coast, which results in a strong cross-coast pressure gradient along the northern and central California coast. The pressure gradient along the southern California coast is also tight, but slackens quickly in the offshore direction. Northwesterly flow is present along the northern and central California coast, while onshore west-southwesterly flow dominates in the California Bight region.

Over the next 12 hours, the eastern Pacific high builds to the northeast over the Pacific Northwest and a low develops just south of the Channel Islands in the California Bight region. The cyclonic turning of the winds at buoy 46025 near Santa Barbara and buoy 46054 near Point Conception indicates that this low is a Catalina Eddy. A tongue of high pressure also develops to the southeast of the low due to the coastward advection of cool, moist marine air (see the 04/1200 UTC analysis). The cross-coast pressure gradient along the central and southern California coast north of the Catalina Eddy weakens



substantially during the early morning hours. During the next 3 hours, the coastal mesoscale ridge continues to propagate north along the southern California coast. Although the coastal mesoscale ridge only reaches an area just north of Point Conception by 04/1500 UTC (not shown), an area of stratus extends along the coast from the southern California Bight region to Monterey Bay (Figure 3.9). While winds under the coastal mesoscale ridge are southeasterly following the coastline, northwesterly flow occurs along the remainder of the California coast.

Over the next 9 hours during the period of maximum diurnal warming, this pattern breaks down. Even though the offshore mesoscale low weakens, a trough remains over the California Bight region. The coastal mesoscale ridge remains north of Point Conception until 04/1600 UTC (not shown), and then begins to retreat southward along the coast. The 04/1800 UTC analysis in Figure 3.8 has an offshore mesoscale low and a coastal ridge that extends north to Santa Barbara with weak southerly along-coast flow. The coastal stratus has retreated southward during this period (see the 04/2116 UTC image in Figure 3.9). By 05/0000 UTC, no evidence of the coastal ridge exists and the winds along the southern California coast switch to southwesterly (onshore) due to the sea breeze circulation (Figure 3.8). Although an area of stratus remains in the southern California Bight region, it appears to be decreasing and thinning (Figure 3.9).

The evolution on 5 June is similar to that on 4 June except the features are somewhat more amplified. In the 05/0600 UTC analysis, the offshore mesoscale low has redeveloped with an area of coastal ridging indicated to the east of the low. Over the next

6 hours, the offshore low deepens further and the coastal mesoscale ridge begins to propagate northward along the coast to buoy 46025 (see the 05/1200 UTC analysis). Winds under the coastal mesoscale ridge are along-coast with a southerly component once again. By 05/1600 UTC (not shown), the coastal ridge has progressed around Point Conception and extends to San Luis Obispo, which is its northernmost extent. On this day, the coastal stratus coincides with the coastal ridge (see the 05/1506 UTC image in Figure 3.9). The coastal ridge only remains north of Point Conception until 05/1800 UTC, then again retreats southward along the coast over the next 6 hours. The coastal ridge breaks down as the offshore low weakens during the period of maximum heating. By 06/0000 UTC, only the trough over the California Bight region remains with no evidence of the coastal ridge. Winds along the coast are southwesterly (onshore) as the sea breeze circulation reaches maximum intensity for this day.

This pattern repeats again on 6 June, except with an overall increase in the sea-level pressure over the southern California Bight region and the coastal stratus extends to Monterey Bay (Figure 3.9). That is, the offshore mesoscale low reamplifies, the coastal mesoscale ridge redevelops to the east of the low and propagates north along the coast to San Luis Obispo, and the features decay during the peak in afternoon heating. Finally, the entire pattern appears to break down on 7 June as the thermal trough over inland southern California weakens and the eastern Pacific high builds onshore over the California Bight region.

In this case, the development of the offshore low, the coastal mesoscale ridge, and the along-coast winds with a southerly component along the southern California coast would seem to indicate the initiation of a CTWR. However, analysis of the synoptic-scale and the mesoscale patterns indicates that this event is more correctly classified as a Catalina Eddy. The evolution of the synoptic-scale pattern in this case only briefly on 5 June produced the pattern required for the development of a CTWR, when the Catalina Eddy extended around Point Conception and reached as far north as San Luis Obispo. The lack of persistent synoptic forcing favorable for a CTWR appears to have prevented this event from evolving into an extended CTWR. Because this case did not evolve into a fully developed CTWR, no further analysis was done on this case.

The development of the offshore low, as well as the coastal ridge, in this case was highly diurnal in nature, which is not a characteristic of CTWRs. The offshore trough over the California Bight region deepens during the night, which may produce a closed low over the California Bight region. This development of an offshore low appears to be an amplification of the Catalina Eddy that results from the northeasterly offshore flow over Point Conception as seen in the eta model analyses for 850 mb at 05/1200 UTC and 06/1200 UTC in Figure 2.5. The flow to the south and east of the offshore low advects cool, marine air toward the coast, which results in the development of the coastal ridge. The coastal ridge propagates along the coast to the area where the coastal northerly jet remains near the coast. The winds under the coastal ridge adjust geostrophically and follow the coast around the offshore low. However, this pattern

breaks down during the morning hours as the sea breeze circulation is reestablished each day. The evolution of this pattern then begins again during the late evening as the sea breeze circulation weakens and breaks down.

#### **D. DEVELOPMENT OF THE OFFSHORE MESOSCALE LOW**

##### **1. Conceptual Model**

One key feature of the two-dimensional and three-dimensional simulations in Skamarock et al. (1998) is the development of an offshore mesoscale low. These simulations provide an excellent conceptual model for comparison with observed events. Figure 3.2 illustrates the evolution of the mesoscale offshore low at 300 m from the three-dimensional simulations. After 24 hours of offshore flow, a noticeable depression in the marine layer depth develops just south of the maximum offshore flow. The low-level coastal northerly jet is displaced offshore and slightly accelerates west of the depression, and the marine layer is displaced away from the coast. As the depression deepens, it is also elongated to the south due to the accelerated flow to the west. Weak onshore flow also develops to the south of the depression. Over the next 12 hours, the depth of the marine layer increases in the region of the onshore flow (not shown). The northward propagation of the elevated marine layer represents the initiation of the CTWR. During Day 1.5 to Day 2.5 after the onset of offshore flow, the wind reversal continues to propagate northward along the coast as the marine layer continues to deepen south of the depression. The depression is cut off from the coast to form a mesoscale low. The

mesoscale low moves slowly southward as the wind reversal propagates north to where the northerly jet has not pushed offshore.

The presence of the offshore mesoscale low may partially explain the deep southerlies associated with some CTWR's. As seen in section C, the evolution of the 21-24 July and 1-4 September 1996 events exhibit some of the same features. However, distinct differences also exist between the simulation from Skamarock et al. (1998) and these two CTWRs. The following sections examine the synoptic-scale and mesoscale forcing of the offshore mesoscale low at the surface in these two events as compared to the Skamarock model in order to more fully understand the development of these CTWRs.

## **2. 21-24 July 1996 Case**

The crucial role of the low-level offshore flow to the development of the CTWR in the Skamarock model is that the marine layer is displaced away from the coast just south of the maximum cross-coast flow. Along-coast cross sections of the cross-coast wind component and temperature from the eta model analyses for the period from 19/1200 UTC to 22/1200 UTC are shown in Figure 3.10. Notice the gradual warming of the lower troposphere, especially below 850 mb. The greatest warming occurs just north of the southern end of the cross section where a region of 28°C develops in the 21/1200 UTC cross section. Although only a weak (<5 m/s) cross-coast wind component below 800 mb is indicated along the entire cross section prior to this time, the soundings and profilers shown in Figure 2.3 suggest this warming is near or just south of the area of

maximum offshore flow at 850 mb. A maximum offshore flow of 5 m/s is indicated at Oakland. The 21/1200 UTC cross section indicates that the cross-coast wind component from the eta model analysis has strengthened considerably ( $>7.5$  m/s) to the north of the temperature maximum with very weak onshore flow to the south. Notice also the lower temperatures near the surface in the region of a weak onshore flow component at this time. This region is south of the offshore mesoscale low and where southerly flow would be expected east of the mesoscale low. In the conceptual model, this advection of cool marine air toward the coast is a response to onshore flow south of the mesoscale low.

Time series of sea-level pressure for the moored coastal buoys and the marine layer depth for the coastal wind profiler sites are shown in Figures 3.11 and 3.12, respectively. The sea-level pressure for the moored coastal buoys is examined to compare the area of minimum-sea level pressures along the coast with the position of the development of the offshore mesoscale low. The marine layer is composed of cool, moist air that is "heavier" than the warm, dry air found away from the coast. Therefore, lower marine layer depth should correspond to lower sea-level pressure, and vice versa. Finally, the northward propagation of the CTWR should be revealed in the sea-level pressure traces.

A decrease in sea-level pressure along the coast from buoy 46042 to buoy 46030 occurs after 19/1800 UTC (Figure 3.11). This decrease in sea-level pressure along the coast may occur in response to the lee troughing and warming above the marine layer associated with lower tropospheric offshore flow across the coastal topography. The

warming appears to be caused by a combination of warm advection across the coast and adiabatic downslope flow. Notice that the highest temperatures (closed 28°C isotherm in Figure 3.10) at 950 mb occur over the area between Point Reyes and buoy 46012 where the lowest sea-level pressures are found (Figure 3.11). No marine layer is detected along the coast from Point Piedras Blancas to Point Arena by 21/0000 UTC, which corresponds to the sea-level pressure minima in this area of the coast at 21/0300 UTC (Figures 3.11 and 3.12). Later, the marine layer appears to be displaced away from the coast by approximately 21/0300 UTC at Point Arena, but maintains a diurnal variation until 21/1800 UTC when the forcing from offshore flow strengthens over the region as indicated in Figures 3.10 and 3.12.

This pattern is consistent with the development of a cyclonic circulation and thermal trough in the lower troposphere near the coast, which is reflected in the 850 mb analysis in Figure 2.3 as well as the profiler winds on those charts. As analyzed in Figure 3.3, the trough begins to elongate southward after 21/1200 UTC in response to accelerated northerly flow west of the area of troughing. Four hours later at 21/1600 UTC, the offshore mesoscale low forms in this area. The location of the mesoscale low at this time corresponds to the 850 mb and 950 mb temperature maximum shown in Figures 2.3 and 3.10, and as indicated on the 21/1800 UTC analysis in Figure 3.4.

The northward propagation of the coastal trough is also evident in Figure 3.11. A minimum in sea-level pressure is reached at approximately 21/0300 UTC from buoy 46014 (Point Arena) to buoy 46042 (Monterey Bay). As the coastal trough propagates

north, sea-level pressure minima are reached later at buoy 46030 (Cape Mendocino) and buoy 46027 (near the California/Oregon border) at approximately 21/1200 UTC and 22/0100 UTC, respectively. The sea-level pressure minima propagate north with the area of strongest offshore flow, highest temperatures, and decreasing marine layer depth as shown in Figures 3.10, 3.11, and 3.12. However, the position of the offshore mesoscale low remains relatively unchanged until this CTWR begins to break down (see Figure 3.4).

The evolution of the mesoscale offshore low in this case is similar to the Skamarock et al. (1998) simulation. The pressure gradient near the coast is relaxed and the marine layer appears to be displaced away from the coast, thus leading to the development of a coastal depression. The strongest pressure gradient is pushed away from the coast (Figure 3.3), which suggests that the coastal northerly jet is pushed offshore. This depression elongates to the south as the northerly jet to the west of the depression accelerates due the tightened pressure gradient (Figure 3.4). Once the coastal ridge propagates north along the coast, the depression/trough is cut off from the coast and a mesoscale low forms offshore. The offshore flow in this case occurs below 850 mb and is generally less than 6 m/s. The maximum increase of temperature in the lower troposphere roughly coincides with the offshore flow maximum. The offshore flow in this case is weaker than that used in the Skamarock model, but the increase in temperature (warming) in the lower troposphere appear to be warmer. In this case, the atmosphere is warmed, as inferred from the building ridge aloft and developing thermal



trough at low levels (Figure 2.3). It appears that the atmospheric warming must be pushed offshore to get a mesoscale response in the lower troposphere.

The lower tropospheric ridging over the Pacific Northwest and the resulting geostrophic offshore flow over the California coast appear to be the mechanism for pushing the warm air offshore. A combination of warm advection, lee troughing, and adiabatic warming from downslope flow that result from the offshore flow across the coastal topography appears to be responsible for the forcing of this event. As discussed in between this event and the Skamarock simulations is the nature of the forcing. In the Skamarock simulations, the forcing at 850 mb is constant, whereas in this event the forcing appears to be modified by the mesoscale circulation that is trapped along the coastal mountain range.

It is also noteworthy that the maximum in marine layer depth along the coast remains at the southern end of the coastal ridge near the base of the offshore trough and mesoscale low during the entire event as noted by Skamarock et al. (1998). This can be seen in the profiler data (Figure 3.12) where the maximum in marine layer depth lies between Bodega Bay and Monterey Bay until 23/0300 UTC, which corresponds to the location of the offshore mesoscale low as seen in Figure 3.4. The maximum marine layer depth shifts north with the northward propagation of the offshore mesoscale low. The wind profiler data indicates that the maximum depth of the marine layer is near Bodega Bay at 23/0300 UTC, then near Point Arena at 23/1800 UTC, which corresponds with the movement of the offshore mesoscale low (Figure 3.4).

### 3. 1-4 September 1996 Case

During the September 1996 event, a significant offshore flow pattern at 850 mb develops over northern California at 1200 UTC 31 August, which is approximately 18 hours prior to the development of a depression in sea-level pressure (Figures 2.4 and 3.6). Along-coast cross sections of the cross-coast wind component and temperature from the eta model analyses are shown in Figure 3.13 for the period from 1200 UTC 30 August to 0000 UTC 02 September. The 30/1200 UTC cross section shows a weak inversion, especially to the north (left side of the cross section). This is consistent with the inversion being weakened by the approaching upper-level trough (see Figure 2.5). The subsequent cross sections show the development of an inversion between 850 mb and 900 mb, particularly over the southern part of the domain. At the initial time (30/1200 UTC), the offshore wind component below 900 mb is weak ( $< 2.5$  m/s) and covers nearly the entire length of the cross-section from Monterey Bay to Cape Mendocino. Onshore flow above 900 mb and to the north of Cape Mendocino is indicated as a short-wave trough approaches the coast. At 31/1200 UTC, the area of the offshore wind component below 850 mb shifts to the north from Point Arena to Cape Mendocino with warming to the south at 850 mb. As this warming occurs in an area of onshore flow, it most likely results from subsidence aloft, and not warm advection, as discussed in the previous chapter (see Figure 2.4). The warming in the lower troposphere reestablishes the inversion capping the marine layer. The development of offshore flow to the north results from a building

synoptic-scale ridge over the Pacific Northwest from the surface to 850 mb as shown in Figure 2.4.

By 01/1200 UTC, the inversion continues to strengthen and becomes shallower over the domain as the lower troposphere continues to warm. The depth of the offshore flow reaches 700 mb near Cape Mendocino and extends horizontally from Point Reyes to at least Cape Mendocino. This 01/1200 UTC along-coast cross section also has evidence of the developing surface trough, or cyclonic circulation, along the coast with a strong offshore wind component ( $> 7.5$  m/s) north of Point Arena and a weak onshore wind component below approximately 960 mb south of Point Reyes. This pattern is consistent with the development of a closed circulation at 850 mb shown in Figure 2.4 and by the profiler winds at 850 mb (Figure 2.4).

The 02/0000 UTC cross section shows that the offshore flow component shifts farther to the north while onshore flow strengthens to the south. For the first time during this event, the highest temperatures (in a layer from 950 mb to 850 mb) coincide with the strongest offshore flow. The decreasing temperatures from the surface to 950 mb in the region of onshore flow south of the mesoscale offshore low indicate an advection of cool marine air toward the coast. The 02/1200 UTC cross section was not available for analysis.

Time series of sea-level pressure for each moored coastal buoy indicate a gradual decrease in sea-level pressure along the central and northern California coast after 31/0000 UTC. By 01/0600 UTC, a noticeable depression in sea-level pressure is present

along the coast from Point Reyes to Point Arena to the south of the offshore flow maximum. A sea-level pressure minimum is reached at approximately 01/1300 UTC over an area extending from buoy 46012 (south of San Francisco Bay) to buoy 46014 (Point Arena). This trough expands offshore with time (Figure 3.6). As the surface trough expands offshore, the pressure gradient to the west tightens, which implies an accelerating northerly flow west of the depression. The surface trough then begins to elongate after 01/1500 UTC in response to the accelerating northerly flow to the west. By 01/1700 UTC, a mesoscale ridge develops along the coast at the south end of the trough and begins propagating to the north (Figure 3.5). At the same time, the wind at buoy 46012 develops a southerly component. Over the next few hours, the coastal ridge and southerly flow propagates northward, and reaches just south of Point Arenas by 01/1900 UTC. Later, minima in sea-level pressure are reached at buoys 46030 (Cape Mendocino) and 46027 (near the California/Oregon border) at approximately 02/0300 UTC, which indicates the northward expansion of the thermal trough. However, the position of the offshore mesoscale low remains relatively unchanged until this CTWR begins to break down, as seen in the July case. This sea-level pressure pattern is very consistent with the evolution at 850 mb shown in Figure 2.5.

Time series of marine layer depth for the coastal wind profiler sites (Figure 3.15) show the effects of the passage of the short-wave trough aloft (see Figure 2.4). No marine layer is detected to the north as shown by the Crescent City profiler after 01/0000 UTC. Farther south, the marine layer depth decreases, which is consistent with the

decreasing sea-level pressure (Figure 14), but maintains a diurnal signature as shown by the Point Arena and Bodega Bay profilers. The displacement of the marine layer away from the coast at Monterey Bay and Point Piedras Blancas is unexplained. An increase of the marine layer depth after 01/1800 UTC at Monterey Bay, Bodega Bay, and Point Arena is consistent with the development of onshore flow and the coastal mesoscale ridge as shown in Figure 3.6. However, the decrease in depth between 02/0200 UTC and 02/0700 UTC at Point Arena is unexplained. The evolution of the marine layer in this event does not correlate as well with the sea-level pressure pattern as in the July 1996 event as discussed in the previous section. The passage of the short-wave trough aloft appears to be the primary feature changing the marine layer depths, especially to the north.

The evolution of this event appears differ significantly from the Skamarock et al. (1998) model and the July case. The offshore mesoscale low in this event does develop as a result of offshore flow at 850 mb and lower tropospheric warming. However, the origin of both the dynamic and thermal forcing appears to be different. As the ridge builds in the mid-troposphere over the eastern Pacific, subsidence ahead of the ridge appears to be responsible for the warming in the lower troposphere. This warming results in a thermal trough and warm-core low to develop in the lower troposphere. Offshore flow then develops over northern California to the north of the trough/closed low at 850 mb as a result of the associated cyclonic flow. Warm advection does not appear to be significant as in the July event, since the warming occurs over the coast. Once the

dynamic forcing (offshore flow) and the thermal forcing are in place, the initial mesoscale response near the surface begins and the offshore mesoscale low forms.

As in the July case, the pressure gradient near the coast is relaxed and the marine layer appears to be displaced away from the coast, thus leading to the development of a coastal depression. The strongest pressure gradient is pushed away from the coast (Figure 3.6), which suggests that the coastal northerly jet is pushed offshore. This depression elongates to the south as the northerly jet to the west of the depression accelerates due the tightened pressure gradient (Figure 3.6). Once the coastal ridge propagates north along the coast, the depression/trough is cut off from the coast and a mesoscale low forms offshore. As in the July case, the maximum marine layer depth along the coast remains tied to the position of the offshore mesoscale low as in the July event and as noted in Skamarock et al. (1998).

## **E. REVERSAL OF THE ALONG-COAST PRESSURE GRADIENT**

### **1. 21-24 July 1996 Case**

As discussed in the previous section, offshore flow across the California coast becomes established at 19/1200 UTC at 850 mb along the California coast (Figure 3.10). The expected effects of the offshore flow are the westward advection of warm air across the coast and a decrease in the marine layer depth, which should result in decreasing sea-level pressure along the coast. Approximately 6 hours after the onset of the offshore flow, sea- level pressure along the coast reaches a maximum, and then begins to decrease

gradually over the next 48 hours (Figure 3.11). The decrease in sea-level pressure can be attributed to the warming atmosphere and suppression of the marine layer, and is consistent with the Skamarock et al. (1998) model. At 21/0000 UTC, no marine layer is detected along the coast between Point Piedras Blancas and Bodega Bay. An along-coast analysis of the marine layer depth from Crescent City to Point Piedras Blancas for 21/0000 UTC indicates higher marine layer depth to the north with a decrease from over 200 meters at the California/Oregon border to 0 m at Bodega Bay (Figure 3.16). Between 19/1200 UTC and 21/0000 UTC, a strong north-south sea-level pressure gradient of 5-6 mb is evident from buoy 46030 to buoy 46012 (Figure 3.16).

Over the next 24 hours, the along-coast gradient in the marine layer depth relaxes, and then ultimately reverses. During this period, moderate ( $>7.5$  m/s) offshore flow develops in the lower troposphere north of Point Arenas as a result of the cyclonic circulation associated with the developing coastal troughing and building ridge over the Pacific Northwest as discussed in the previous section. The offshore flow and continued warming act to lower the marine layer depth and the sea-level pressure from Point Arenas to the California/Oregon border, and is consistent with the Skamarock et al. (1998) model. During this same period, weak onshore flow begins at 21/0900 UTC to the south of the coastal trough and developing offshore mesoscale low as in the Skamarock et al. (1998) model. The expected deepening of the marine layer in response to the onshore flow begins after 21/1500 UTC at Point Piedras Blancas. The onshore flow pushes cool, moist marine air toward the coast, and results in a deepening of the marine layer as the

marine air piles up against the coastal mountain ranges. After 21/0600 UTC, the along-coast sea-level pressure gradient begins to weaken. A general rise in sea-level pressure along the coast from buoy 46042 to buoy 46014 begins between 21/1200 UTC and 21/1500 UTC. This rise in sea-level pressure occurs approximately 3-6 hours prior to the development of a MBL from Monterey Bay to Bodega Bay, and can be attributed to the atmospheric tidal cycle in which sea-level pressure should rise after 1200 UTC. Between 21/1200 UTC and 21/1800 UTC the along-coast sea-level pressure gradient reverses with higher sea-level pressure to the south. At 21/1800 UTC, the sea-level pressure at buoy 46013 is approximately 2 mb higher than the sea-level pressure at buoy 46027. The along-coast gradient in marine layer depth does not correlate well with the along-coast sea-level pressure gradient at this time. The marine layer depth gradient remains slightly positive from the California/Oregon border to Point Arena with a slope from 100 m to 0 m. However, a reversal in the gradient occurs to the south as the marine layer (150 m in depth) develops near Point Piedras Blancas. The reversal in the marine layer depth gradient to the south corresponds to the time that the wind at buoy 46012 develops a weak southerly component.

In the succeeding hours, the surface winds develop more of a southerly component and increase slightly in strength as the marine layer depth gradient increases. The propagation of the surface southerly wind transition and coastal ridge begins once the gradient in marine layer depth reverses after 21/1800 UTC. Between 21/1800 UTC and 22/0000 UTC, the along-coast gradient in marine layer depth increases along the entire



domain. The largest gradient is between Monterey Bay (250 m) and Point Arena (0 m). During this period, the along-coast sea-level pressure gradient between buoy 46013 and buoy 46027 increases to approximately 3 mb. This sea-level pressure gradient is maintained through the remainder of this event. However, the along-coast sea-level pressure gradient south of buoy 46013 remains positive from north to south, and does not reverse until after 22/0000 UTC. This pattern does not correlate with the marine layer depth changes over this area during this period. By 22/0300 UTC, the along-coast gradients in marine layer depth and sea-level pressure are reversed along the entire domain, but remain strongest between Bodega Bay and Point Arena. Over the next 36 hours, the along-coast marine layer depth gradient between Bodega Bay and the California/Oregon border remains between 150-200 m, while the sea-level pressure gradient remains at approximately 2 mb.

The reversal in the along-coast sea-level pressure gradient is consistent with the evolution of the CTWR in the Skamarock and that observed in past CTWRs (e.g. Ralph et al. 1998). Sea-level pressure and marine layer depth decrease along the coast in the region of offshore flow. As the coastal trough and low develops at the surface, onshore flow develops to the south, and thus results in increasing marine layer depth and sea-level pressure to the south. Once the gradients in marine layer depth and sea-level pressure reverse occurs, then southerly flow begins along the coast east of the offshore mesoscale low.

## 2. 1-4 September 1996 Case

Crucial to the reversal of the along-coast gradients in marine layer depth and sea-level pressure in this case is the passage of a migratory short-wave trough in the low- and mid-troposphere across the northern California coast. Along-coast depictions of sea-level pressure and marine layer depth (Figure 3.17) show the decreasing sea-level pressure along the northern California coast and the weakening along-coast pressure gradient. The difference in sea level pressure between buoy 46030 and buoy 46042 decreases from 6 mb at 31/0000 UTC to 4 mb at 01/0000 UTC. The marine layer has been eliminated or the depth has been significantly reduced along the coast north of Point Arena by 01/0000 UTC (Figure 3.17) as a result of the passage of the migratory short-wave trough. However, the along-coast gradients are positive from north to south at this time from at least Cape Mendocino southward.

Once offshore flow is established at 850 mb, the along-coast gradients in marine layer depth and sea-level pressure begin to relax between Bodega Bay and the California/Oregon border. At approximately 01/1200 UTC, a minimum in sea-level pressure is reached along the coast in the vicinity of buoy 46013, as shown in Figures 3.14 and 3.17. However, a corresponding minimum in marine layer depth is not evident. By 01/1500 UTC, a weak onshore flow component develops at buoy 46012 south of the coastal trough as expected. Between 01/1200 UTC and 01/1800 UTC, the along-coast gradients in sea-level pressure and marine layer depth reverse between Bodega Bay and the California/Oregon border as shown in Figure 3.17. At 01/1800 UTC, the along-coast

marine layer depth gradient is 300 m, and the along-coast sea level pressure gradient is approximately 2 mb between Bodega Bay and the California/Oregon border. The reversal in these along-coast gradients coincides with the development of a southerly surface wind component at buoy 46012. By 01/1900 UTC, light southerly winds ( $< 2.5$  m/s) reach Point Arena. Over the next 6 hours, the along-coast sea-level pressure gradient increases to over 4 mb between Bodega Bay and the California/Oregon border by 02/0000 UTC. However, the along-coast gradient in marine layer depth actually decreases over this same area, but increases to 400 m from Monterey Bay to the California/Oregon border at this same time. Over the next 15 hours, the along-coast gradients remain strong as shown in Figure 3.17. After 02/1500 UTC, the along-coast gradient in marine layer depth slightly relaxes as the MBL begins to develop along the extreme northern California coast. Six hours later, the along-coast sea level pressure gradient begins to relax.

As in the July case, the reversal in the along-coast sea-level pressure gradient is consistent with the evolution of the CTWR in the Skamarock and that observed in past CTWRs (e.g. Ralph et al. 1998). However, the passage of a deep migratory short-wave trough significantly contributes to the decrease of marine layer depth and sea-level pressures north of Cape Mendocino, and thus the reversal in the along-coast gradient of both, which differs from the July case and is not indicated in the Skamarock et al. (1998). Sea-level pressure and marine layer depth decrease along the coast in the region of offshore flow. As the coastal trough and low develop at the surface, onshore flow

develops to the south, and thus results in increasing marine layer depth and sea-level pressure to the south. Once the gradients in marine layer depth and sea-level pressure are reversed, then southerly flow begins along the coast east of the offshore mesoscale low.

## **F. PROPAGATION AND VERTICAL EXTENT OF THE CTWR**

### **1. 21-24 July 1996 Case**

As discussed in Section C, this CTWR is initiated at 21/1500 UTC. The transition to southerly flow at the surface initially propagates poleward at approximately 6-7 m/s and reaches Bodega Bay by 21/2000 UTC and Point Arena by 22/0200 UTC. This propagation speed closely matches that observed in a 1982 event (Dorman 1985) and in Kelvin wave simulations by Dorman (1985), but is slower than the 11.9 m/s observed in the 10-11 June 1994 CTWR (Ralph et al. 1998). During the initial hours of this event, the southerly wind transition lags the deepening of the marine layer (e.g., by 2 hours at Bodega Bay). As this disturbance begins to propagate along the coast, the southerly wind transition moves ahead of the deepening marine layer (by approximately 2 hours at Point Arena), which is also observed in the 10-11 June 1994 CTWR (Ralph et al. 1998). An analysis of aircraft data for 22/0000 UTC (not shown) indicates that the southerly wind transition aloft develops earlier than at the surface, prior to the deepening of the marine layer along the coast. Southerly flow of at least 2.5 m/s extends well north of Point Arenas in a layer from 100 m to 500 m. Weaker southerly flow ( $< 2.5$  m/s) extends farther north to Cape Mendocino in a layer from 600 m to 1000 m.

The southerly wind transition stalls at Point Arena for approximately 8 hours. The CTWR then begins to propagate northward along the coast at an accelerated speed of 9.8 m/s (Figure 3.4) and reaches Cape Mendocino at 22/1400 UTC, which more closely agrees with the 10-11 June 1994 CTWR (11.9 m/s). The southerly wind transition continues to accelerate and reaches the California/Oregon border, which indicates a propagation speed of approximately 15 m/s. The deepening of the marine layer at this location also lags the southerly wind transition as earlier in the event (by approximately 8 hours). Aircraft data for 22/1800 UTC and 22/2100 UTC show that southerly flow in a layer from 100 m to 1200 m coincides with the northward extent of southerly flow at the surface. This differs from the aircraft observations of wind structure at 22/0000 UTC, when the flow aloft extended north of the surface feature, which seems to indicate that the vertical wind structure of the CTWR undergoes change during the event.

The southerly wind transition continues to propagate to the north along the coast and reaches North Bend, OR between 23/0800 UTC and 23/1200 UTC. The speed of propagation can not be determined due to a lack of surface observations along the southern Oregon coast between 23/0800 UTC and 23/1200 UTC. The depth changes of the marine layer along the Oregon coast can not be evaluated due to a lack of data.

## **2. 1-4 September 1996 Case**

As discussed in section C, the initiation of this coastally trapped wind reversal occurs at 01/1700 UTC, when the wind at buoy 46012 first develops a southerly wind component. The transition to southerly flow at the surface rapidly propagates (30-35 m/s)

to the north along the coast and reaches Bodega Bay at 01/1800 UTC and Point Arena at 01/1900 UTC (Figure 3.6). This rapid transition to southerly flow suggests an ageostrophic response to the along-shore pressure gradients in sea-level pressure and marine layer depth. The deepening of the marine layer lags the surface southerly transition at Bodega Bay by approximately 5 hours and at Point Arena by approximately 12 hours (Figure 3.15). At both locations, the depth of the marine layer actually decreases for several hours after the southerly wind transition before deepening. Aircraft data for 01/2200 UTC (not shown) show that the southerly winds are contained in a very narrow band along the coast, which roughly corresponds to the width of the mesoscale ridge of high pressure at the surface. The horizontal extent of southerly flow appears to increase slightly offshore above 600 m.

The surface southerly wind transition stalls twice between Cape Mendocino and Point Arena, and does not reach Cape Mendocino until 02/1300 UTC. Aircraft data for 02/0200 UTC indicate a layer from 100 m to 1200 m of southerly winds that coincide with the northward extent of the surface southerlies. This is similar to the July event. At 02/2200 UTC, the southerly wind transition reaches Arcata, its northern-most extent. Aircraft data for 02/2100 UTC show a shallow layer (100-400 m) of southerly winds that coincide with the northernmost extent (Arcata) of the southerly transition at the surface. Above 400 m, southerly winds only extend approximately 50 km north of Point Arena, with northerly flow along the coast north of this area. This vertical distribution of winds is quite different from the July event in which southerly flow extended through a

much deeper layer (1200 m). This vertical distribution appears to indicate that the CTWR has begun to decay above the surface. Although the southerly wind transition fails to reach the California/Oregon border, the marine layer does deepen as far north as Crescent City wind profiler site (Figure 3.15).

## Evolution of a Coastally-Trapped Disturbance

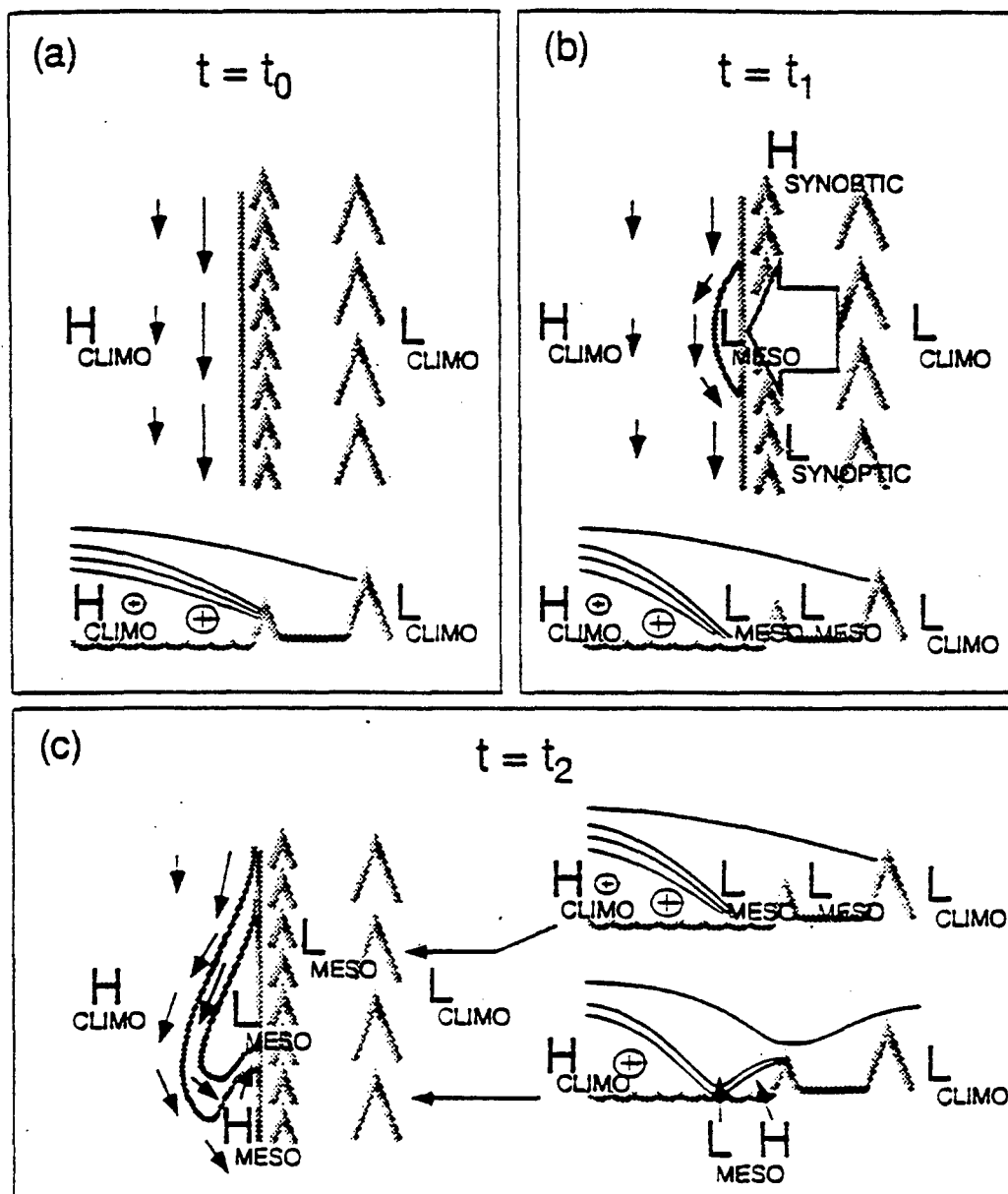


**Figure 3.1.** Summary of a coastally trapped wind reversal (from Skamarock et al. 1998).



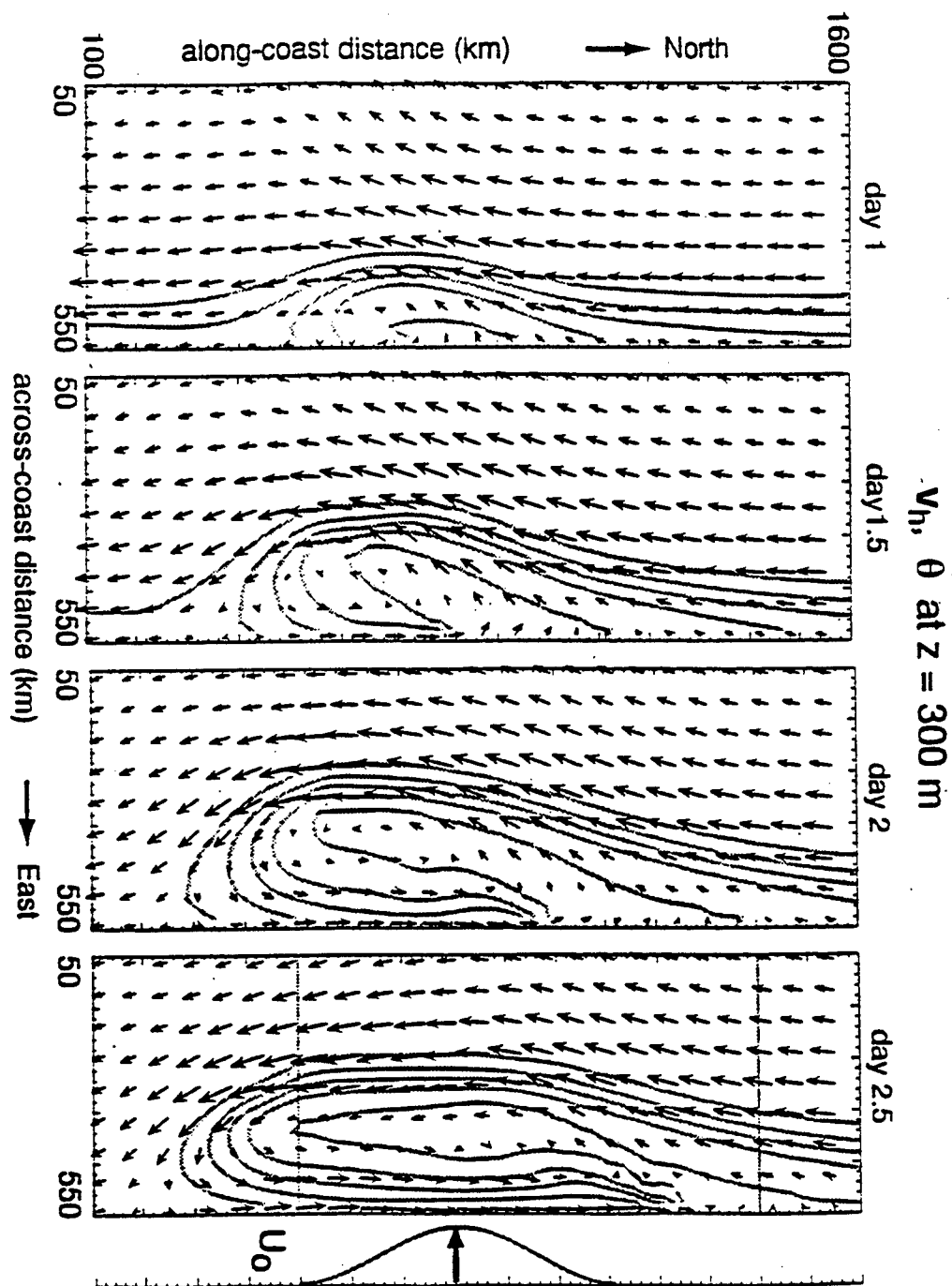


**Figure 3.2.** Horizontal cross-sections at  $z = 300$  m from the reference simulation. Potential temperature is contoured in gray with a contour interval of  $2^\circ$  K. Maximum wind vectors are approximately 14 m/s. The coastal mountains intersect the plane at  $x = 540$  m. The position of the imposed offshore flow is indicated on the right (from Skamarock et al. 1998).

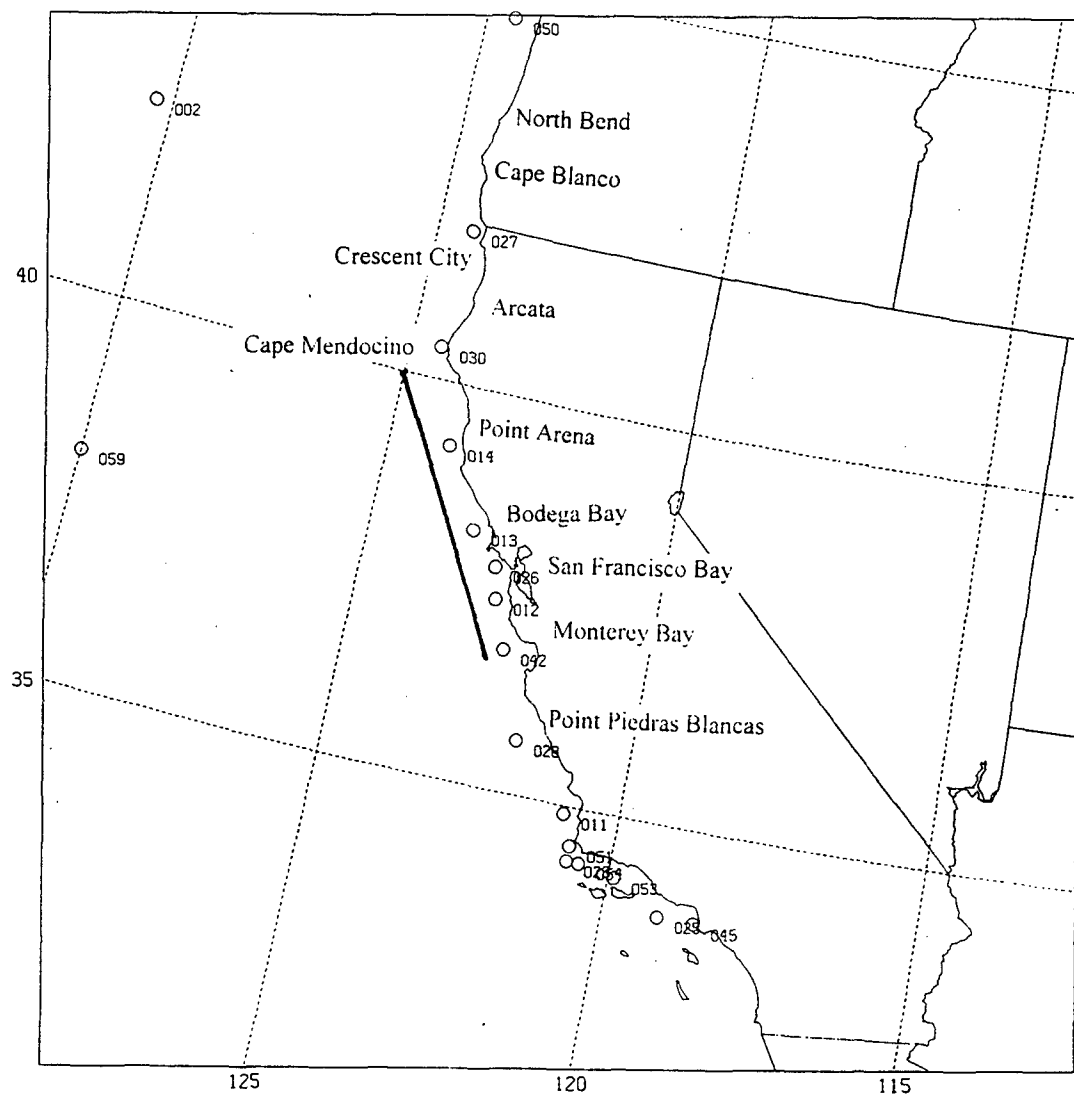
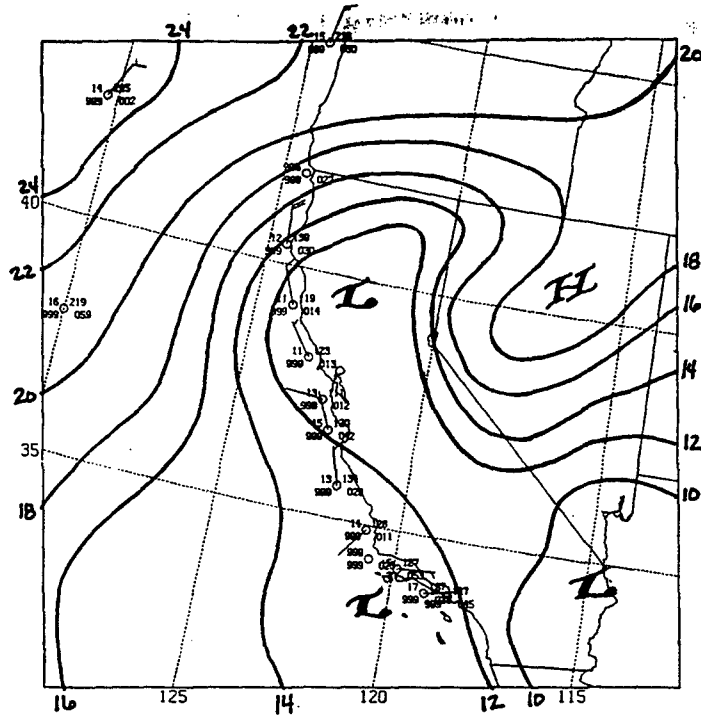


**Figure 3.3.** Domain for the hand-drawn mesoscale analyses of sea level pressure. Contour interval is 2 mb. Selected moored buoy locations and the track for the along coast cross-sections are denoted.

82

1200 UTC - 21 JULY 1996



1800 UTC - 21 JULY 1996

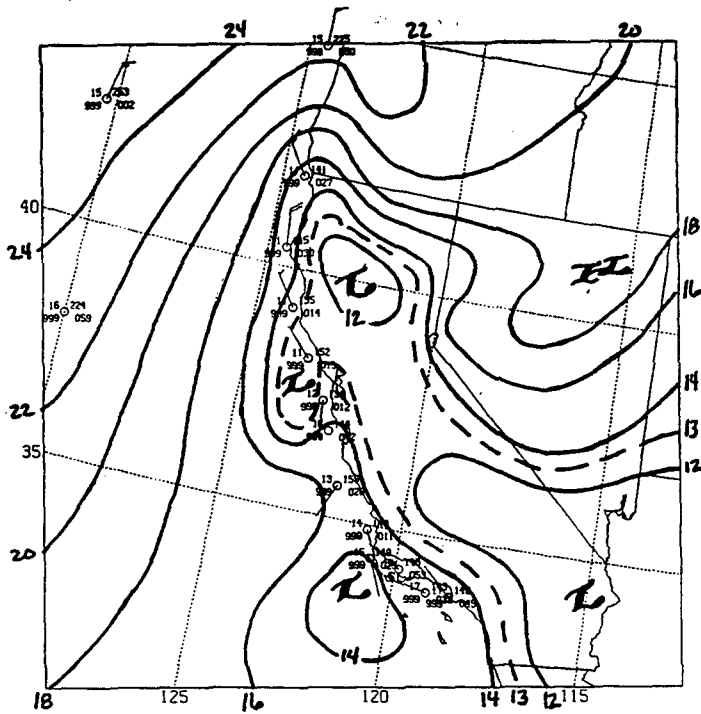


Figure 3.4 (cont.)

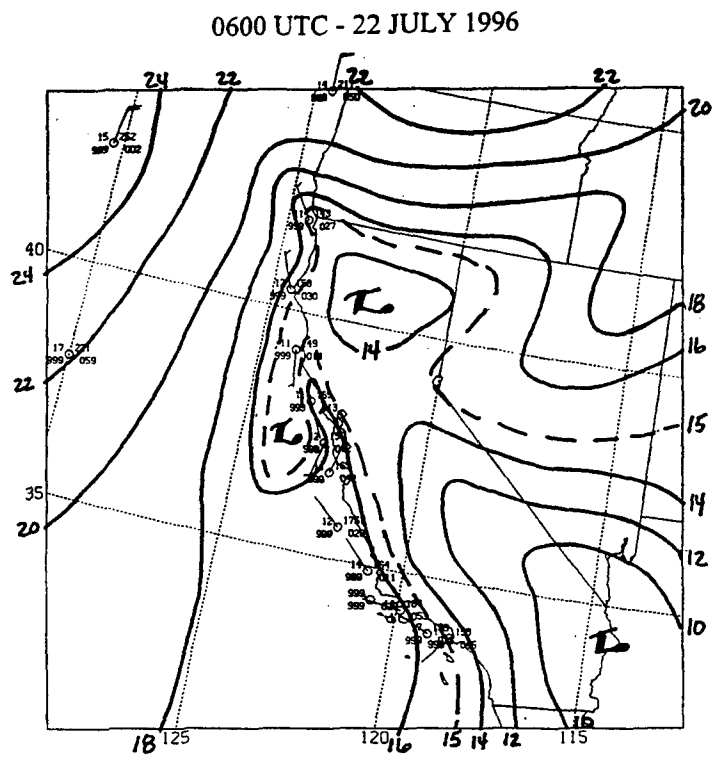
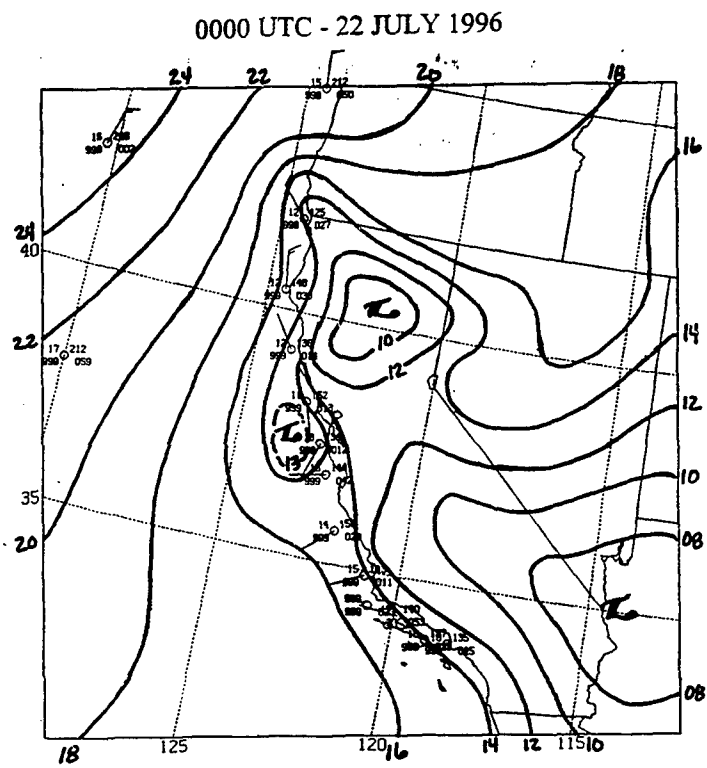
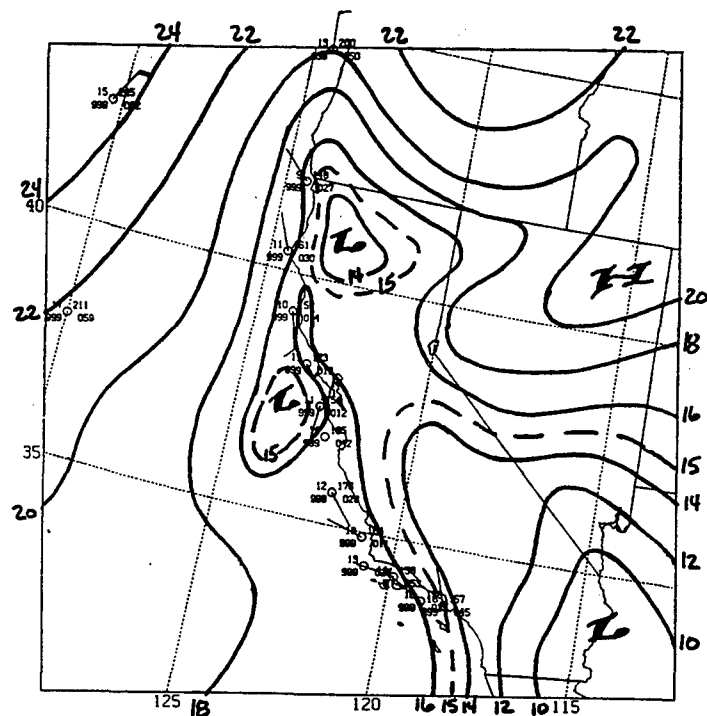


Figure 3.4 (cont.)

1200 UTC - 22 JULY 1996



1500 UTC - 22 JULY 1996

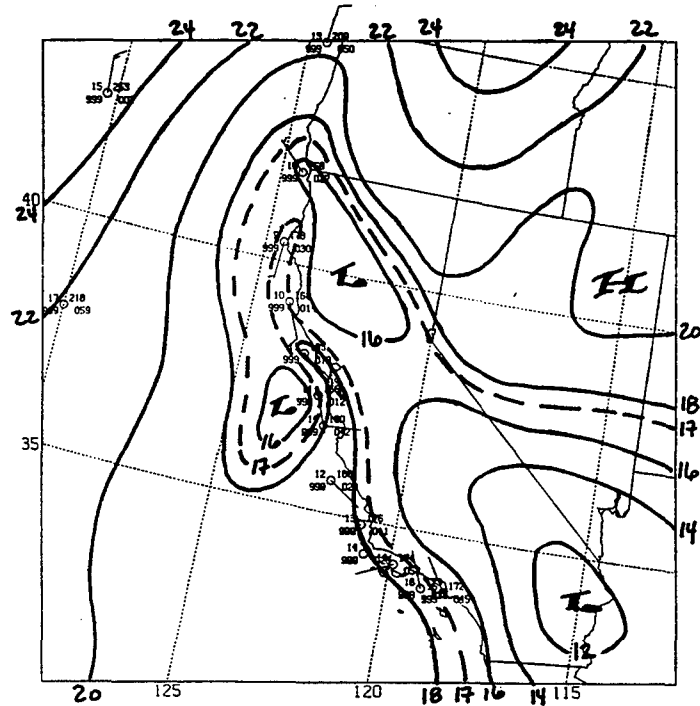
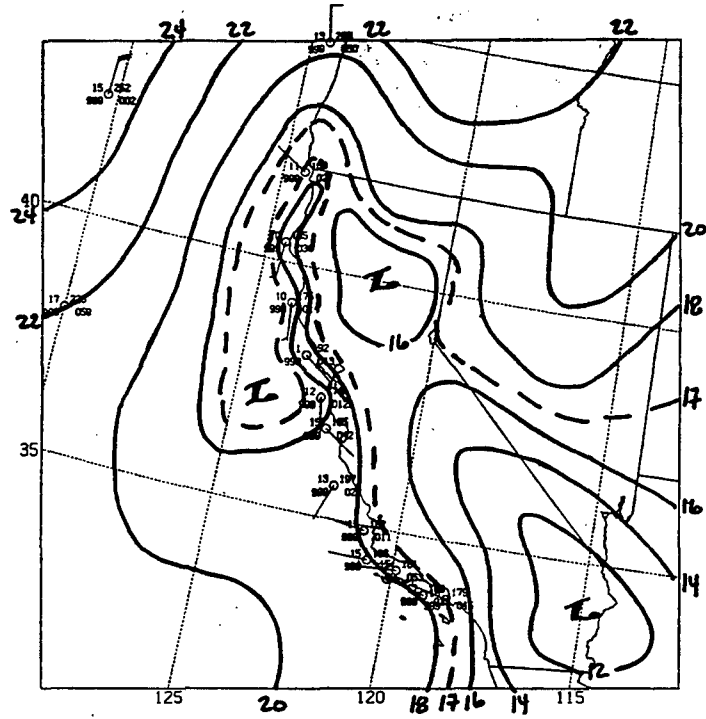


Figure 3.4 (cont.)

1800 UTC - 22 JULY 1996



0000 UTC - 23 JULY 1996

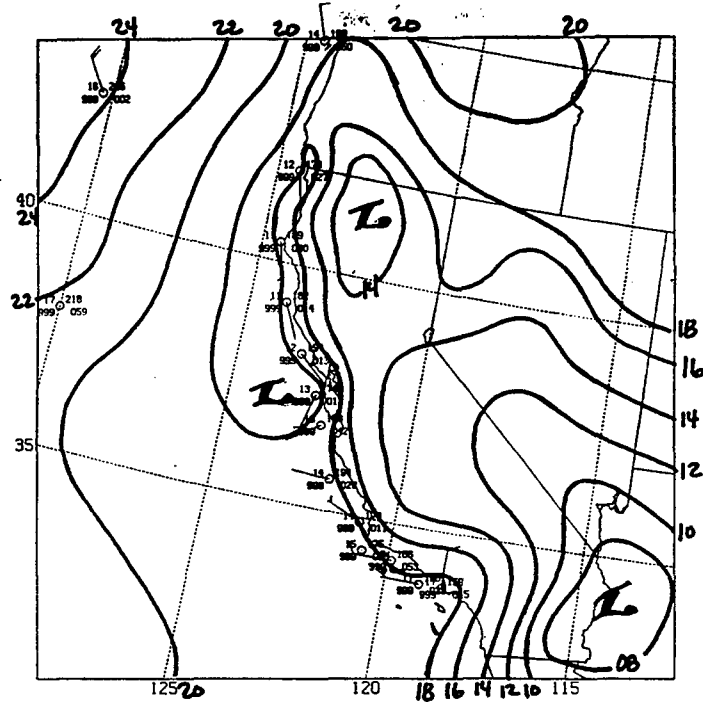
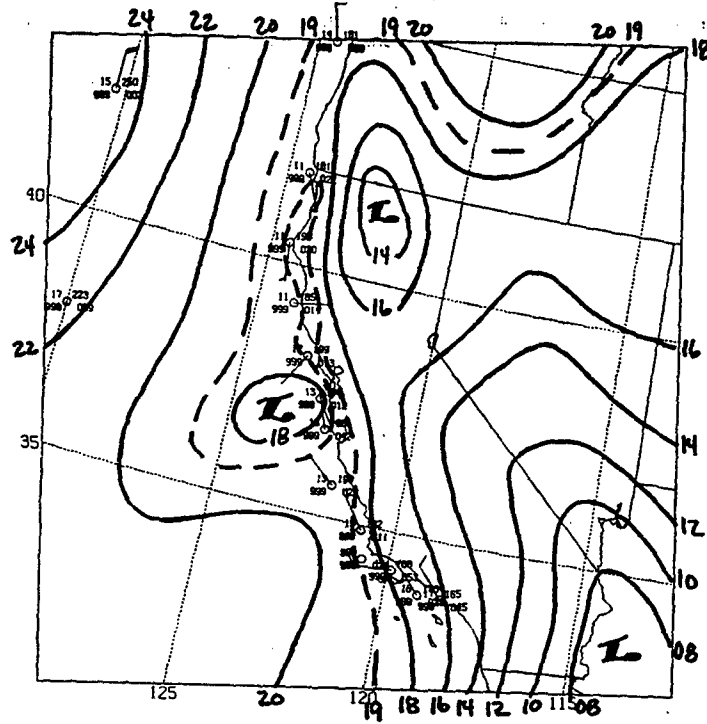


Figure 3.4 (cont.)

0600 UTC - 23 JULY 1996



1200 UTC - 23 JULY 1996

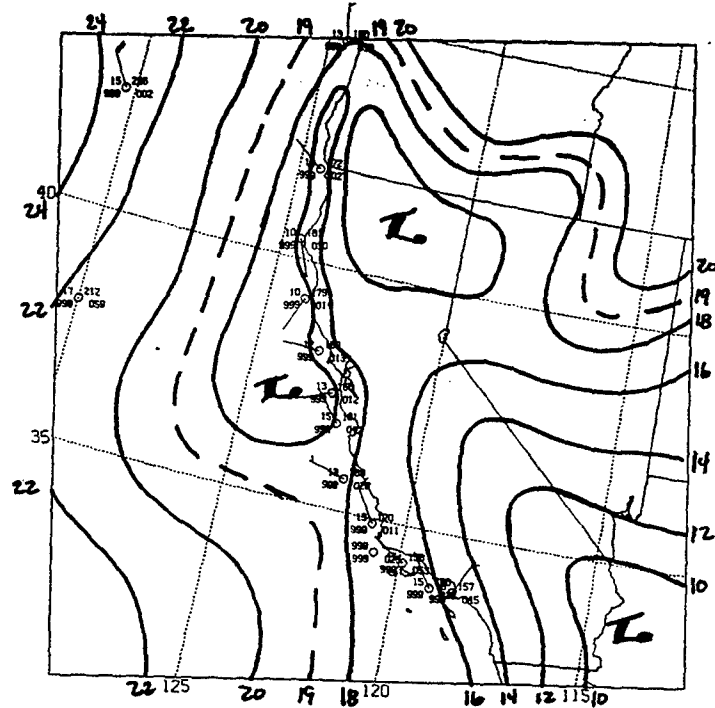
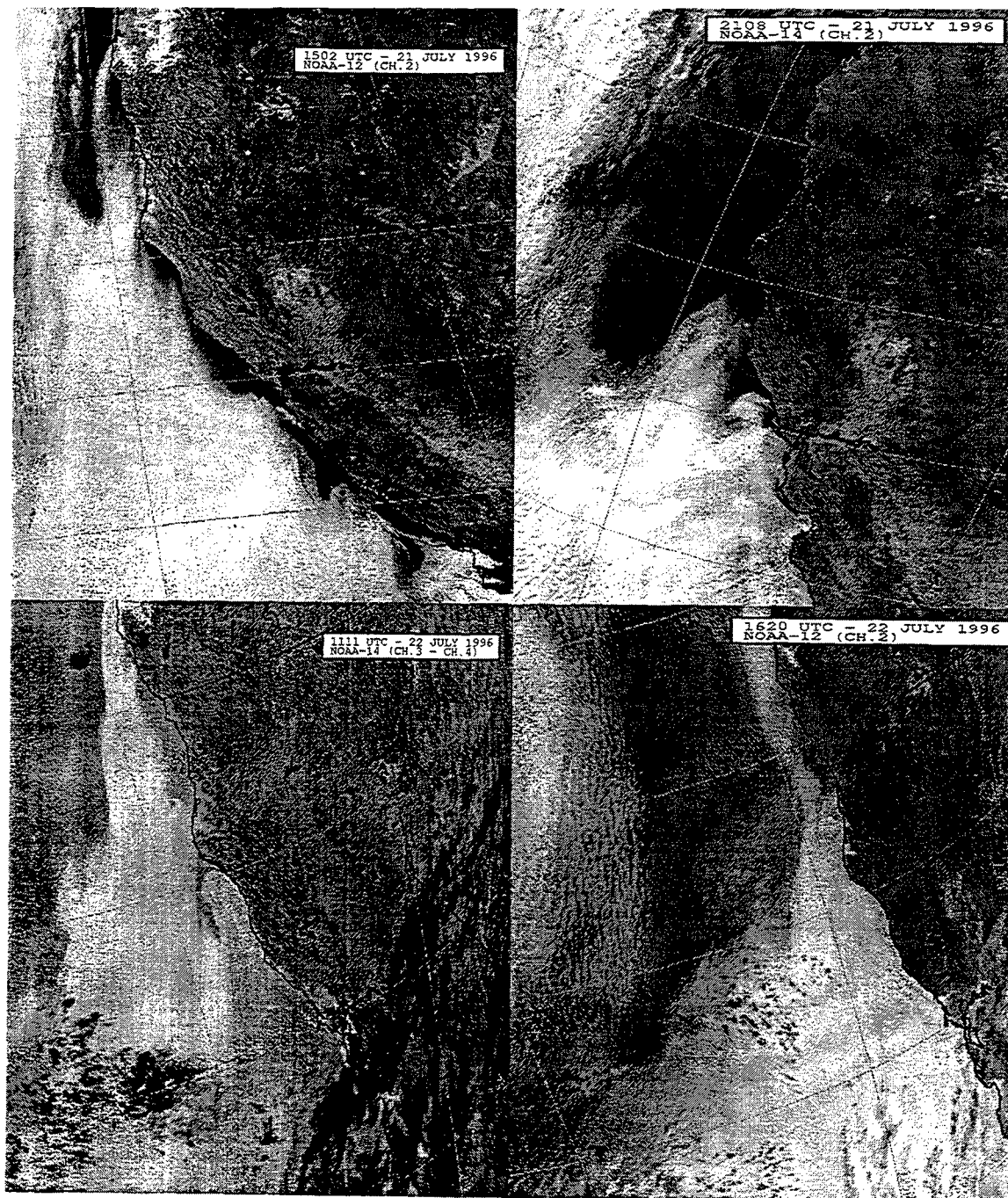


Figure 3.4 (cont.)





**Figure 3.5.** Satellite imagery from NOAA polar orbiting satellites for the 21-24 July 1996 coastally trapped wind reversal. Horizontal horizontal resolution is 1.1 km.



Figure 3.5 (cont.)

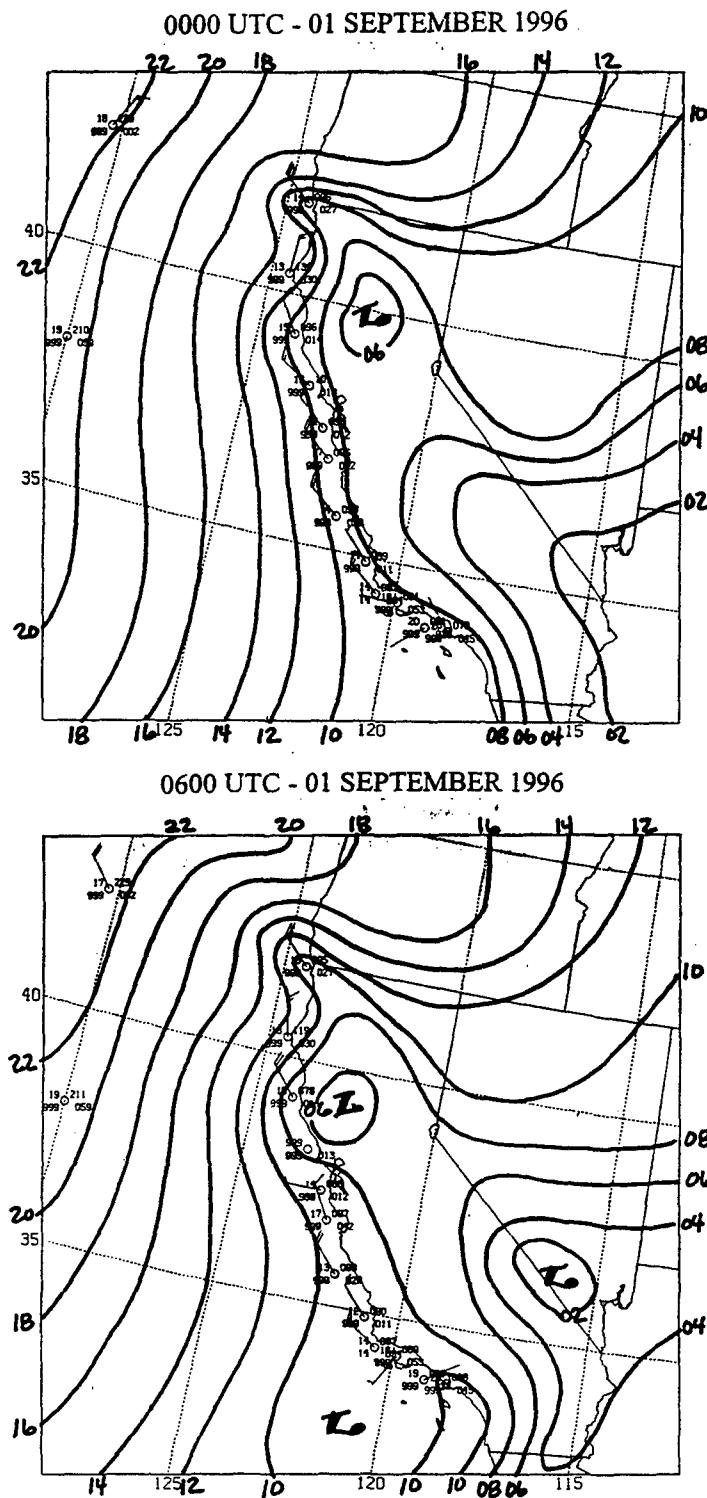


**Figure 3.6.** Surface evolution of the September 1996 coastally trapped wind reversal as depicted by hand-drawn analyses of sea-level pressure. Contour interval is 2 mb.

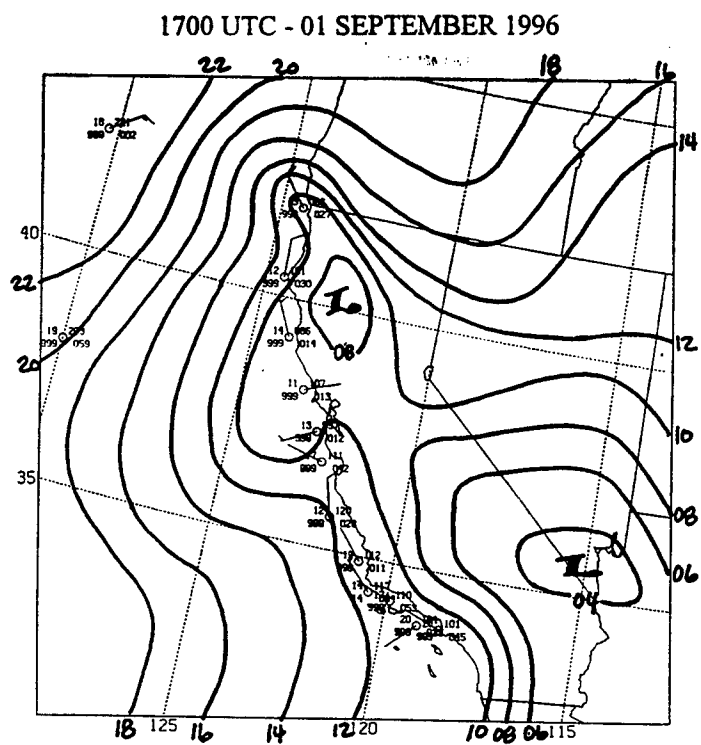
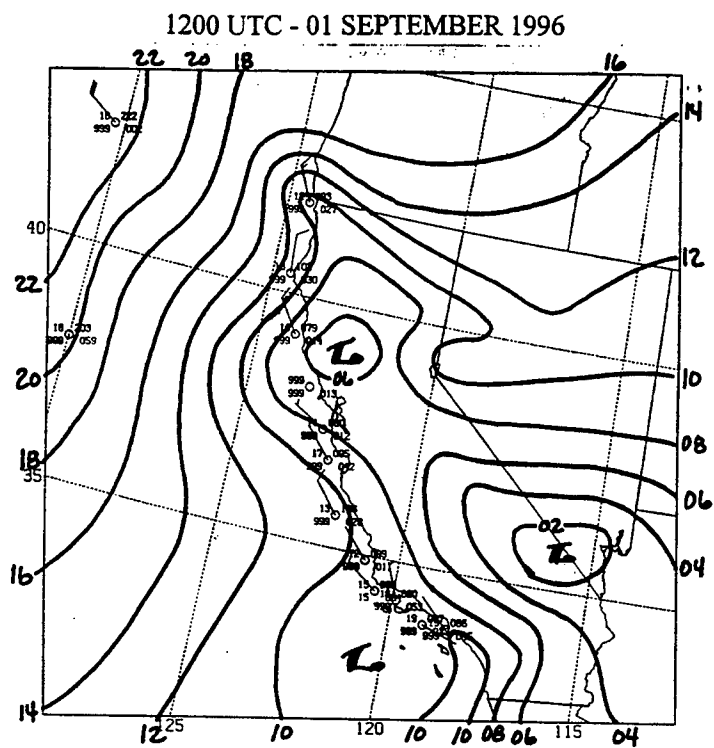


Figure 3.6 (cont.)

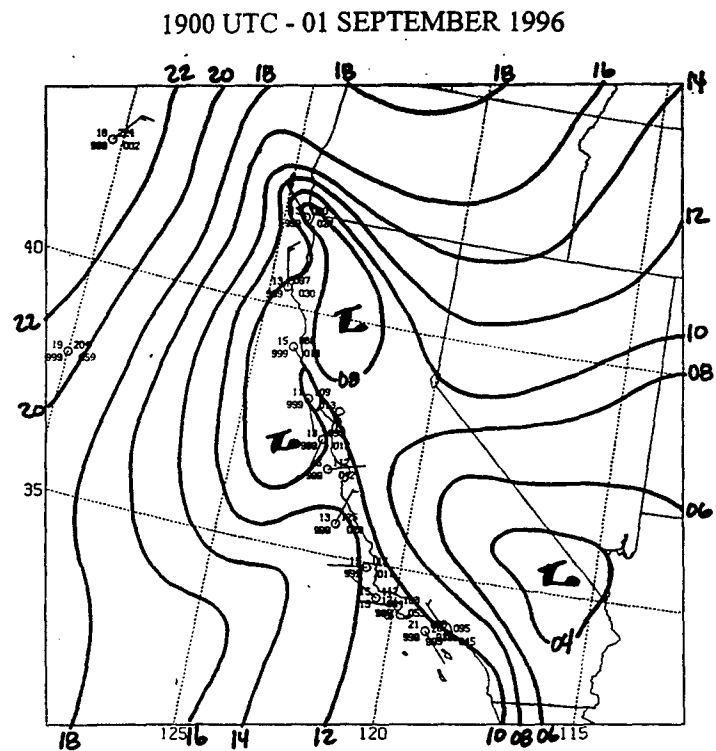
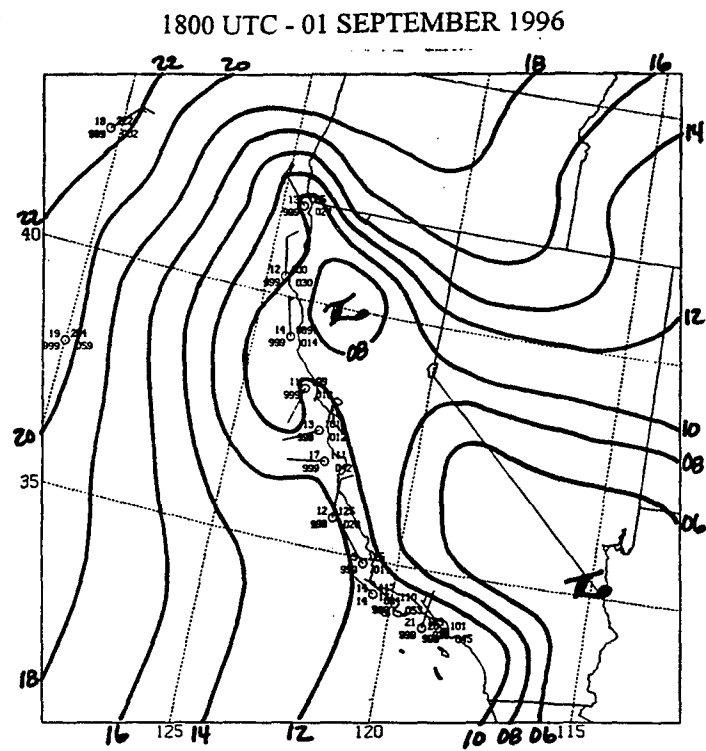


Figure 3.6 (cont.)

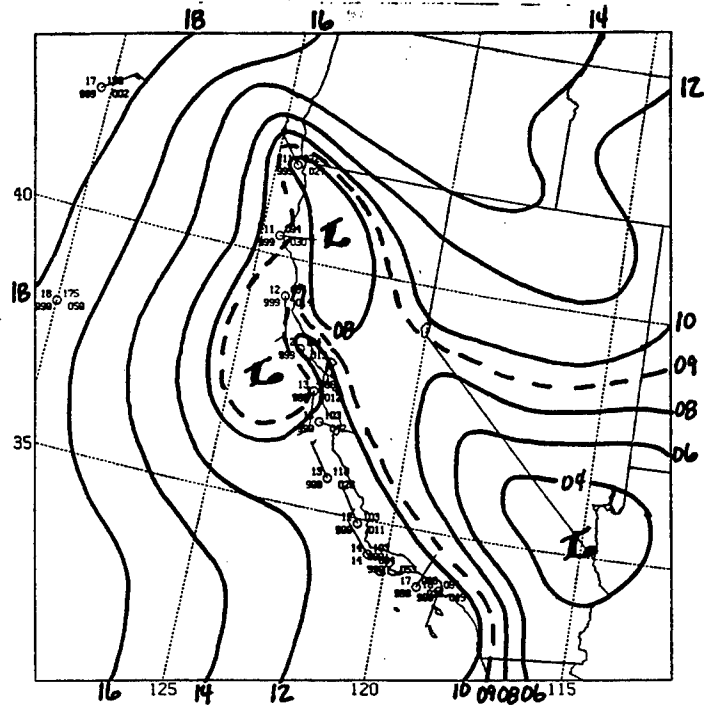
This is a hand-drawn weather map of the Western Pacific region, showing pressure contours, isobars, and various weather symbols. The map includes latitude and longitude markings and is labeled with handwritten numbers and letters.

**Geographic Features and Markings:**

- Latitude:** 16, 18, 20, 35 (on the left); 02, 04, 06, 08, 10 (on the right).
- Longitude:** 125, 120, 115 (at the bottom); 12, 10, 08, 06, 04 (on the right).
- Isobars:** Solid lines representing pressure levels, with values such as 990, 995, 1000, 1005, 1010, 1015, 1020, 1025, 1030, 1035, 1040, 1045, 1050, 1055, 1060, 1065, 1070, 1075, 1080, 1085, 1090, 1095, 1100, 1105, 1110, 1115, 1120, 1125, 1130, 1135, 1140, 1145, 1150, 1155, 1160, 1165, 1170, 1175, 1180, 1185, 1190, 1195, 1200, 1205, 1210, 1215, 1220, 1225, 1230, 1235, 1240, 1245, 1250, 1255, 1260, 1265, 1270, 1275, 1280, 1285, 1290, 1295, 1300, 1305, 1310, 1315, 1320, 1325, 1330, 1335, 1340, 1345, 1350, 1355, 1360, 1365, 1370, 1375, 1380, 1385, 1390, 1395, 1400, 1405, 1410, 1415, 1420, 1425, 1430, 1435, 1440, 1445, 1450, 1455, 1460, 1465, 1470, 1475, 1480, 1485, 1490, 1495, 1500, 1505, 1510, 1515, 1520, 1525, 1530, 1535, 1540, 1545, 1550, 1555, 1560, 1565, 1570, 1575, 1580, 1585, 1590, 1595, 1600, 1605, 1610, 1615, 1620, 1625, 1630, 1635, 1640, 1645, 1650, 1655, 1660, 1665, 1670, 1675, 1680, 1685, 1690, 1695, 1700, 1705, 1710, 1715, 1720, 1725, 1730, 1735, 1740, 1745, 1750, 1755, 1760, 1765, 1770, 1775, 1780, 1785, 1790, 1795, 1800, 1805, 1810, 1815, 1820, 1825, 1830, 1835, 1840, 1845, 1850, 1855, 1860, 1865, 1870, 1875, 1880, 1885, 1890, 1895, 1900, 1905, 1910, 1915, 1920, 1925, 1930, 1935, 1940, 1945, 1950, 1955, 1960, 1965, 1970, 1975, 1980, 1985, 1990, 1995, 2000, 2005, 2010, 2015, 2020, 2025, 2030, 2035, 2040, 2045, 2050, 2055, 2060, 2065, 2070, 2075, 2080, 2085, 2090, 2095, 2100, 2105, 2110, 2115, 2120, 2125, 2130, 2135, 2140, 2145, 2150, 2155, 2160, 2165, 2170, 2175, 2180, 2185, 2190, 2195, 2200, 2205, 2210, 2215, 2220, 2225, 2230, 2235, 2240, 2245, 2250, 2255, 2260, 2265, 2270, 2275, 2280, 2285, 2290, 2295, 2300, 2305, 2310, 2315, 2320, 2325, 2330, 2335, 2340, 2345, 2350, 2355, 2360, 2365, 2370, 2375, 2380, 2385, 2390, 2395, 2400, 2405, 2410, 2415, 2420, 2425, 2430, 2435, 2440, 2445, 2450, 2455, 2460, 2465, 2470, 2475, 2480, 2485, 2490, 2495, 2500, 2505, 2510, 2515, 2520, 2525, 2530, 2535, 2540, 2545, 2550, 2555, 2560, 2565, 2570, 2575, 2580, 2585, 2590, 2595, 2600, 2605, 2610, 2615, 2620, 2625, 2630, 2635, 2640, 2645, 2650, 2655, 2660, 2665, 2670, 2675, 2680, 2685, 2690, 2695, 2700, 2705, 2710, 2715, 2720, 2725, 2730, 2735, 2740, 2745, 2750, 2755, 2760, 2765, 2770, 2775, 2780, 2785, 2790, 2795, 2800, 2805, 2810, 2815, 2820, 2825, 2830, 2835, 2840, 2845, 2850, 2855, 2860, 2865, 2870, 2875, 2880, 2885, 2890, 2895, 2900, 2905, 2910, 2915, 2920, 2925, 2930, 2935, 2940, 2945, 2950, 2955, 2960, 2965, 2970, 2975, 2980, 2985, 2990, 2995, 3000, 3005, 3010, 3015, 3020, 3025, 3030, 3035, 3040, 3045, 3050, 3055, 3060, 3065, 3070, 3075, 3080, 3085, 3090, 3095, 3100, 3105, 3110, 3115, 3120, 3125, 3130, 3135, 3140, 3145, 3150, 3155, 3160, 3165, 3170, 3175, 3180, 3185, 3190, 3195, 3200, 3205, 3210, 3215, 3220, 3225, 3230, 3235, 3240, 3245, 3250, 3255, 3260, 3265, 3270, 3275, 3280, 3285, 3290, 3295, 3300, 3305, 3310, 3315, 3320, 3325, 3330, 3335, 3340, 3345, 3350, 3355, 3360, 3365, 3370, 3375, 3380, 3385, 3390, 3395, 3400, 3405, 3410, 3415, 3420, 3425, 3430, 3435, 3440, 3445, 3450, 3455, 3460, 3465, 3470, 3475, 3480, 3485, 3490, 3495, 3500, 3505, 3510, 3515, 3520, 3525, 3530, 3535, 3540, 3545, 3550, 3555, 3560, 3565, 3570, 3575, 3580, 3585, 3590, 3595, 3600, 3605, 3610, 3615, 3620, 3625, 3630, 3635, 3640, 3645, 3650, 3655, 3660, 3665, 3670, 3675, 3680, 3685, 3690, 3695, 3700, 3705, 3710, 3715, 3720, 3725, 3730, 3735, 3740, 3745, 3750, 3755, 3760, 3765, 3770, 3775, 3780, 3785, 3790, 3795, 3800, 3805, 3810, 3815, 3820, 3825, 3830, 3835, 3840, 3845, 3850, 3855, 3860, 3865, 3870, 3875, 3880, 3885, 3890, 3895, 3900, 3905, 3910, 3915, 3920, 3925, 3930, 3935, 3940, 3945, 3950, 3955, 3960, 3965, 3970, 3975, 3980, 3985, 3990, 3995, 4000, 4005, 4010, 4015, 4020, 4025, 4030, 4035, 4040, 4045, 4050, 4055, 4060, 4065, 4070, 4075, 4080, 4085, 4090, 4095, 4100, 4105, 4110, 4115, 4120, 4125, 4130, 4135, 4140, 4145, 4150, 4155, 4160, 4165, 4170, 4175, 4180, 4185, 4190, 4195, 4200

93

1200 UTC - 02 SEPTEMBER 1996



1500 UTC - 02 SEPTEMBER 1996

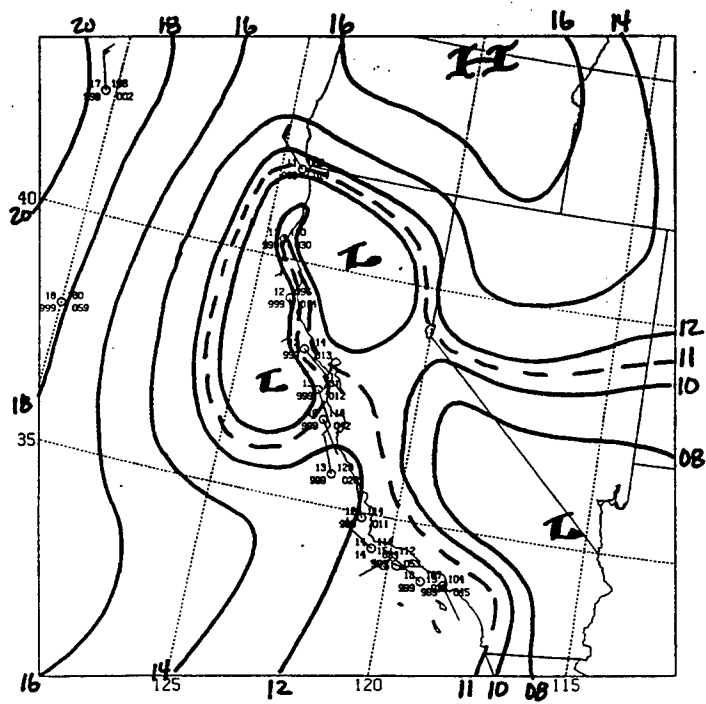
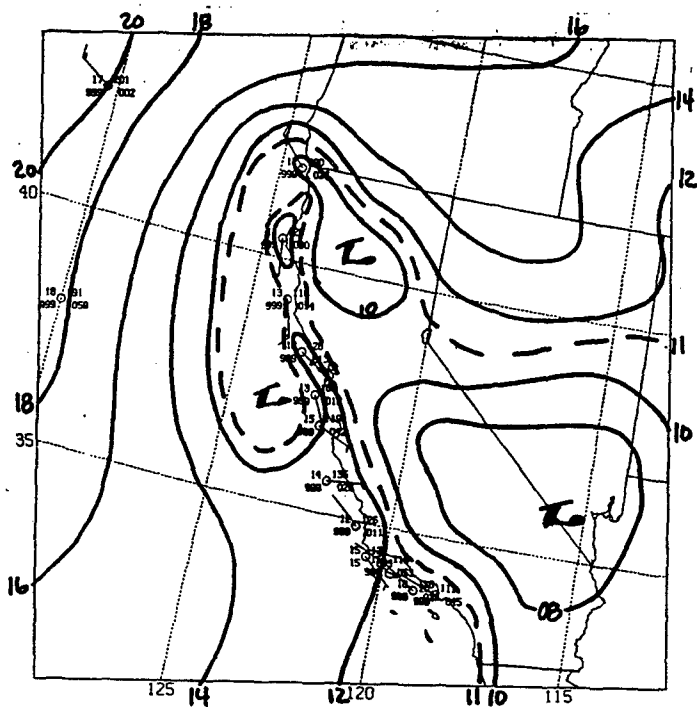


Figure 3.6 (cont.)

1800 UTC - 02 SEPTEMBER 1996



0000 UTC - 03 SEPTEMBER 1996

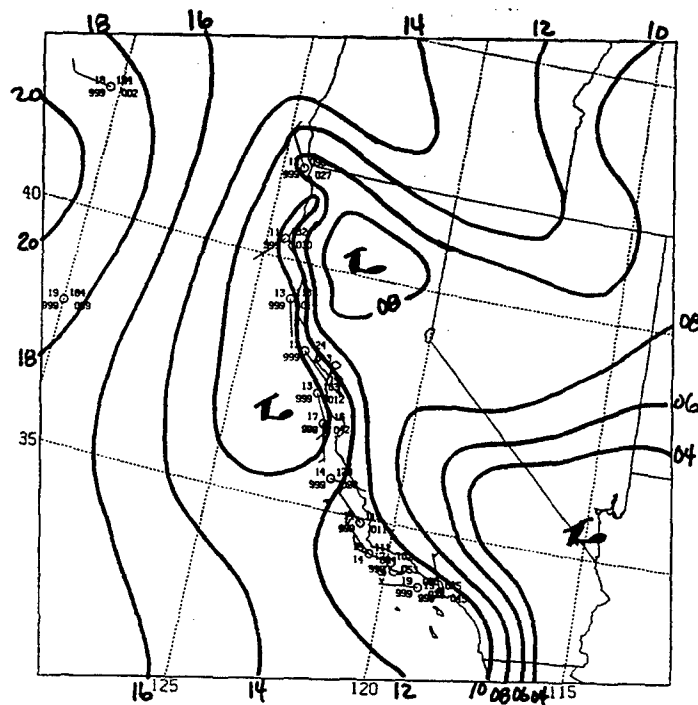
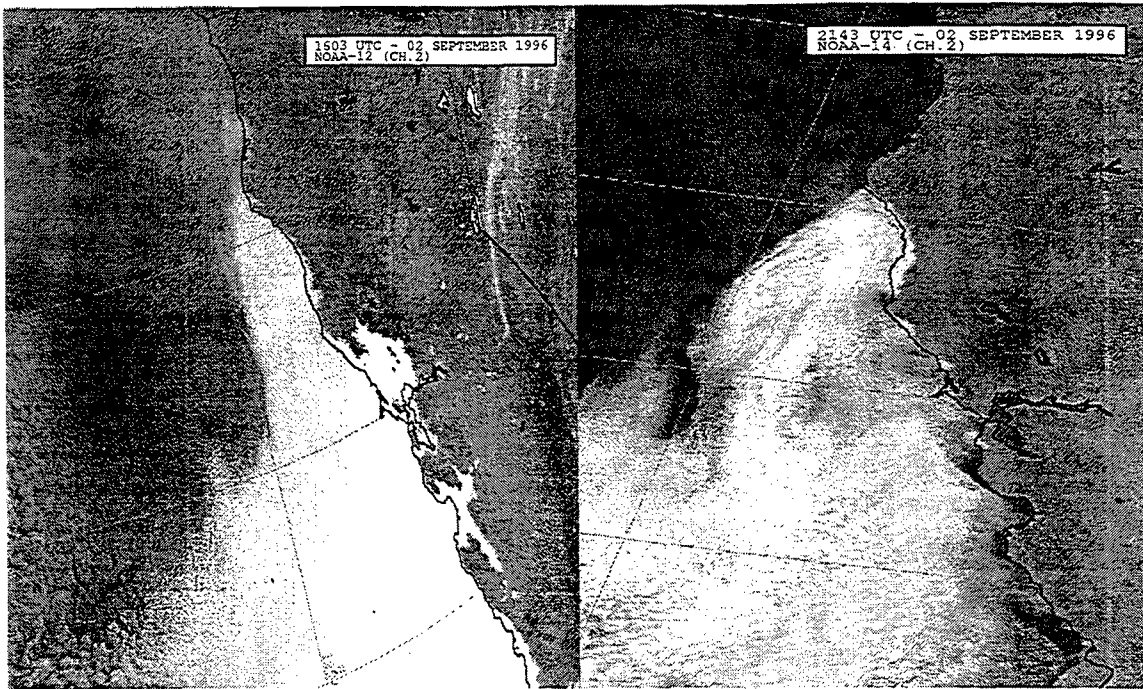


Figure 3.6 (cont.)





**Figure 3.7.** Satellite imagery from NOAA polar orbiting satellites for the 01-04 September 1996 coastally trapped wind reversal. Horizontal horizontal resolution is 1.1 km



**Figure 3.7 (cont.)**

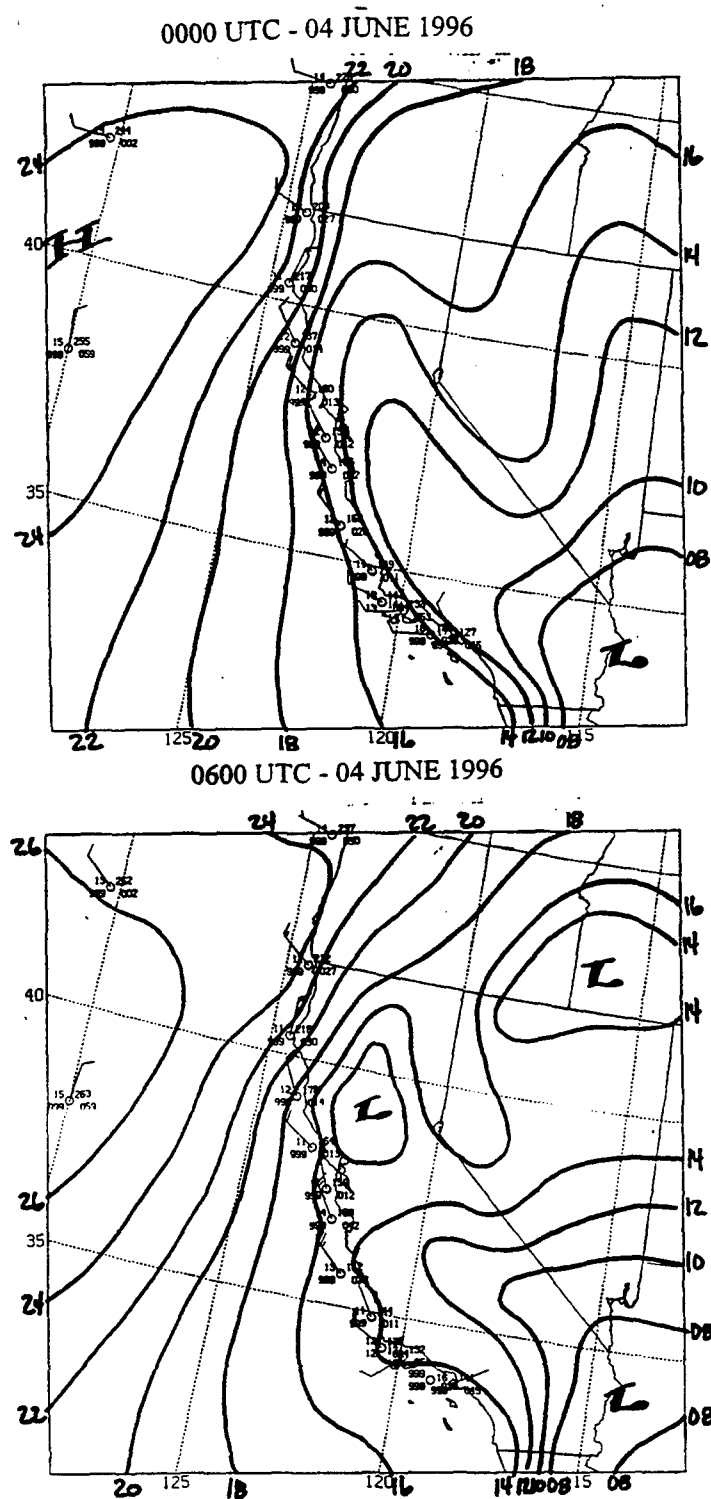
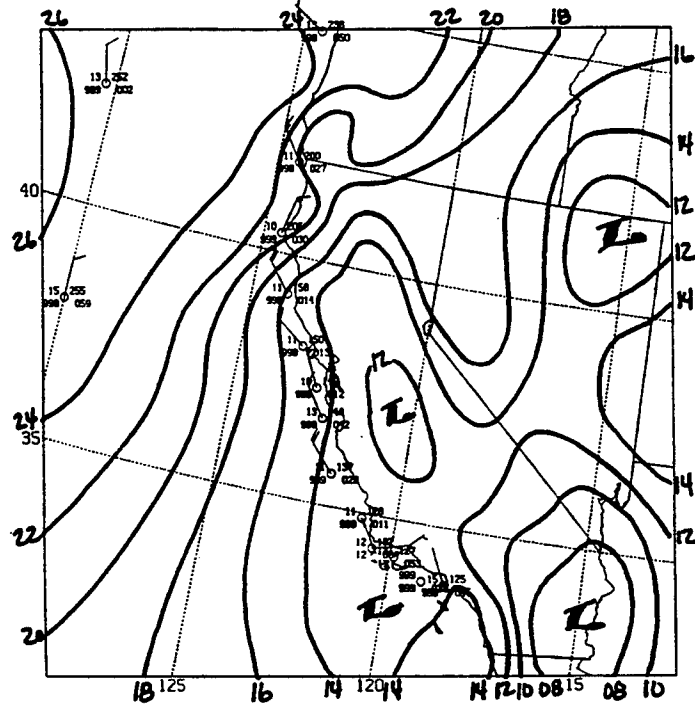


**Figure 3.8.** Surface evolution for 04-07 June 1996 as depicted by hand-drawn analyses of sea-level pressure. Contour interval is 2 mb.

1200 UTC - 04 JUNE 1996



1800 UTC - 04 JUNE 1996

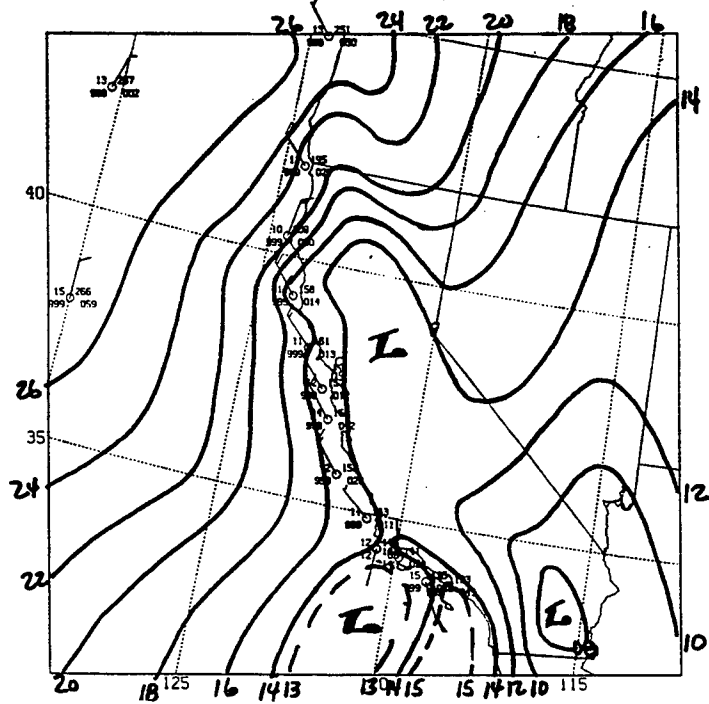
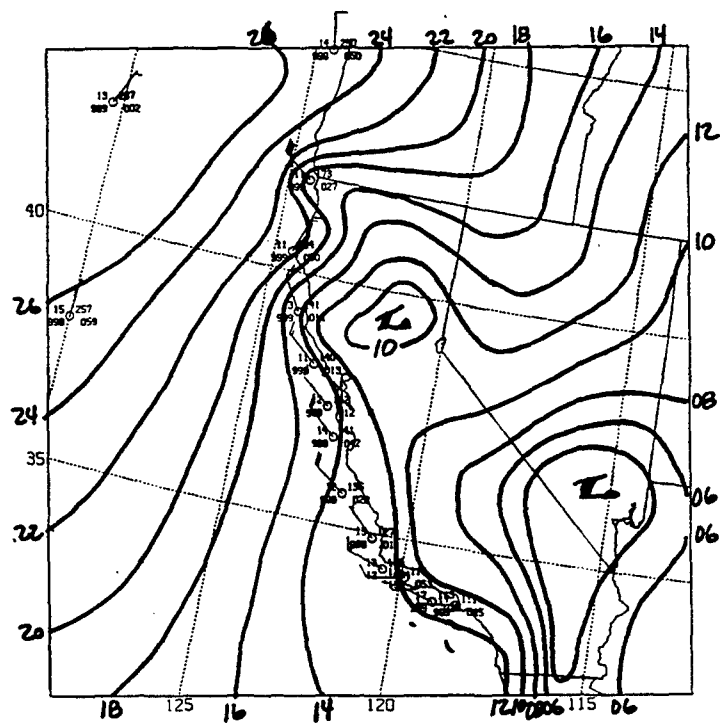


Figure 3.8 (cont.)

0000 UTC - 05 JUNE 1996



0600 UTC - 05 JUNE 1996

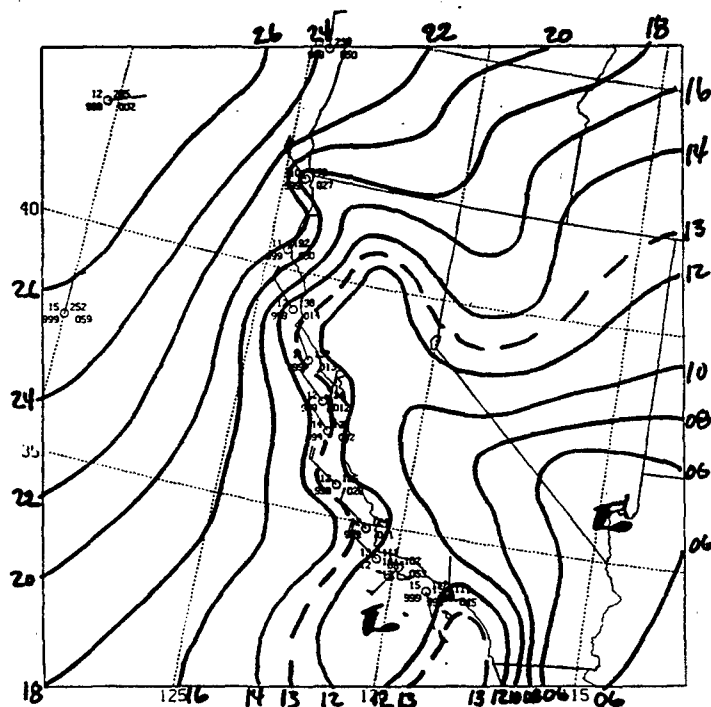
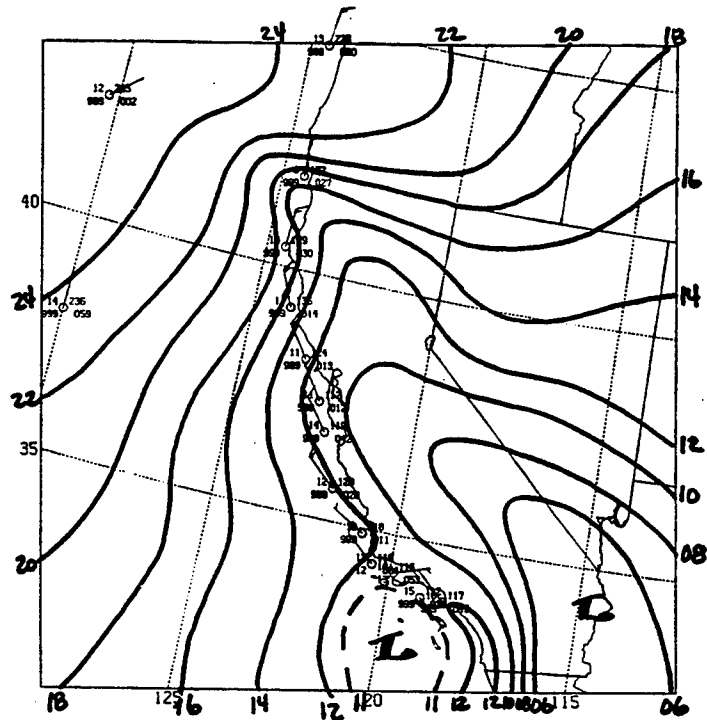


Figure 3.8 (cont.)

1200 UTC - 05 JUNE 1996



1800 UTC - 05 JUNE 1996

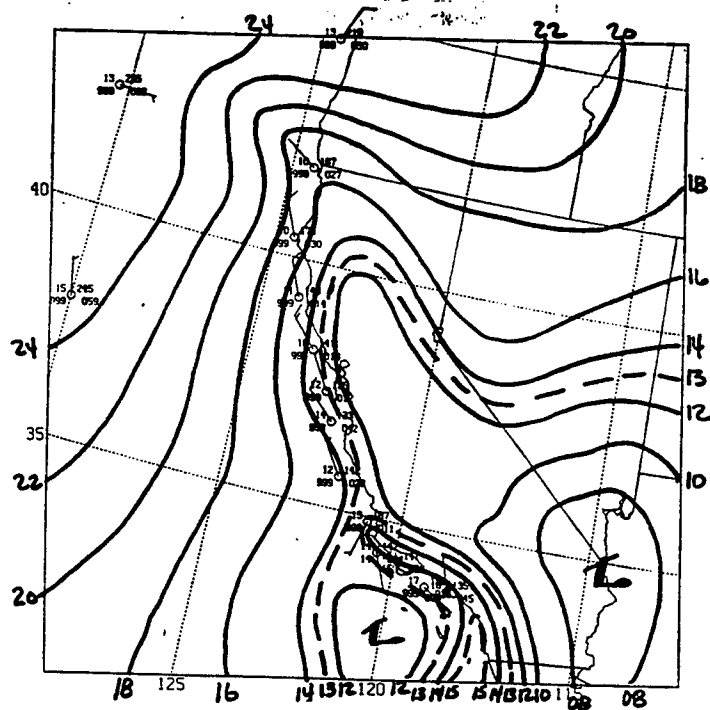


Figure 3.8 (cont.)

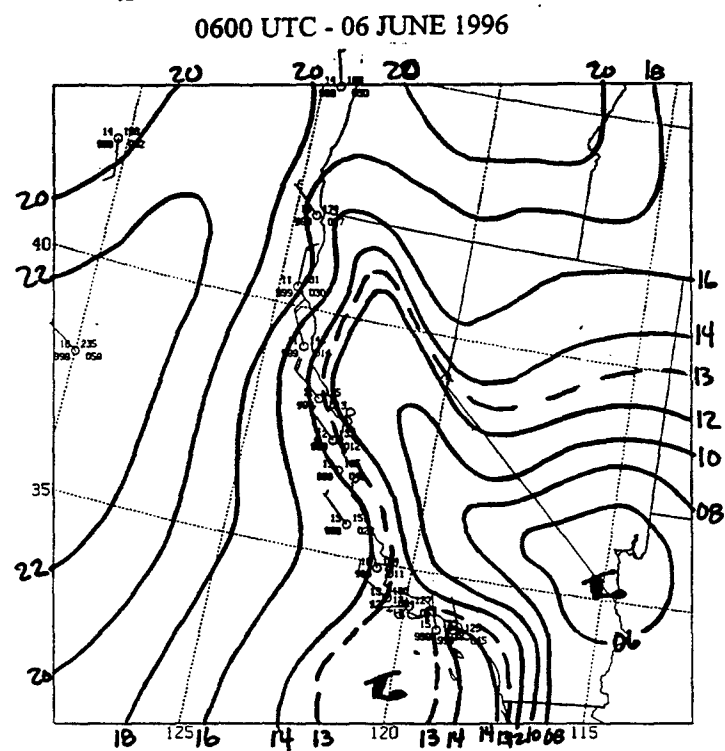
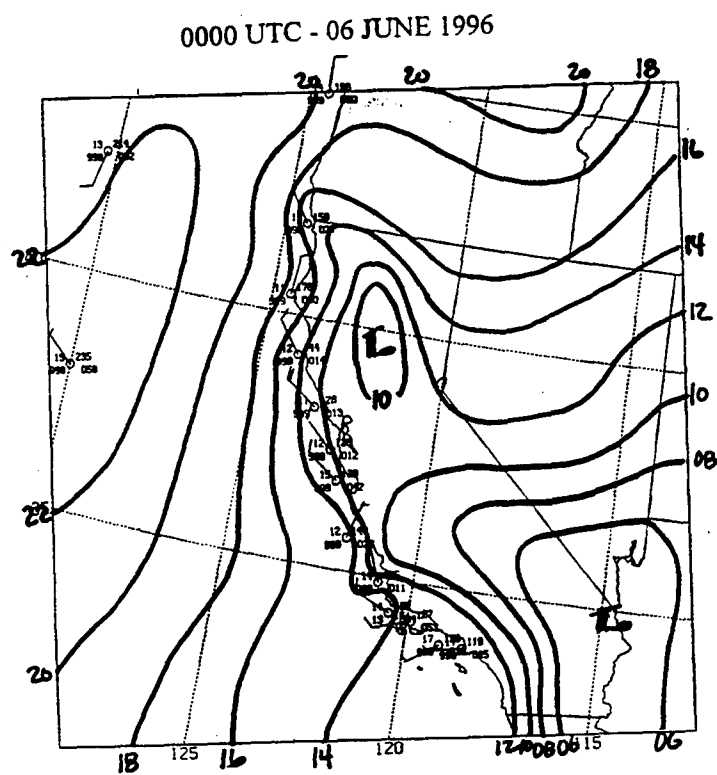
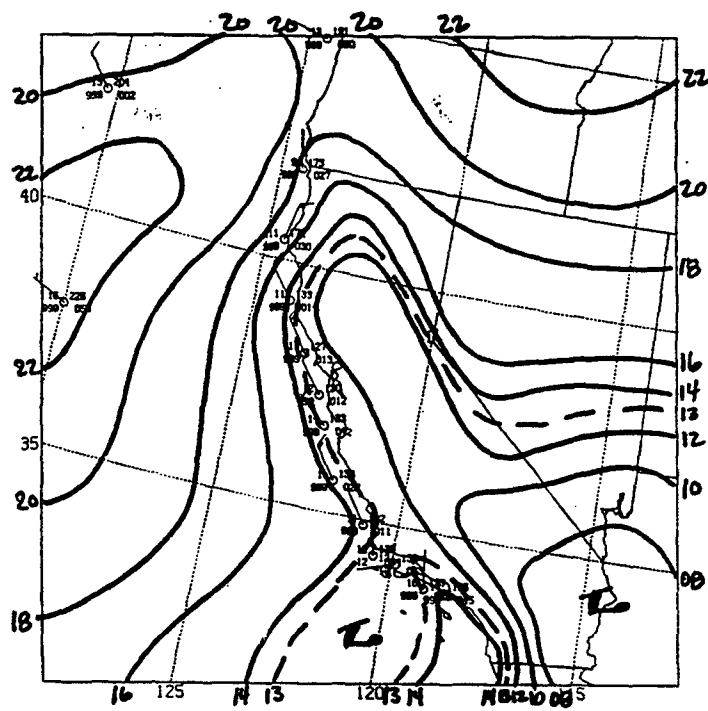


Figure 3.8 (cont.)

1200 UTC - 06 JUNE 1996



1800 UTC - 06 JUNE 1996

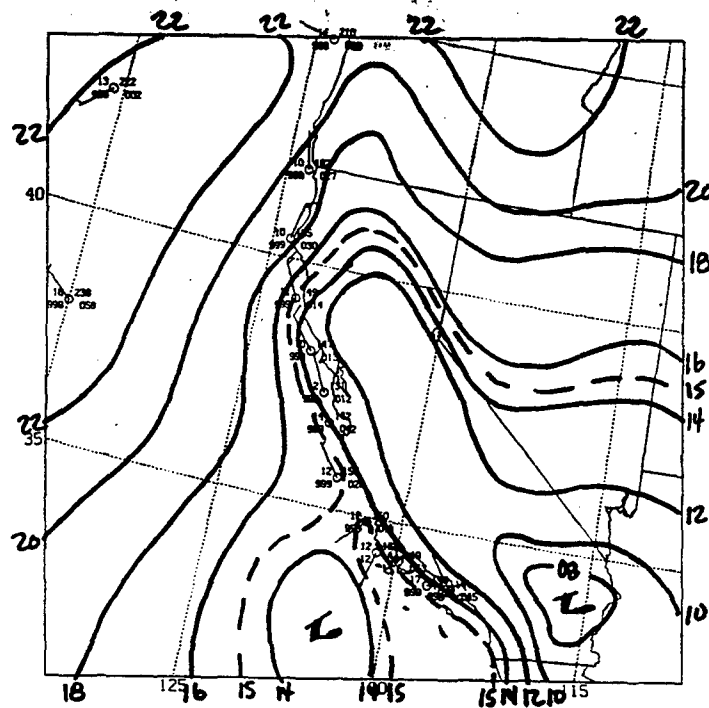


Figure 3.8 (cont.)



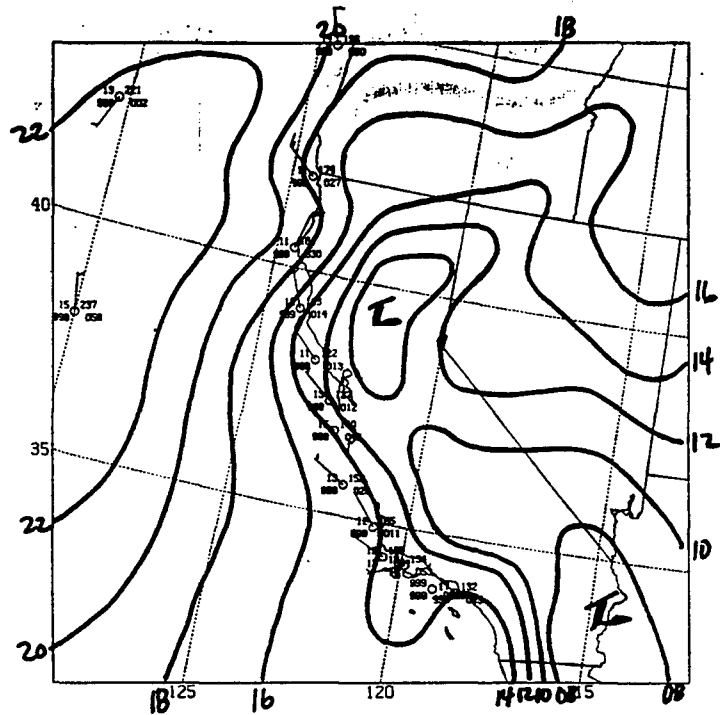
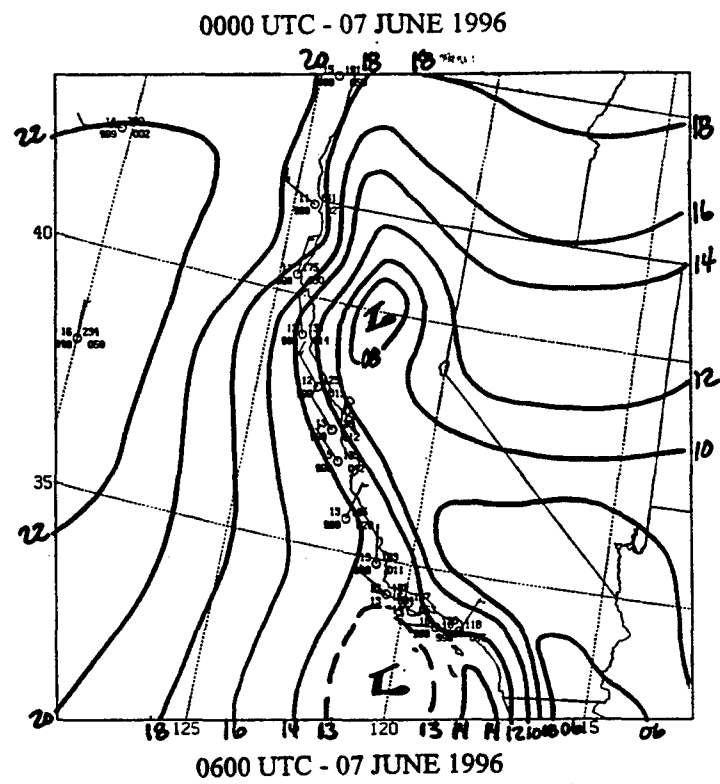
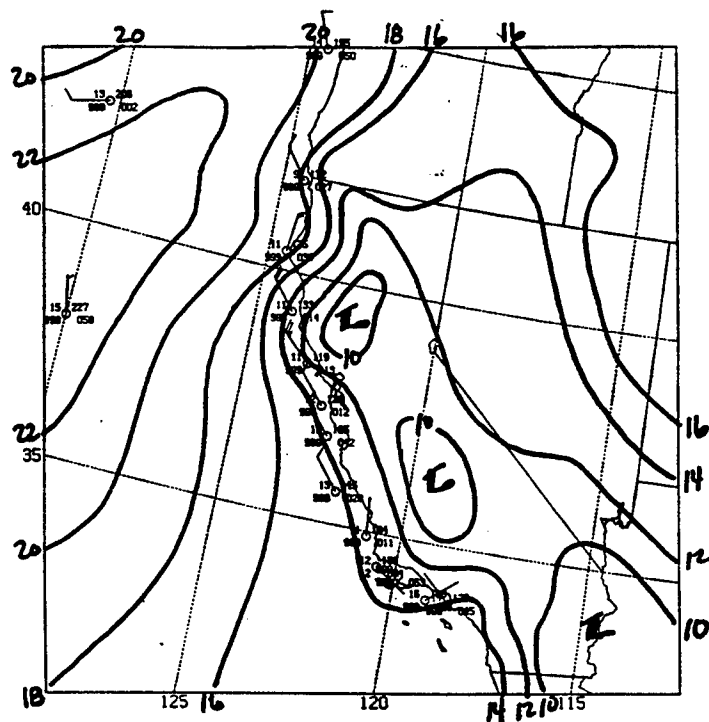


Figure 3.8 (cont.)

1200 UTC - 07 JUNE 1996



1800 UTC - 07 JUNE 1996

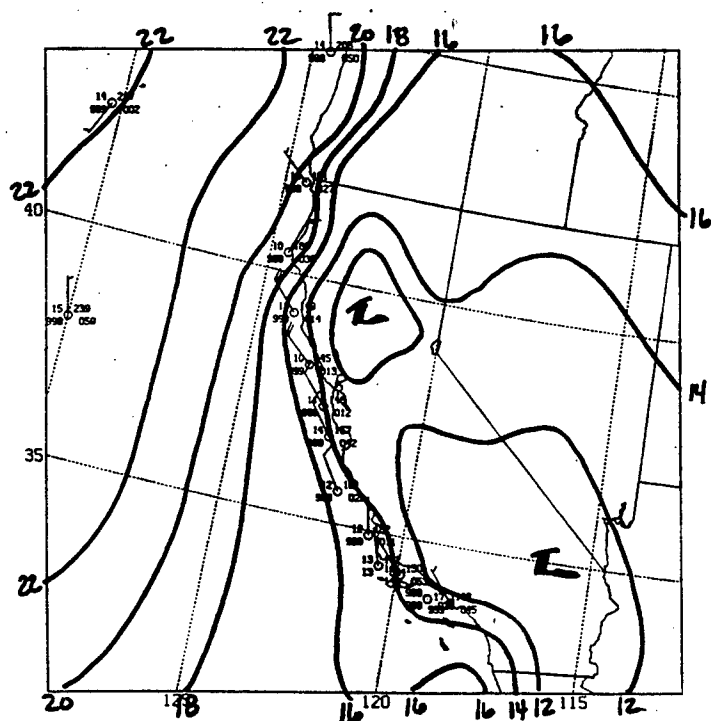
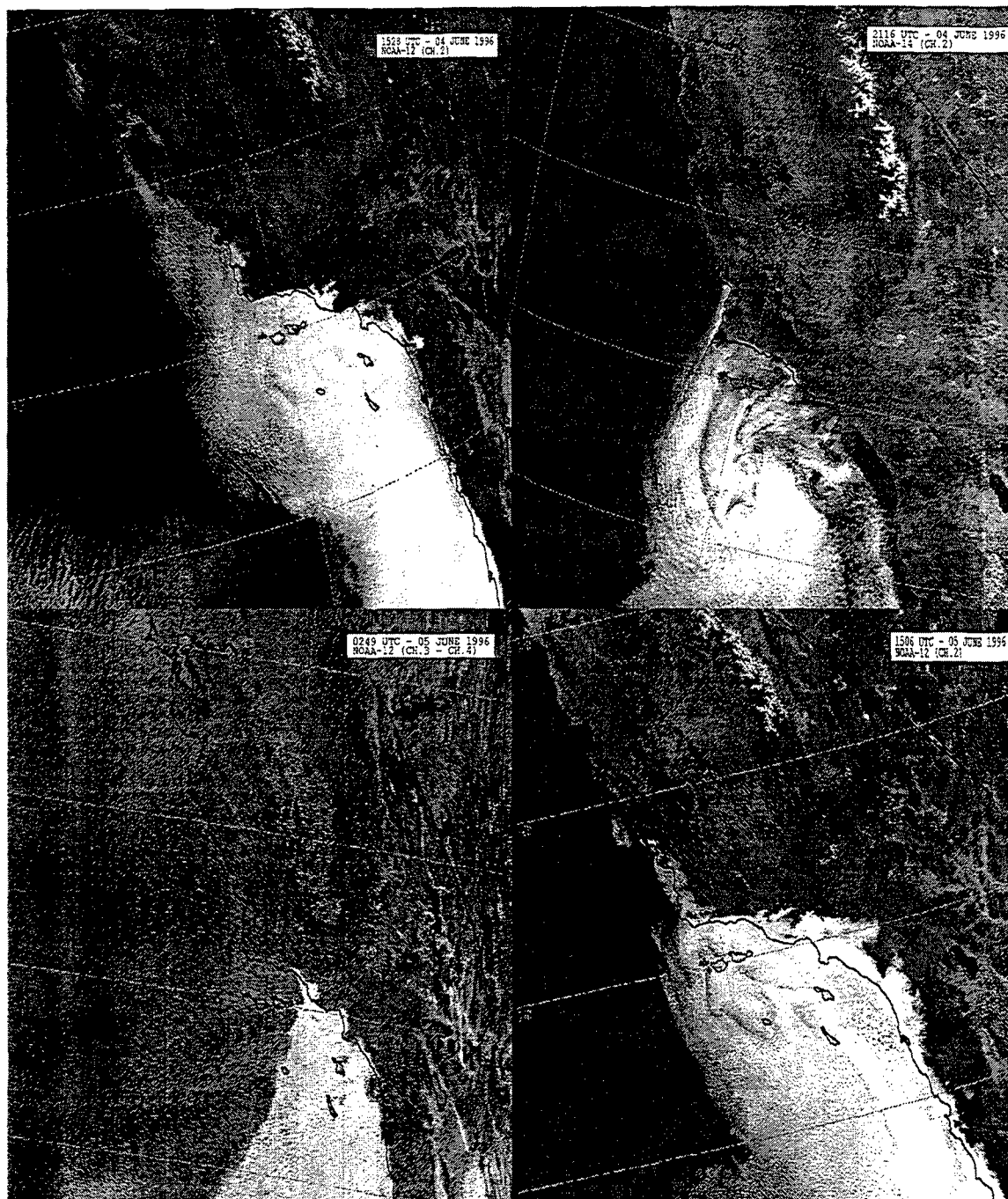
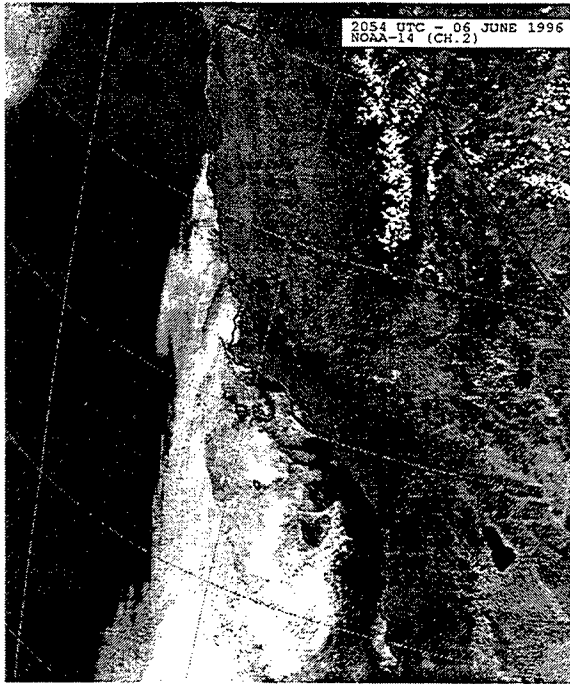


Figure 3.8 (cont.)



**Figure 3.9.** Satellite imagery from NOAA polar orbiting satellites for the 04-06 June 1996. Horizontal horizontal resolution is 1.1 km.



**Figure 3.9 (cont.)**

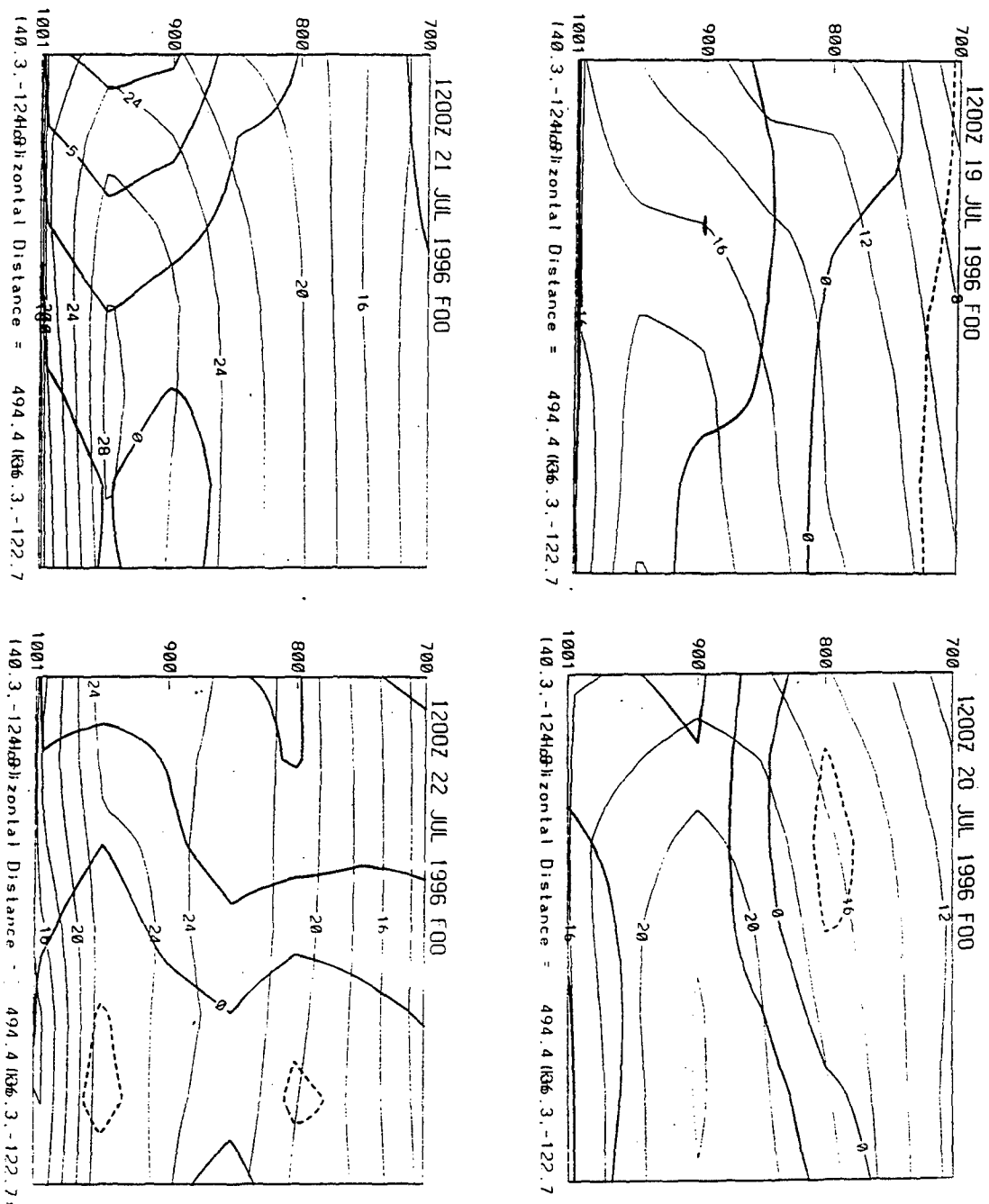


**Figure 3.10.** Along-coast vertical cross sections of the cross-coast wind component (thicker lines) and temperature for the 21-24 July 1996 coastally trapped wind reversal. Contour intervals are 2.5 m/s and 2° C respectively. Negative values (dashed lines) indicate for the cross-coast wind component indicate an onshore direction.

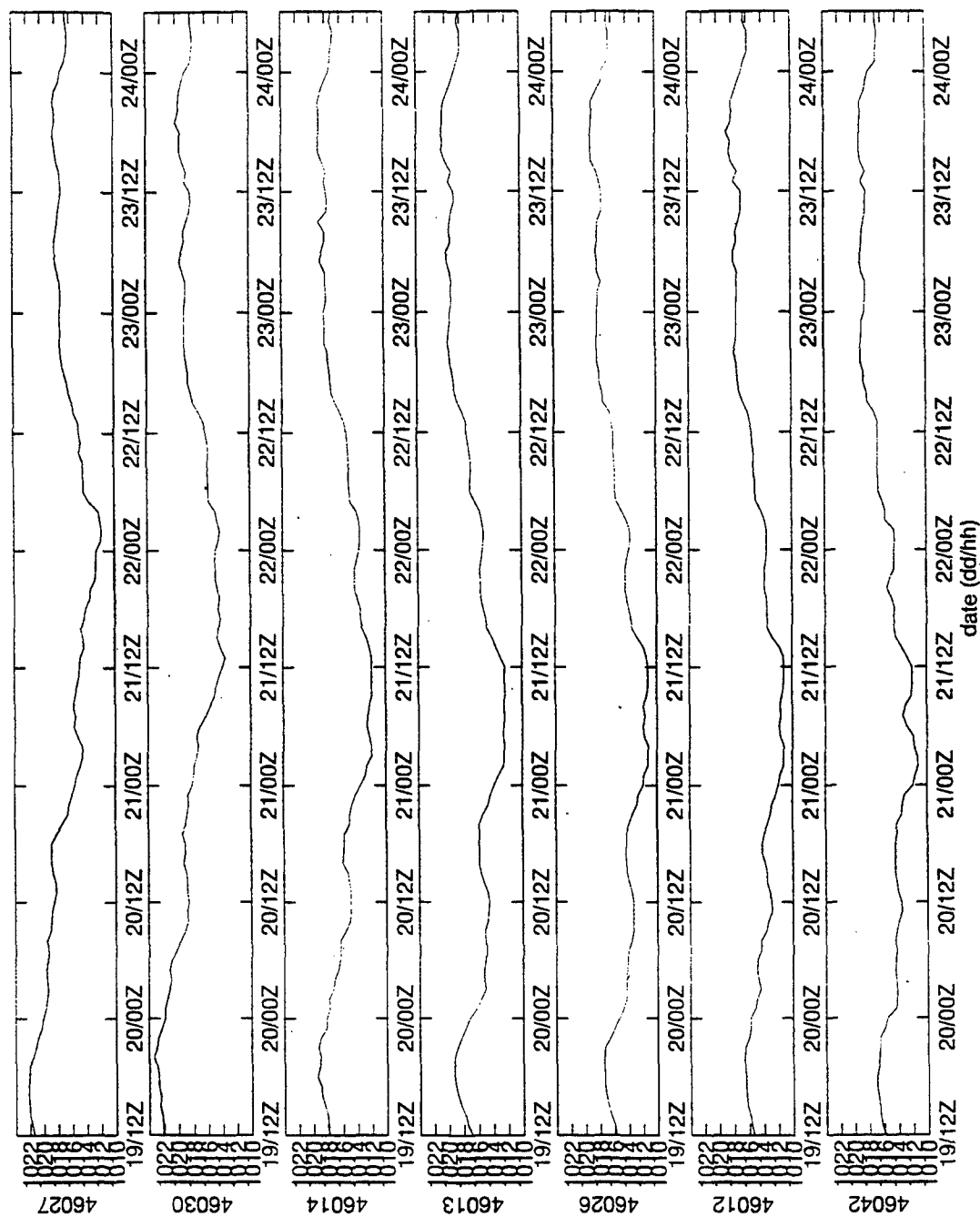


**Figure 3.11.** A time series of sea-level pressure for the moored coastal buoys for the period from 1200 UTC 19 July to 0600 UTC 24 July. Units for sea-level pressure (y-axis) are millibars.

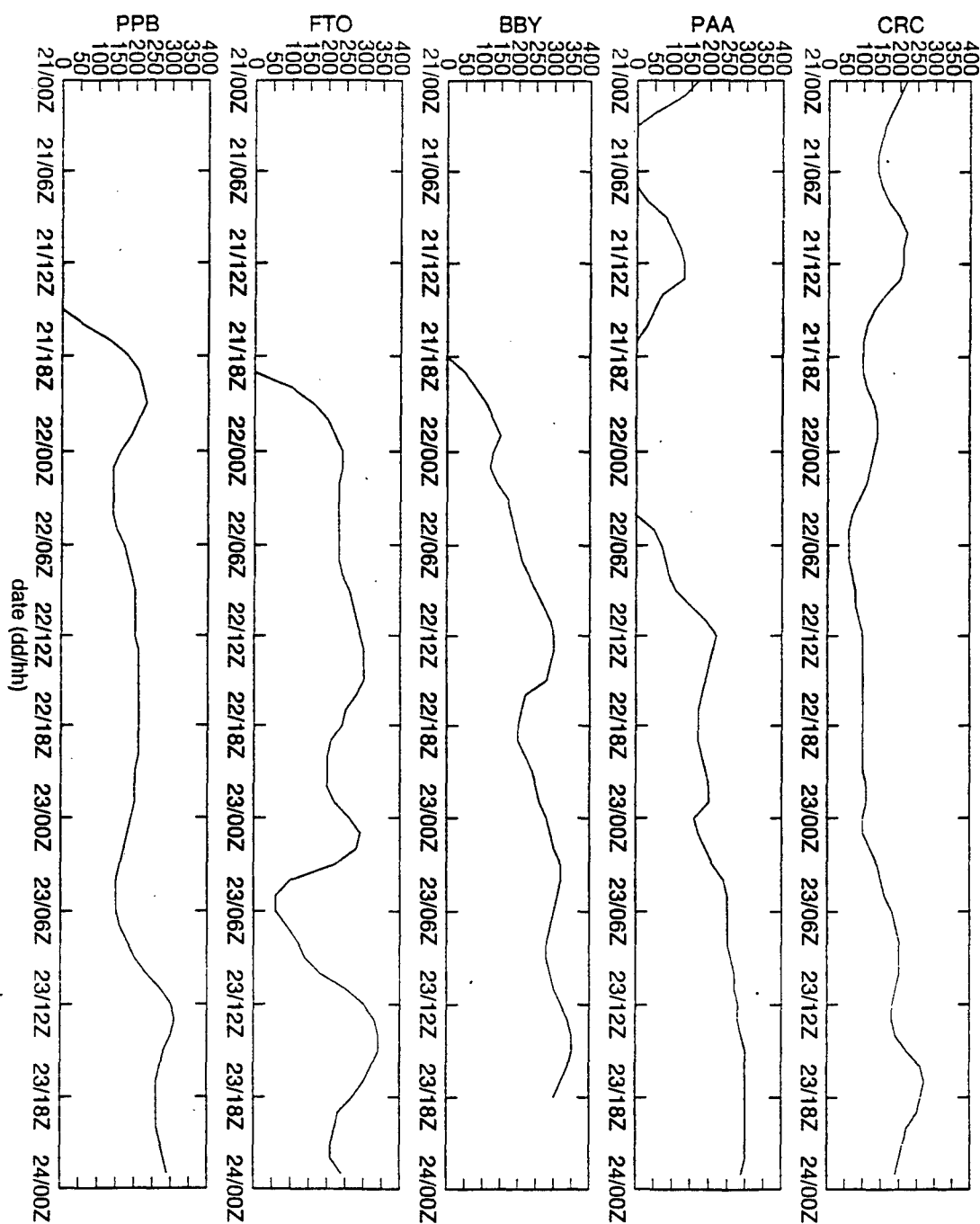


**Figure 3.12.** A time series of marine layer depth for the coastal wind profiler sites at Point Piedras Blancas (PPB), Monterey Bay (FTO), Bodega Bay (PPB), Point Arena (PAA), and Crescent City (CRC) for the period from 0000 UTC 21 July to 2300 UTC 23 July. Units for the marine layer depth (y-axis) are meters.

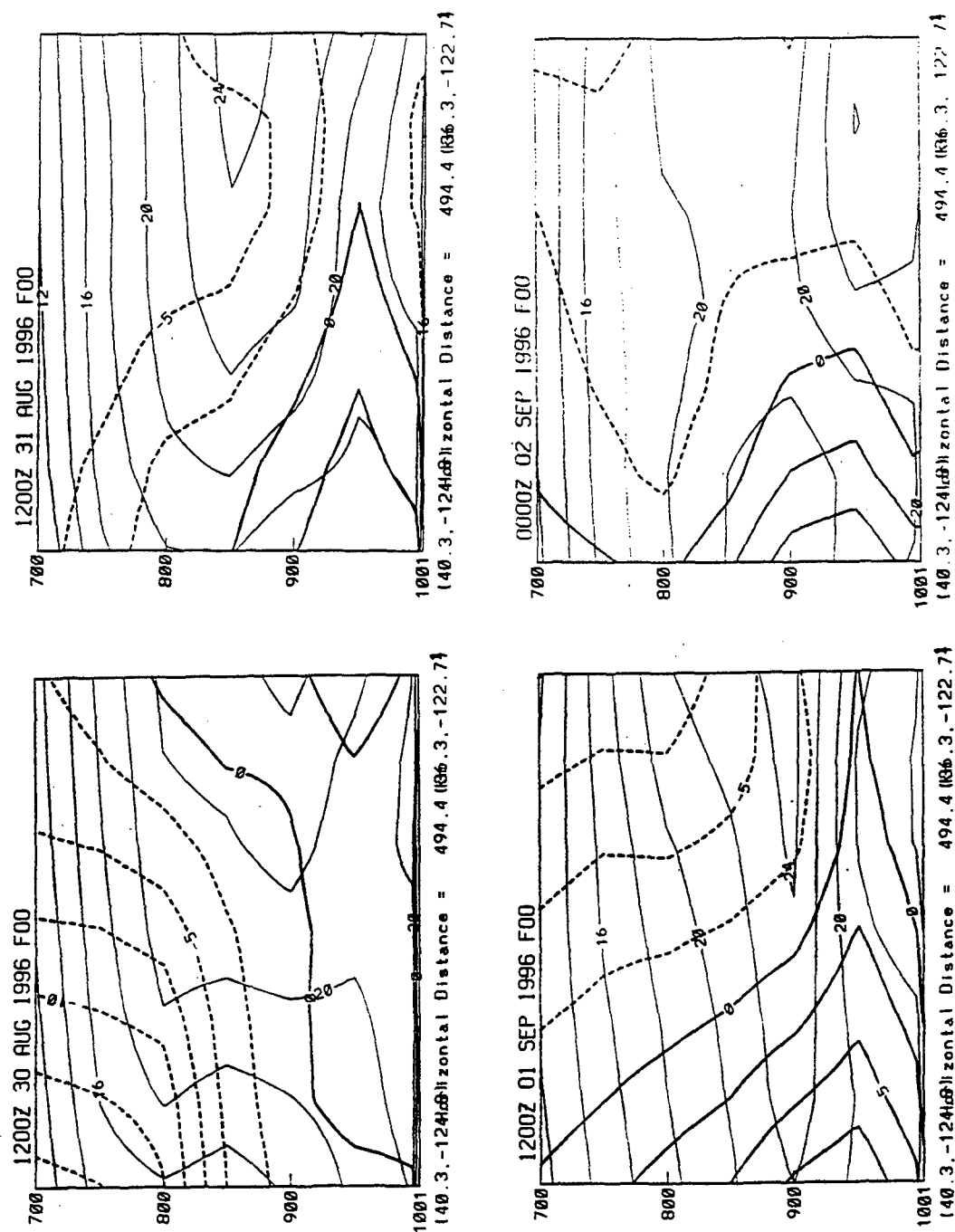


**Figure 3.13.** Along-coast vertical cross sections of the cross-coast wind component (dashed lines) and temperature for the 1-4 September 1996 coastally trapped wind reversal. Contour intervals are 2.5 m/s and 2° C respectively. Negative values (dashed lines) for the cross-coast wind component indicate an onshore direction.



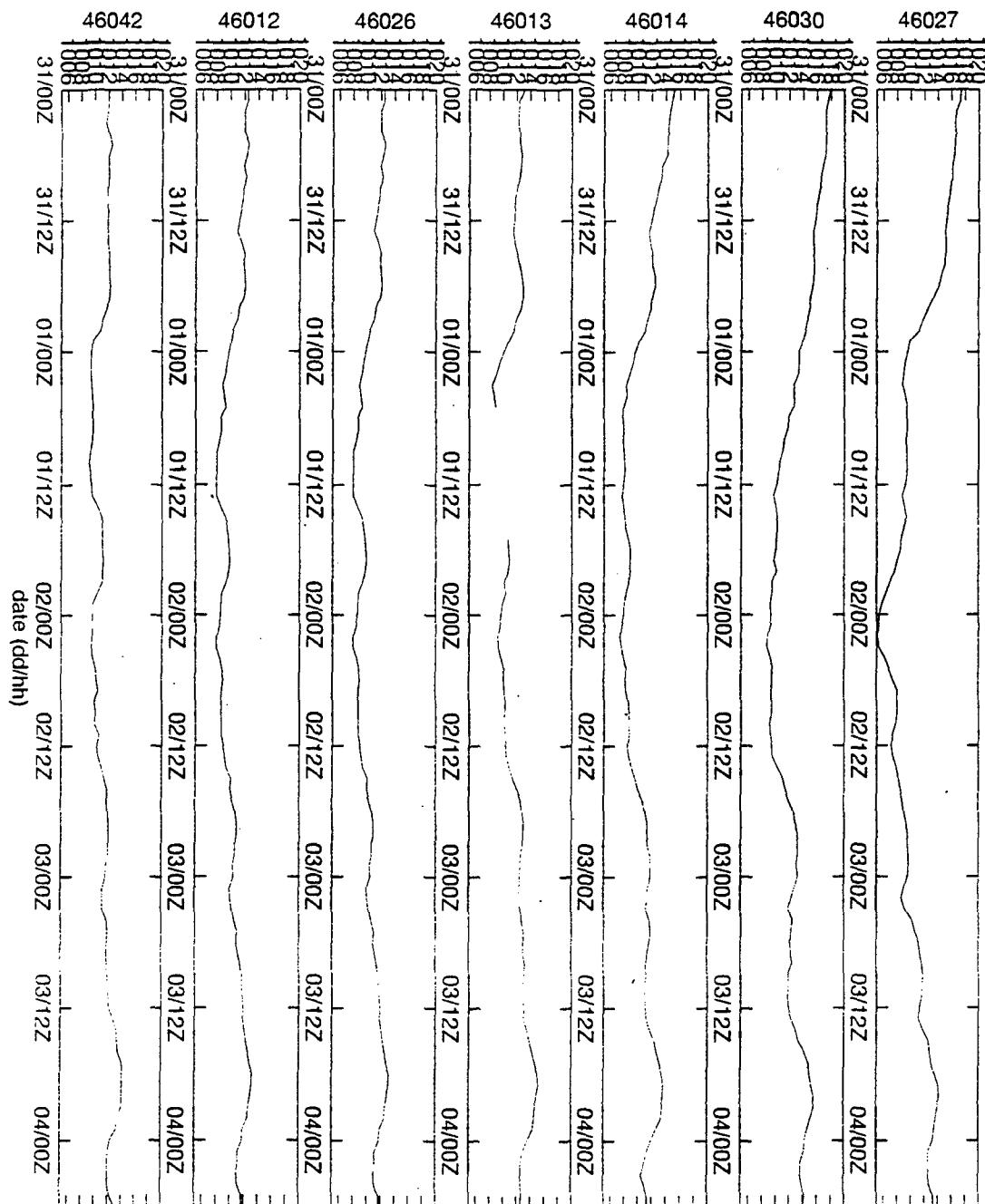


**Figure 3.14.** A time series of sea-level pressure for the moored coastal buoys for the period from 0000 UTC 31 August to 0600 UTC 04 September. Units for sea-level pressure (y-axis) are millibars.

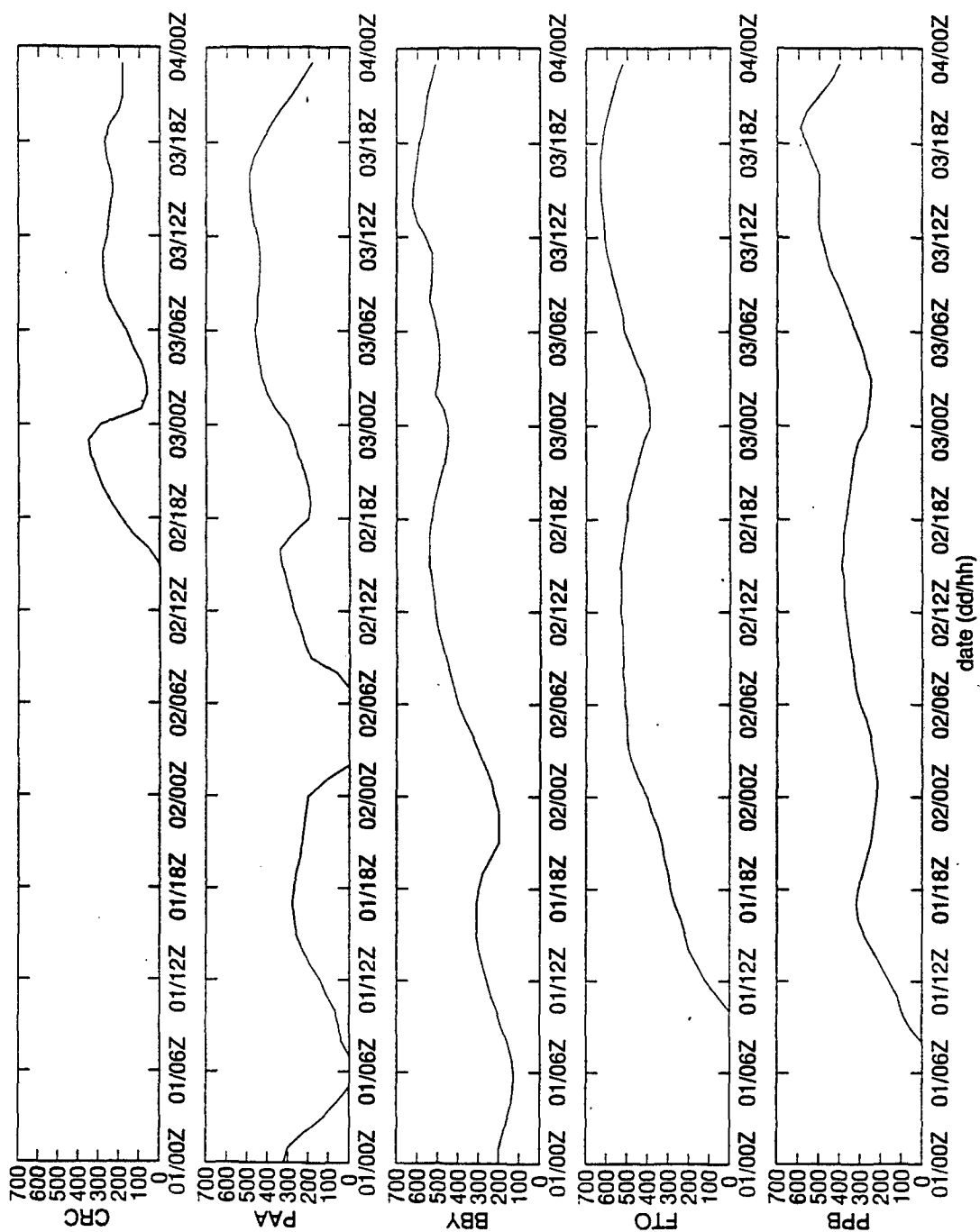


**Figure 3.15.** A time series of marine layer depth for the coastal wind profiler sites at Point Piedras Blancas (PPB), Monterey Bay (FTO), Bodega Bay (BBY), Point Arena (PAA), and Crescent City (CRC) for the period from 0000 UTC 01 September to 2300 UTC 03 September. Units for the marine layer depth (y-axis) are meters.

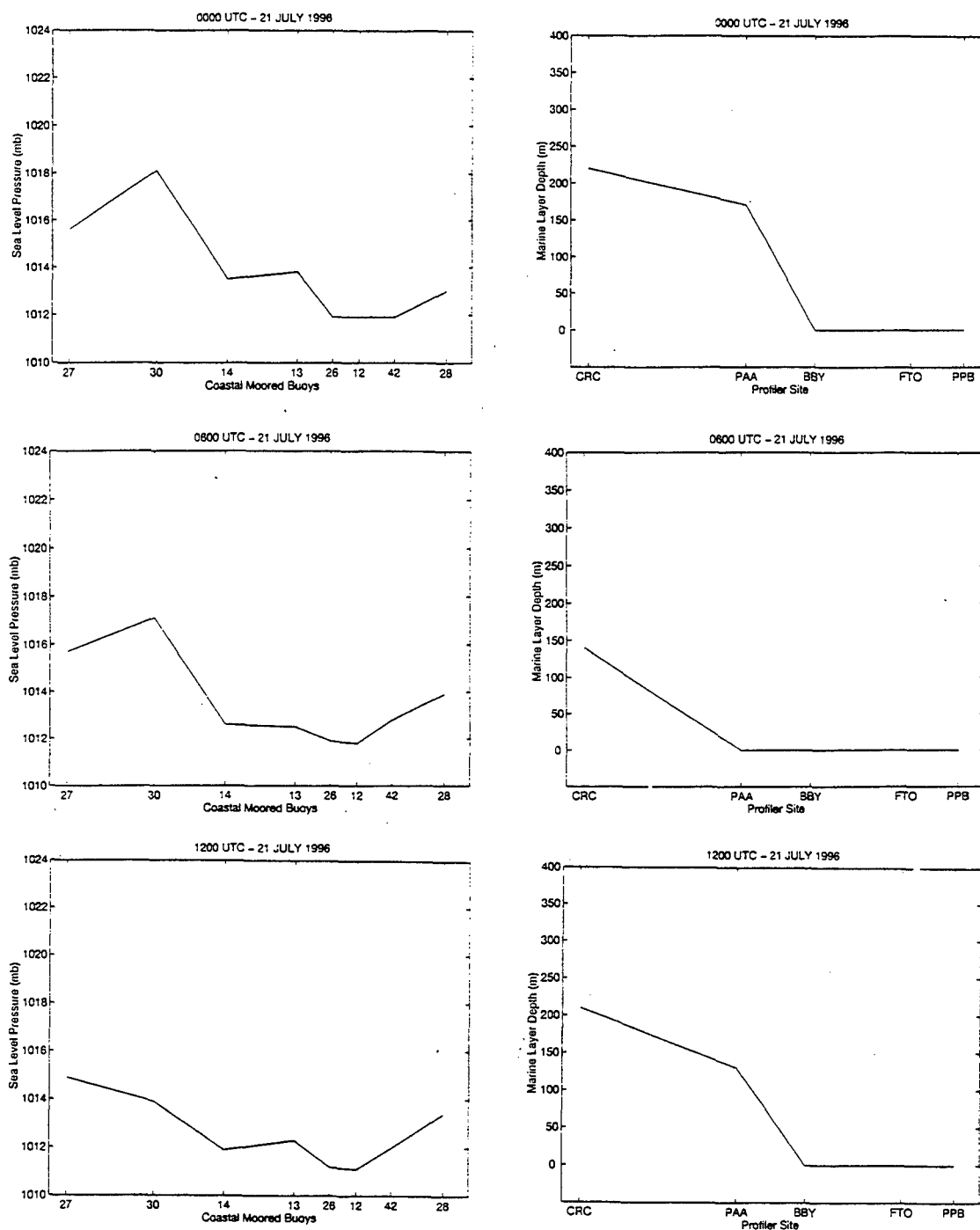


**Figure 3.16.** A series of along-coast depictions of sea-level pressure for the moored coastal buoys and marine layer depth for the coastal wind profiler sites for the 21-24 July 1996 coastally trapped wind reversal. Units for sea-level pressure and marine layer depth are millibars and meters, respectively.

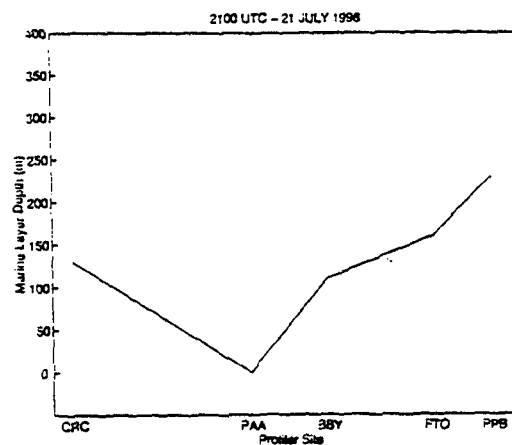
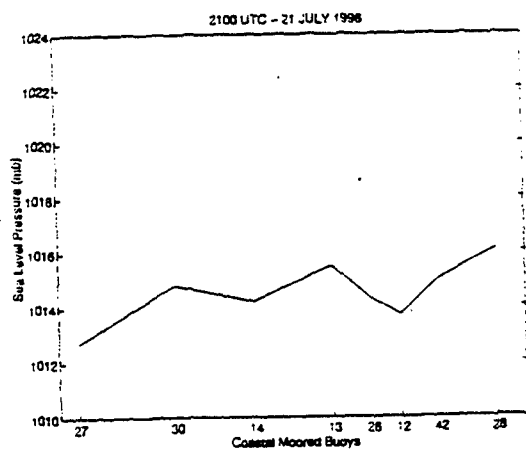
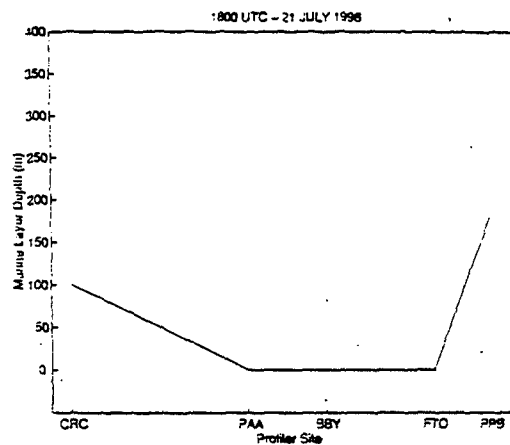
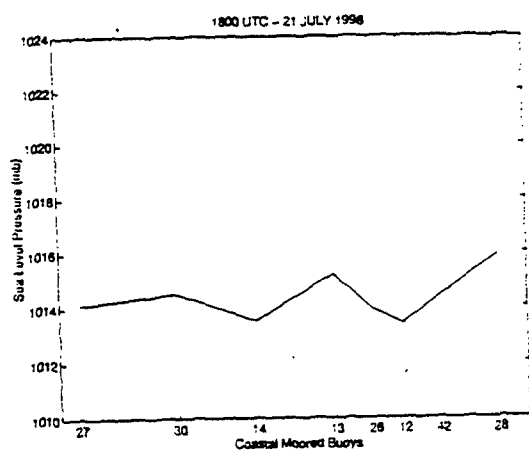
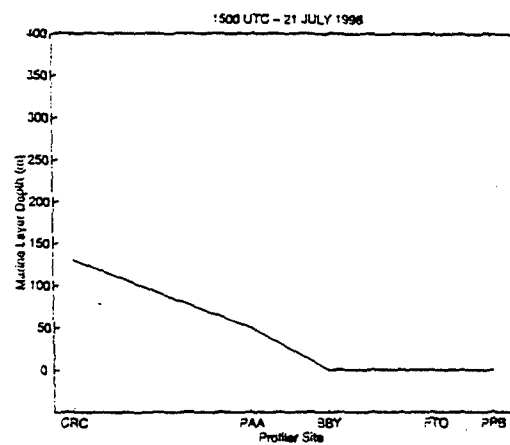
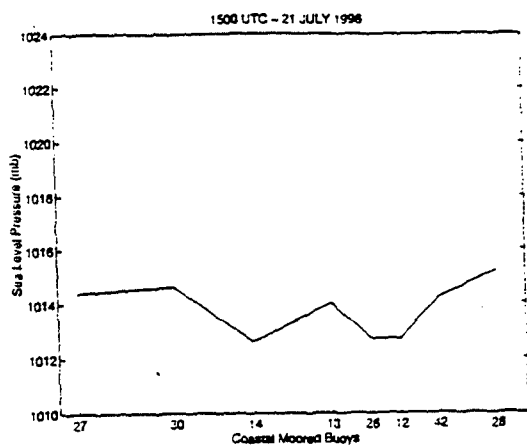


Figure 3.16 (cont.)

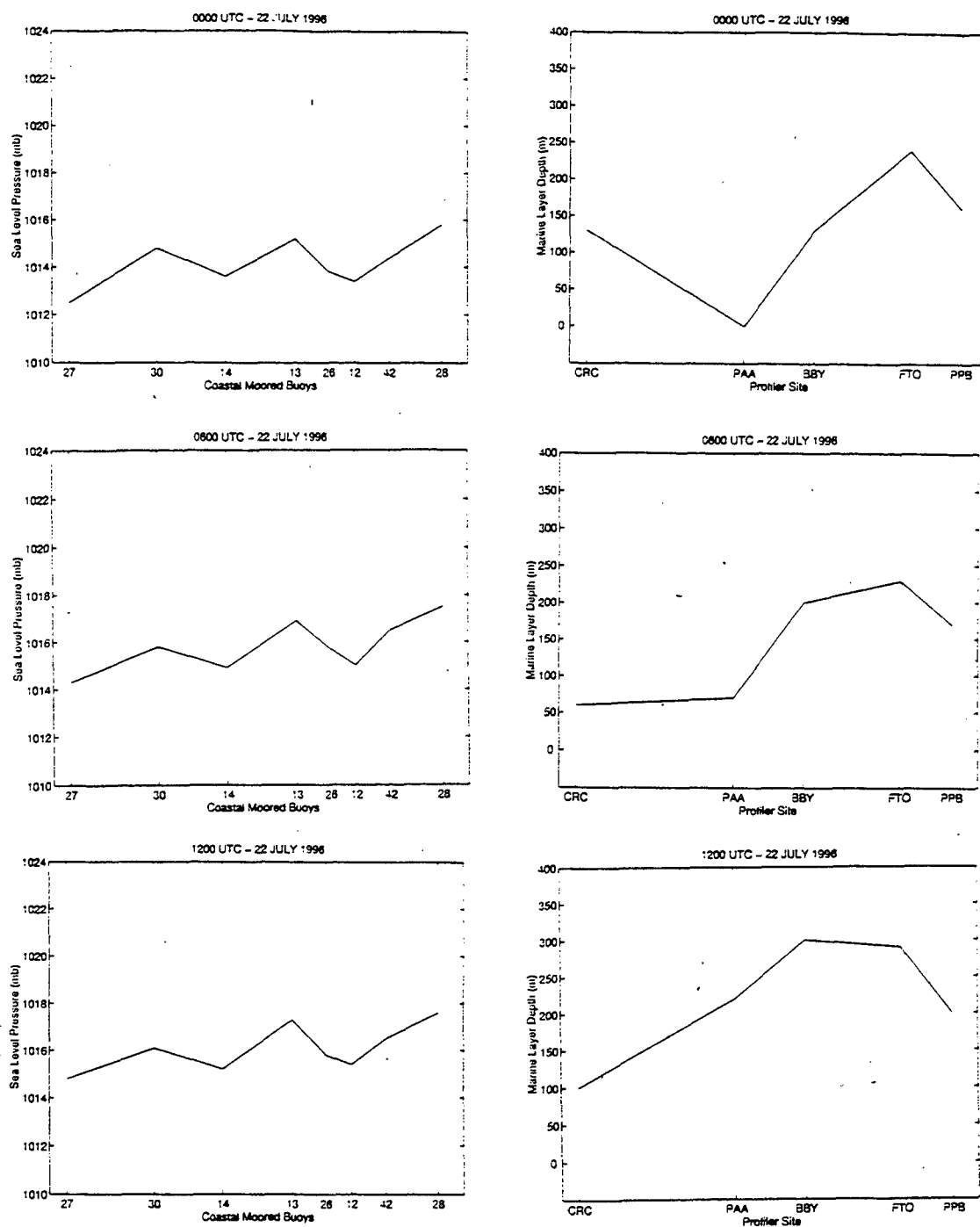
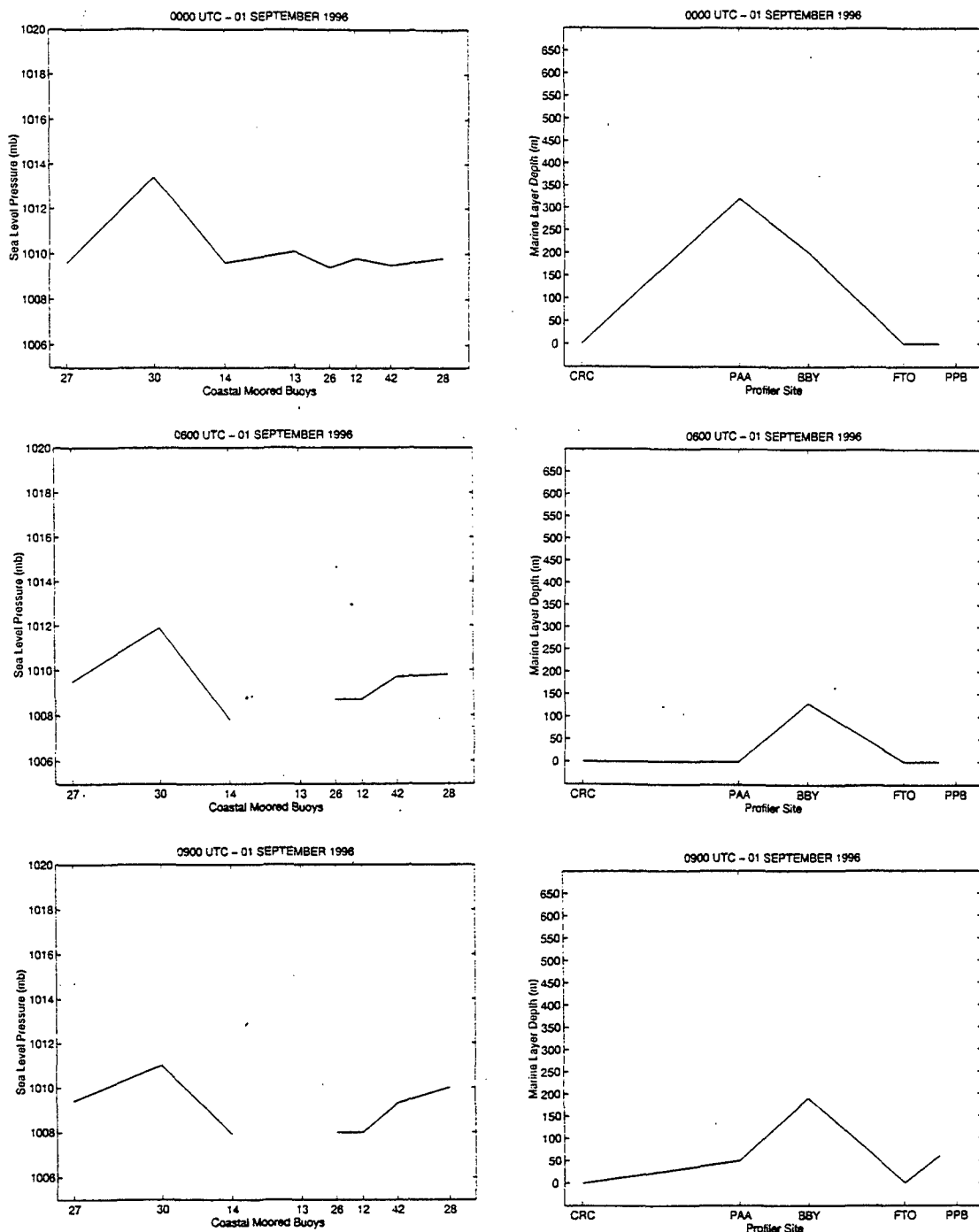


Figure 3.16 (cont.)



**Figure 3.17.** A series of along-coast depictions of sea-level pressure for the moored coastal buoys and marine layer depth for the coastal wind profiler sites for the 1-4 September 1996 coastally trapped wind reversal. Units for sea-level pressure and marine layer depth are millibars and meters, respectively.

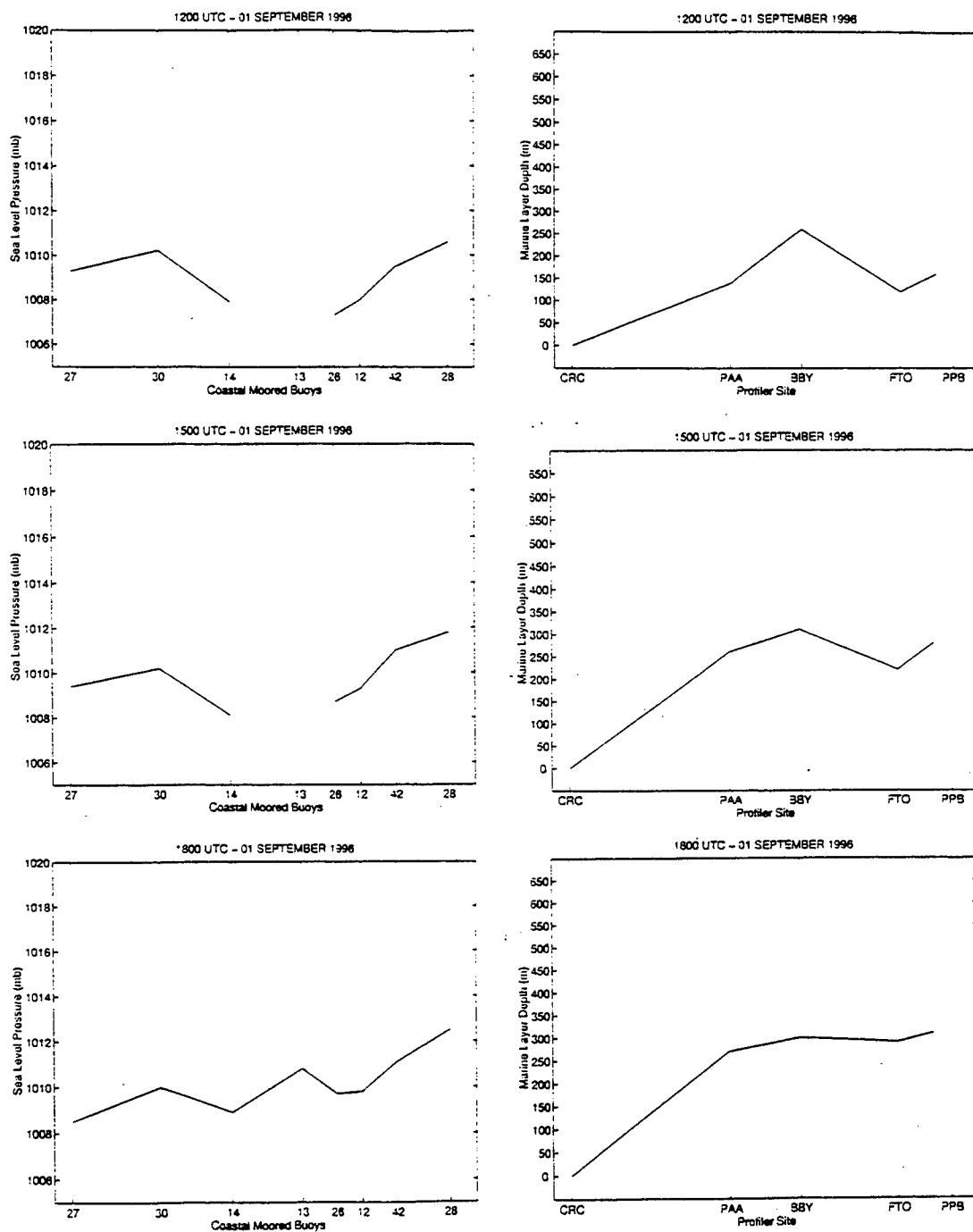


Figure 3.17 (cont.)

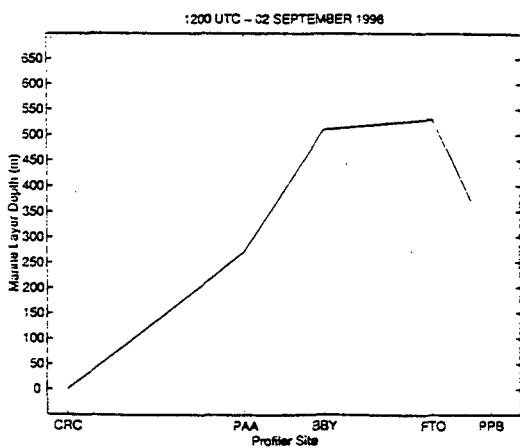
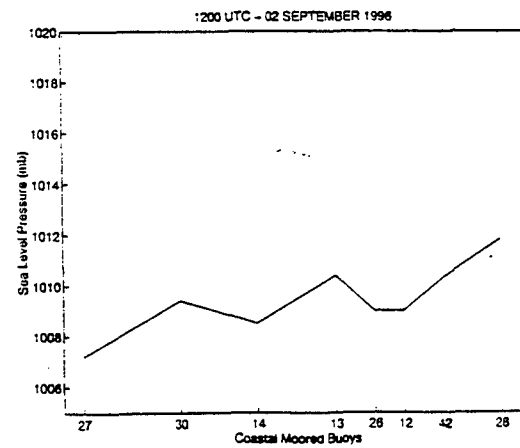
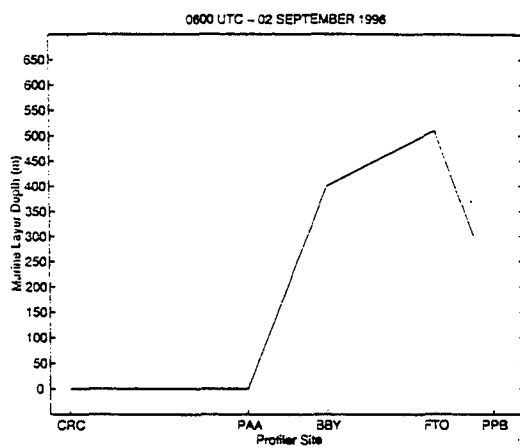
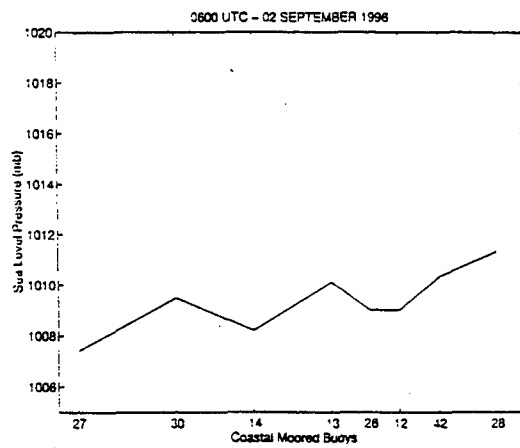
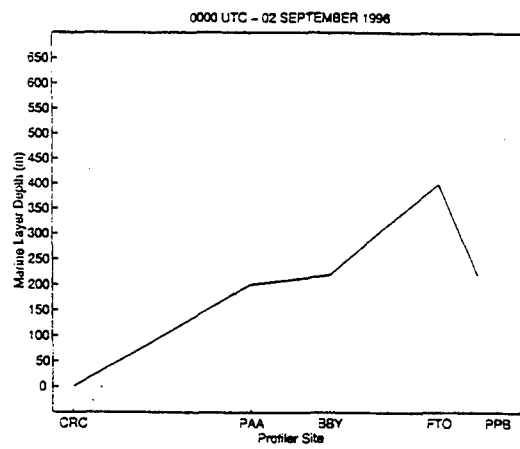
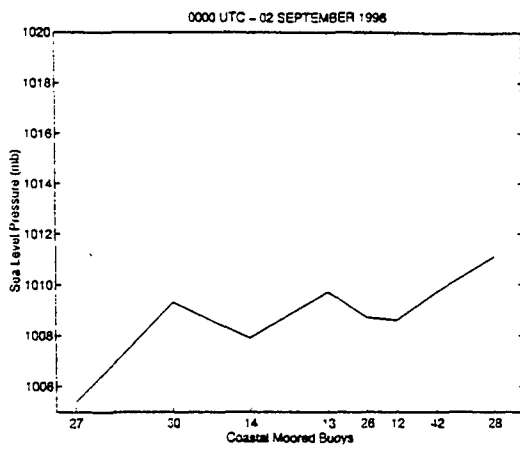


Figure 3.17 (cont.)



#### IV. SUMMARY AND CONCLUSIONS

The present study has examined three cases from a field experiment in 1996 that appear to have the characteristics of a CTWR. Each case was analyzed to determine the associated synoptic-scale forcing and the respective mesoscale structures. The observed synoptic-scale forcing was compared with the results of a climatological study conducted by Mass and Bond (1996). Results of a modeling study by Skamarock et al. (1998) were used to create a conceptual model for comparison with the observed evolution of the mesoscale structure of each case. Results of this study showed that only two cases, July and September, can be classified as CTWRs. Although the June case did appear to possess some characteristics of a CTWR, this case is more correctly classified as a Catalina Eddy event.

The study showed that variability does exist in the synoptic-scale forcing associated with a CTWR. A common feature, found in both the July and September events, was the atmospheric warming that occurred over the U.S. west coast. The synoptic-scale forcing, which produced the warming, occurs in different ways in the two cases. In the July event, synoptic-scale warm advection from the south occurs over the western U.S. with a building ridge in the mid-troposphere and developing thermal trough in the lower troposphere. This scenario differs from the Mass and Bond composites, which indicate a building ridge over the eastern Pacific in the mid-troposphere (500 mb). In the September event, the atmospheric warming occurs as a result of a subsidence

associated with a building ridge in the mid-troposphere over the eastern Pacific. The subsidence that occurs in the northwesterly flow ahead of the ridge appears to be responsible for the warming in the lower troposphere. This warming occurs over the coast, and results in thermal troughing lower troposphere along the California coast. This pattern more closely resembles the Mass and Bond composites at 500 mb.

Another key aspect for the initiation of CTWR is the development of offshore flow (dynamic forcing) in the lower troposphere. In the July event, a building ridge over the Pacific Northwest and thermal troughing over inland California in the lower troposphere produce a geopotential height pattern, which results in offshore flow at 850 mb over northern California. The offshore flow interacts with the coastal topography, and results in the advection of warm air offshore, the westward movement of the thermal trough across the coast, and the relaxation the along-coast pressure gradient. This synoptic-scale evolution in the lower troposphere closely resembles that found in the Mass and Bond composites at 850 mb and the surface. Although a weak ridge also builds over the Pacific Northwest in the lower troposphere during the September case, offshore flow does not develop in the lower troposphere along the northern California coast until after the movement of the thermal trough across the coast. This sequence of events in the September case suggests that the offshore flow at 850 mb is primarily the result of the cyclonic flow around the thermal trough at the coast rather than ridging over the Pacific Northwest. No indications were found of any westward advection of warm air across the coast in the lower troposphere as in the July event.

Once the atmosphere along the coast is warmed and offshore flow is established in the lower troposphere, the evolution of the offshore mesoscale low and initiation of the CTWR for the both July and September events are similar to the Skamarock et al. (1998) model. Many features of the Skamarock model are found in both events, including: (i) warming of the lower troposphere over the coast; (ii) offshore migration of the coastal northerly jet; (iii) suppression or offshore displacement of the marine layer; (iv) development of the offshore mesoscale low; and (v) development of southerly flow along the coast on the east side of the mesoscale low. However, the initiation of the September CTWR appears to be much more synoptically driven. For instance, the suppression or offshore displacement of the marine layer along the coast results from the passage of a short-wave trough rather than offshore flow. The thermal forcing that contributes to the development of the offshore mesoscale low appears to result from subsidence warming associated with a synoptic-scale ridge over the eastern North Pacific rather than offshore flow in the lower troposphere as in the July event.

The propagation characteristics of both events appear to be at least partially influenced by the duration and movement of the synoptic-scale forcing. The July event propagates farther north than the September event, and can be attributed to the fact that the synoptic forcing shifts to the north and persists throughout the event. The synoptic forcing in the September is more progressive and breaks down much faster. The gradual surface southerly wind transition and initial propagation speed (6-7 m/s), and more uniform propagation of the July CTWR suggest that this event fits the Kelvin wave

interpretation. The initial rapid transition to southerly flow and less uniform propagation throughout the event suggest that the September CTWR fits the interpretation of an ageostrophic response to the along-shore pressure gradients produced by orography and the synoptic-scale flow as noted in past studies (Mass et al. 1986; Mass and Albright 1988; Overland and Bond 1994).

A reversal in the along-coast sea-level pressure and marine layer depth gradients occurs in both cases and contribute to the initiation of the CTWRs. The reversal of the gradients in the September case is influenced to greater extent by the synoptic-scale flow than in the July event. Southerly flow is initially evident in layer from the surface to approximately 1200 m for both events. However, the depth of the layer of southerly flow for the September event decreases significantly (surface to 400 m) as this CTWR matures, and can be attributed to the progressive nature of the synoptic forcing.

Many competing ideas exist regarding the evolution and governing dynamics of CTWRs. This analysis of the July and September CTWRs reveals two distinct synoptic-scale forcing patterns that can result in the evolution of a CTWR and two interpretations of their governing dynamics. Since only two cases are examined here, it can not be concluded that only two types of forcing produce this mesoscale phenomenon. However, the results of this study do indicate that CTWRs can not be classified solely on a single type of synoptic-scale forcing or a single set of governing dynamics.

This study does provide a basis for further examination of past and future CTWRs based on these two scenarios. It is recommended that additional cases be examined based

on the synoptic-scale characteristics in these two events, and the subsequent mesoscale response in the lower troposphere. It is also recommended that aircraft data be collected over an area of probable CTWR development prior to the initiation of the actually CTWR.

## LIST OF REFERENCES

- Arakawa, A., and V. R. Lamb, 1977: Computational design of the basic dynamical processes of the UCLA general circulation model. *Methods in Computational Physics*, **17**, Academic Press, 173-265.
- Betts, A. K., and M. T. Miller, 1986: A new convective adjustment scheme. Part II: Single column tests using GATE wave, BOMEX, and arctic air-mass data sets. *Quarterly Journal of the Royal Meteorological Society*, **112**, 693-709.
- Black, T. L., 1988: The step-mountain eta coordinate regional model: A documentation. NOAA/NWS/NMC, 47 pp.
- Black, T. L., 1994: The new NMC mesoscale eta model: Description and forecast examples. *Weather and Forecasting*, **9**, 265-278.
- Bond, N. A., C. F. Mass, and J. E. Overland, 1996: Coastally trapped wind reversals along the United States West Coast during the warm season. Part 1: Climatology and temporal evolution. *Monthly Weather Review*, **124**, 430-445.
- DiMego, G. J., 1988: The National Meteorological Center Regional Analysis and Forecast System. *Monthly Weather Review*, **116**, 977-1000.
- Dorman, C. E., 1985: Evidence of Kelvin waves in California's marine layer and related eddy generation. *Monthly Weather Review*, **113**, 827-839.
- Dorman, C. E., 1987: Possible role of gravity currents in northern California's coastal summer wind reversals. *Journal of Geophysics Research*, **92**, 1497-1506.
- Dykes, J. D., 1991: Multispectral analysis of nighttime low clouds over the ocean. M.S. thesis, Naval Postgraduate School, 42 pp.
- Gerrity, J. P., Jr., T. L. Black, and R. F. Treadon, 1994: The numerical solution of the Mellor-Yamada 2.5 turbulent kinetic energy equation in the eta model. *Monthly Weather Review*, **122**, 1640-1646.
- Janjic, Z. I., 1990: The step-mountain eta coordinate model: Physical package. *Monthly Weather Review*, **118**, 1429-1443.
- Janjic, Z. I., 1994: The step-mountain eta coordinate model: Further developments of the convection, viscous sublayer, and turbulence closure schemes. *Monthly Weather Review*, **122**, 927-945.

- Joseph, D., 1980: Navy 10-minute global elevation values. National Center for Atmospheric Research Notes on Fleet Numerical Weather Center Terrain Data Set; 3 pp. [Available from the National Center for Atmospheric Research, P.O. Box 3000, Boulder, CO 80307.]
- Liu, W. T., K. B. Katsaros, and J. B. Businger, 1979: Bulk parameterizations of air-sea exchanges of heat and water vapor including the molecular constraints at the interface. *Journal of Atmospheric Sciences*, **36**, 1722-1735.
- Mangarella, P. A., A. J. Chambers, R. L. Street, and E. Y. Hsu, 1973: Laboratory studies of evaporation and energy transfer through a wavy air-water interface. *Journal of Physical Oceanography*, **3**, 93-101.
- Mass, C. F., M. D. Albright, and D. J. Brees, 1986: The onshore surge of marine air into the Pacific Northwest: A coastal region of complex terrain. *Monthly Weather Review*, **114**, pp. 2602-2627.
- Mass, C. F., and M. D. Albright, 1988: Reply. *Monthly Weather Review*, **116**, 2407-2410.
- Mass, C. F., and N. A. Bond, 1996: Coastally trapped wind reversals along the United States West Coast during the warm season. Part II: Synoptic evolution. *Monthly Weather Review*, **124**, 446-461.
- Mass, C. F., and M. D. Albright, 1987: Coastal southerlies and along-shore surges of the west coast of North America: Evidence of mesoscale topographically trapped response to synoptic forcing. *Monthly Weather Review*, **115**, 1707-1738.
- Mellor, G. L., and T. Yamada, 1974: A hierarchy of turbulence closure models for planetary boundary layers. *Journal of Atmospheric Sciences*, **31**, 1791-1806.
- Mellor, G. L., and T. Yamada, 1982: Development of a turbulence closure model for geophysical fluid problems. *Review of Geophysics, Space Physics*, **20**, 851-875.
- Mesinger, F., 1984: A blocking technique for representation of mountains in atmospheric models. *Riv. Meteor. Aeronaut*, **44**, 195-202.
- Mesinger, F., and W. G. Collins, 1987: Review of the representation of mountains in numerical weather prediction models. *Observation, Theory, and Modeling of Orographic Effects, Seminar Notes*, **2**, European Center for Medium Range Weather Forecasting, 1-28.

- Mesinger, F., S. Nickovic, D. Gavrilov, and D. G. Deaven, 1988: The step-mountain coordinate: Model description and performance for cases of Alpine lee cyclogenesis and a case of Appalachian redevelopment. *Monthly Weather Review*, **116**, 1493-1518.
- Nuss, W. A., 1996: *Coastal Meteorology Science Plan*. Naval Postgraduate School, NPS-MR-96-001, 1-26.
- Nuss, W. A., 1998: Synoptic-scale structure and the character of coastally trapped disturbances. *Preprints of the Second Conference on Coastal Atmospheric and Oceanic Prediction*, 11-16 January 1998, Phoenix, AZ, 186-193.
- Overland, J. E., and N. A. Bond, 1994: The influence of coastal orography: The Yakutat storm. *Monthly Weather Review*, **121**, 1388-1397.
- Ralph, F. M., L. Armi, J. M. Bane, C. E. Dorman, W. D. Neff, P. J. Neiman, W. A. Nuss, and P. O. G. Persson, 1998: Observations and analysis of the 10-11 June 1994 coastally trapped disturbances. *Monthly Weather Review*, **126**, 2435-2465.
- Reason, C. J. C., and D. G. Steyn, 1992: The dynamics of coastally trapped mesoscale ridges in the lower atmosphere. *Journal of the Atmospheric Sciences*, **49**, 1677-1692.
- Rogers, E., D. G. Deaven, and G. J. DiMego, 1995: The regional analysis system for the operational "early" eta model: Original 80-km configuration and recent changes. *Weather and Forecasting*, **4**, 810-825.
- Skamarock, W. C., R. Rotunno, and J. B. Klemp, 1998: Models of coastally trapped disturbances. Submitted to the *Journal of the Atmospheric Sciences* 10 March 1998.
- Thompson, W. T., T. Haack, J. D. Doyle, and S. D. Burk, 1997: A non-hydrostatic mesoscale simulation of the 10-11 June 1994 coastally trapped wind reversal. *Monthly Weather Review*, **125**, 3211-3230.
- Thompson, W. T., and J. M. Bane, 1998: Modeling and observations of coastally trapped wind reversals. *Preprints of the Second Conference on Coastal Atmospheric and Oceanic Prediction*, 11-16 January 1998, Phoenix, AZ, 194-201.



## INITIAL DISTRIBUTION LIST

	No. Copies
1. Defense Technical Information Center ..... 8725 John J. Kingman Rd, STE 0944 Ft. Belvoir, VA 22060-6218	2
2. Dudley Knox Library ..... Naval Postgraduate School 411 Dyer Rd Monterey, CA 93943-5101	2
3. Chairman (Code OC/Gd) ..... Department of Oceanography Naval Postgraduate School Monterey, CA 93943-5122	1
4. Chairman (Code MR/Wx) ..... Department of Meteorology Naval Postgraduate School Monterey, CA 93943-5114	1
5. Dr. Wendell A. Nuss, (Code MR/Nu) ..... Department of Meteorology Naval Postgraduate School Monterey, CA 93943-5122	3
6. Dr. Russell L. Elsberry, (Code MR/Es) ..... Department of Meteorology Naval Postgraduate School Monterey, CA 93943-5122	1
7. Scott Sandgathe ..... Office of Naval Research 800 N. Quincy St. Arlington, VA 22217-5660	1
8. Dr. William T. Thompson ..... Naval Research Laboratory Code 7541 7 Grace Hopper Ave. Monterey, CA 93943	1

9. John Bane ..... 1  
Marine Sciences Program  
University of North Carolina  
Chapel Hill, NC 27599-3300
10. Dr. Clifford Mass ..... 1  
Department of Atmospheric Sciences (AK-40)  
University of Washington  
Seattle, WA 98195
11. LCDR Steven P. Sopko ..... 2  
P.O. Box K  
Hobart, IN 46342